HYDROMAGNETIC INSTABILITY IN THE EARTH'S CORE

by

CHRISTOPHER JOHN LAMB

A thesis submitted to the Faculty of Science, University of Glasgow, for the degree of Doctor of Philosophy

Department of Mathematics,
University of Glasgow,
March, 1994

To my family

Contents

Preface

This thesis is submitted to the University of Glasgow in accordance with the requirements for the degree of Doctor of Philosophy.

To my supervisor, Prof. D.R. Fearn, I wish to express sincere gratitude for his help, encouragement and advice throughout the three years of my research. Thanks are also due to the other members of the MHD group at the University of Glasgow for support and helpful discussion and to Prof. R.W. Ogden and the staff and research students within the Department of Mathematics for their assistance.

I must also thank the Science and Engineering Research Council of Great Britain for the provision of a Research Studentship.

Finally, I thank my family and friends (with a special thanks to Chris for the roof and light refreshments) for their support and understanding throughout my time at University.

Summary

In this thesis we investigate aspects of the Earth's magnetic field with a view to further understanding the physical processes at work in the Earth's core which act to maintain the geomagnetic field against ohmic decay. In particular, we consider problems relating to the stability of the Earth's magnetic field.

The basic model of the Earth's fluid outer core we adopt throughout, chosen to simplify the problem whilst retaining the important features, is that of a cylindrical annulus of electrically conducting, incompressible fluid rotating rapidly about its axis. In this annulus we impose a toroidal magnetic field and velocity field which both depend only on the distance from the axis of rotation. This basic state is then perturbed and its stability investigated.

In the first problem we consider in Chapter 2 the annulus is unbounded in the direction of the axis of rotation. We extend the problem solved by Fearn (1988) to include an inner core of finite conductivity and allow the mantle to be a perfect insulator or a perfect conductor. The effect of varying the inner core conductivity on the magnetic field strength required for the onset of instability is investigated and the result in the limit of an insulating inner core compared with that of Fearn (1988) to serve as a check on the results.

In Chapter 3 the same model is extended to include a finitely conducting layer at the base of the mantle as a model for the D'' layer. The inner core conductivity is in most cases assumed to be equal to that of the outer core and the influence of the D'' layer on instability is investigated. The results are compared with those of the previous Chapter in the appropriate limits.

In the final problem considered we extend the linear stability analysis into the weakly nonlinear regime. The annulus is bounded in the direction of the axis of rotation by perfectly conducting plates and the cylindrical walls are assumed to be perfectly insulating. To simplify the analysis the magnetostrophic approximation is made. Using a multiple scales expansion technique an amplitude equation is derived and the coefficients evaluated to determine if the instabilities are of sub- or supercritical type. As a check on the results the geostrophic flow that arises in the nonlinear regime is used as input into the linear code and its effect on the field strength required for

instability investigated.

The calculations in this thesis were carried out on the University of Glasgow's IBM 3090-150E/VF mainframe computer. The graphics have been produced using the GHOST80 graphics package. The results of Chapters 2 and 3 can also be found in Lamb (1994a,b).

CHAPTER 1

Introduction

1.1 General Introduction

The task of understanding the physical processes at work in the Earth's core which act to maintain the geomagnetic field against dissipative losses is an immense one. The highly nonlinear nature of the governing equations coupled with a comparative ignorance of many of the important parameters makes progress difficult. Nonetheless, advances have been made by approaching the problem from several different perspectives and it is the aim of the work presented here to further understanding of one of these, namely, the stability of the Earth's magnetic field.

Although the attracting properties of lodestones were known to the ancient Chinese and Greeks as early as the third century B.C. it was not until the mid-sixteenth century that measurements of declination, the angle between geographic and magnetic north, led Gerhard Mercator to realise that the source of attraction for compass needles was terrestrial. Later, in 1600, William Gilbert published the influential treatise *De Magnete*, credited by some with being the first scientific textbook although some of the fundamental concepts of magnetism were recorded as early as 1269 by Petrus Peregrinus in *Epistola de Magnete*. From measurements of inclination Gilbert concluded that the Earth itself is a great magnet, one of the first physical properties to be attributed to the Earth as a whole. This important step was followed in 1634 by the discovery by Henry Gellibrand that the magnetic field was not constant in time, a fact he deduced from measurements of declination.

Many of the early measurements of geomagnetic properties were motivated by their use as a navigational aid. Nowadays extensive measurements are made across the globe. Accumulated over the centuries these direct measurements have yielded a great deal of useful information. As well as showing the observable part

of Earth's field to be predominantly dipolar in structure (the toroidal part of the field, believed to be the stronger part, cannot be observed because the bulk of the mantle is insulating) they have revealed some of the non-constant features, the secular (or temporal) variation, and in particular the westward drift of some large scale features of the field (eg. Bloxham, Gubbins and Jackson, 1989). In the latter parts of last century palaeomagnetism began to reveal data covering much longer timescales. Palaeomagnetists were able to extract information on the intensity and direction of the geomagnetic field dating back hundreds of millions of years from rocks formed from cooling of lava and sedimentation. Over these geological timescales the average intensity of the field has been almost constant but the polarity was found to have reversed at irregular intervals of between a hundred thousand and a million years although there have been long periods in which no reversals have taken place.

Although Gilbert had asserted that the geomagnetic field originated from within the Earth it was Gauss in 1834 who brought a mathematical approach to the problem and showed the bulk of the field had its source deep within the Earth. However, permanent magnetism cannot be retained at the temperatures in the deep interior of the Earth and the diffusion timescale for a magnetic field in the Earth is $O(10^5)$ years. It follows therefore from the long term consistency of intensity and time dependent nature of the geomagnetic field (i.e., secular variation, polarity reversals) that the geomagnetic field is not due to permanent magnetisation but that some regeneration process is at work. It is now believed that the geomagnetic field is generated by a dynamo operating in the fluid outer core of the Earth. Conducting fluid moves through a magnetic field inducing electric currents and associated with these currents is a magnetic field which can act to reinforce the original field. As it grows stronger the field will act to inhibit those motions which are enhancing it.

The most obvious obstacle to progress in modelling the Earth is our inability to directly sample the interior and consequent dependence on inferring information

indirectly. It was 1906 before R. Oldham concluded that the Earth has a molten core from the observation that, after an earthquake, only longitudinal waves are detected on the opposite side of the Earth from the epicentre. The general nature and constituents of the Earth's interior are now fairly well established from seismic observations and, as technology improves, from high temperature and pressure experiments. We now know that the 3485km radius core consists of a solid inner part of radius 1220km of almost pure iron and a fluid outer part made up of iron alloyed with smaller quantities of other elements. The identity of these other elements is still debated but oxygen and sulphur are thought likely to be the most abundant alloying elements with silicon, magnesium and nickel amongst the other possible candidates. The core is surrounded by the solid mantle of oxide and silicate minerals and the properties of this region are currently the subject of much research. An overview of the core's features can be found in Jeanloz (1990).

Planetary dynamo action is only possible in a conducting fluid region making the outer core the only feasible location within the Earth. Several possible sources of energy to drive the dynamo have been considered. The most commonly adopted in models to date is a uniform distribution of heat sources giving rise to thermal convection (eg. Roberts, 1968; Fearn, 1979; Fearn and Proctor, 1983a) but it is now thought there is an insufficient amount of radioactive material in the core to provide the necessary heat. Precession as a source has also been ruled out on energetic and other grounds (Loper, 1989) and current thinking favours compositional convection as the main energy source for the geodynamo (eg. Gubbins, 1977; Fearn, 1989; Loper, 1989). The idea is that as the Earth cools the iron part of the outer core freezes out, releasing latent heat and leaving behind lighter compositionally buoyant material. This buoyant material will then rise up through the outer core driving convection and providing energy for the dynamo.

The problems facing anyone hoping to produce a realistic model of the geodynamo are daunting. They must solve a set of highly nonlinear 3-D partial differential equations in a spherical geometry. The model must reproduce fea-

tures such as secular variation and polarity reversals involving widely disparate timescales (eg. reversals occur at irregular intervals of the order of 10^5–10^6 years but the field takes only 5000–10000 years to reverse). They are further hindered by the so called 'anti-dynamo theorems' the most famous of which is Cowling's theorem which states that a steady axisymmetric poloidal magnetic field cannot be maintained by axisymmetric motions [this was later generalised to axisymmeytic toroidal fields by Backus and Chandresekhar (1956) and the non-steady case by Backus (1957)], making asymmetry an inherent part of the problem. Yet another problem is that some of the relevant parameters are not well known, for example viscosity and mantle conductivity. It is only recently that advances in computer technology have made a full numerical solution to the geodynamo problem a realistic possibility and because of the difficulties outlined above a great deal of work to date has concentrated on particular aspects of the problem.

One such approach is the kinematic dynamo, in which a flow is prescribed and the induction equation (see §2.2.1) solved, ignoring the reaction of the field on the flow, to determine if a growing magnetic field results (eg. Gubbins, 1973; Kumar and Roberts, 1975 and for an introduction to kinematic dynamos Soward, 1989). The aim here is to establish which types of flow produce dynamo action, particularly with behaviour reflecting the geodynamo. The actual flow in the Earth is not well known although constraints on the flow near the core-mantle boundary (CMB) can be made from extrapolation of the magnetic field at the surface down into the lower mantle (eg. Gubbins, 1982,1991; Bloxham and Jackson, 1991).

A complimentary approach, and the one we adopt in this thesis, is a stability analysis of some prescribed magnetic and velocity field. Such an approach has proved very fruitful in isolating important aspects of the dynamo problem and a wealth of literature now exists on the various classes of instability which may have a role to play in the dynamics of the Earth's core. Broadly speaking instabilities can be divided into thermally driven instability (see eg. Eltayeb and Kumar, 1977; Fearn, 1979; Drew, 1991) and magnetically driven instability (eg. Acheson,

1972; Fearn, 1983b). We are interested only in the latter here. Many studies have concentrated on the mathematically simpler plane layer geometry (eg. Soward, 1979; Fearn and Proctor, 1983b; Kuang and Roberts, 1990,1991,1992) but cylindrical (Roberts and Loper, 1979; Fearn, 1983b; Fearn and Weiglhofer, 1992) and spherical (Fearn and Proctor, 1983a; Fearn and Weiglhofer; 1991a,1991b) models have also been investigated. A variety of instability types have been uncovered: dynamic instability (Malkus 1967), buoyancy catalysed instability (Roberts and Loper, 1979; Soward, 1979; Acheson, 1980), exceptional instability (Roberts and Loper, 1979; Fearn, 1988), field gradient (ideal) instability (Acheson, 1972,1973; Fearn, 1983b,1988) and resistive instability (Fearn, 1983b,1984,1988; Fearn and Weiglhofer, 1992; Kuang and Roberts, 1990,1991,1992) but it is the latter two that are now thought most likely to be relevant to the Earth. The properties of magnetically driven instability are further discussed in §1.2.

These studies (and numerous others) are important in understanding both the generation of the geomagnetic field and its characteristics. To date, dynamo models have concentrated on axisymmetric mean field models in which the essential asymmetry (Cowling's theorem) is included via some prescribed α-effect [a mechanism for the generation of poloidal (toroidal) field from toroidal (poloidal) field]. Braginsky (1964,1967) proposed that this asymmetry is provided by asymmetric instabilities of the axisymmetric mean field. Instabilities will also place constraints on the strength of the fields that can be maintained since they are an additional drain on the available energy. In addition, Hide (1966) first suggested that the secular variation may be due to travelling hydromagnetic waves and recent statistical analysis (McFadden and Merril, 1992) has supported the view that internal fluid instability in the core is responsible for polarity reversals. All of these provide motivation for further investigation of magnetically driven instability in the Earth.

1.2 Magnetic Instability

The number of studies devoted to magnetic instability is now considerable (see

§1.1). An obvious but important consideration in such studies is the choice of the magnetic field. Many authors have adopted a field of the form

$$\mathbf{B} = B_M s^* \hat{\phi}, \tag{1.1}$$

where s^* is cylindrical radius and B_M a constant. Two important effects are incorporated here: field curvature (so $\mathbf{B} = B\hat{\phi}$) and field strength depending on radius (so $B = s^*$). Such a choice is made because the Earth's field is believed to be predominantly toroidal and because it greatly simplifies the mathematics. Malkus (1967) found dynamical instability of such a field but the large field strengths required led him to dismiss it as being geophysically irrelevant. Roberts and Loper (1979) found an 'exceptional' instability which is absent when the magnetostrophic approximation is made or in the presence of perfectly conducting boundaries. We discuss this exceptional instability further in Chapter 3. They also considered buoyancy catalysed instability of (1.1). Such instability must be magnetically driven because either a top-heavy *or* a bottom-heavy density gradient can have a destabilising effect. This was further investigated by Soward (1979). However, while the choice of field $B = s^*$ simplifies the analysis it has the disadvantage of removing certain important classes of instability.

Acheson (1972,1973,1983) adopted a local analysis in a cylindrical geometry to investigate more general magnetic fields. His local analysis makes the assumption that the instability mechanism operates on lengthscales short in comparison with the annulus width, ignores the effect of the boundaries and expands the perturbation variables in the form

$$f \sim \exp[i(ls + m\phi + nz - \omega t)], \tag{1.2}$$

where (s^*, ϕ, z^*) are cylindrical polar coordinates, $s = s^*/s_o, z = z^*/s_o$, s_o is the outer radius, f is any of the perturbation variables and $l >> 1$. His earlier work (1972,1973) is concerned with the diffusionless limit in which the preferred modes have $n >> 1$. He showed that dynamical instability in a cylindrical geometry must drift westward and that the high field strength required for Malkus' instability was

a result of his choice of magnetic field. With diffusive effects included Acheson (1983) established a stability criterion for ideal instability (ideal, in this context, implies the instability persists in the diffusionless limit, not the absence of diffusive effects). For a magnetic field and velocity profile of the form

$$\mathbf{B}_0 = B_M s F(s)\hat{\phi}, \qquad \mathbf{U}_0 = U_M s\Omega(s)\hat{\phi}, \tag{1.3}$$

this can expressed in terms of a parameter Δ where, in the absence of stratification

$$\Delta = \frac{s}{F^2}\frac{d}{ds}(F^2 - \Re_m\Omega) \tag{1.4}$$

where U_0 is the fluid velocity relative to rotating axes and $\Re_m$, the modified magnetic Reynolds number

$$\Re_m = \frac{U_M \tau_s}{s_o}, \tag{1.5}$$

is a measure of the strength of differential rotation. Instability arises when

$$\Delta > \Delta_c = m^2\left(1 + \frac{l^2}{n^2}\right) + \left(\frac{l^2+n^2}{m\Lambda F^2}\right)^2, \tag{1.6}$$

[cf. Acheson 1983 Eq(3.1)]. The parameter Λ can be regarded as a measure of the field strength or, alternatively as an inverse measure of magnetic diffusion and is defined by

$$\Lambda = \tau_\eta/\tau_s, \tag{1.7}$$

where τ_η is the magnetic diffusion timescale and τ_s is the slow magnetohydrodynamic timescale

$$\tau_\eta = s_o^2/\eta, \qquad \tau_s = 2\Omega_0/\Omega_A^2, \tag{1.8}$$

Ω_0 is the rotation frequency of the system and Ω_A the Alfvén frequency

$$\Omega_A = B_M/s_o(\mu\rho_0)^{1/2}. \tag{1.9}$$

where μ is magnetic permeability and ρ_0 fluid density. With sufficiently large Λ and n the stability condition (1.6) becomes

$$\Delta > m^2. \tag{1.10}$$

The slow timescale τ_s (slow because in the Earth's core $\Omega_A << \Omega_0$) is a natural timescale for instability arising in diffusionless rapidly rotating systems, the analogue of the Alfvén timescale in a non-rotating system. Provided Δ satisfies $\Delta > m^2(1 + l^2/n^2)$ the condition (1.6) can be rewritten in terms of a minimum value of Λ, i.e., instability exists for a given value of Δ if $\Lambda > \Lambda_c$ where

$$\Lambda_c = \frac{1}{mF^2}(l^2 + n^2)\left[\Delta - m^2\left(1 + \frac{l^2}{n^2}\right)\right]^{-1/2}. \tag{1.11}$$

It is apparent from (1.10) or (1.11) that the most unstable mode is $m = 1$. In the diffusionless limit $\Lambda \to \infty$ the instability persists and the growth rate p tends to a constant; hence these instabilities are also termed ideal instabilities. The above indicates there are two basic requirements for ideal instability. The first is geometric; the field must increase sufficiently rapidly with distance from the axis of rotation [condition (1.6) with (1.4)]. This led Acheson to term this type of instability "field gradient instability". The second requirement is energetic. The instability must be able to extract sufficient energy from the field to counteract diffusive effects. Consider (1.7); as Λ is decreased from some supercritical value the instability timescale and the diffusive timescale become more evenly matched until eventually diffusion acts rapidly enough to dampen out the instability.

Fearn (1983b,1984,1985,1988) found global numerical solutions to the problem in a cylindrical geometry and confirmed that many of the results of Acheson's local analysis carried over to the global results. In this case the boundaries act as a restriction so that global solutions will not necessarily satisfy $l >> 1$ and boundary conditions cannot be ignored. Also, on the short lengthscales entailed by $n >> 1$ diffusion becomes an important effect so $n \geq O(1)$ is more reasonable. Nonetheless, the numerical solutions proved the local analysis to be a good guide to ideal instability. Fearn also found a second important class of instability: resistive instability. Resistive instability was already well known in non-rotating magnetohydrodynamics [eg. Furth, Killeen and Rosenbluth (1963)] and the principle effect of rotation is in modification of the timescale. Again instability arises

when $\Lambda > \Lambda_c$ but in this case the growth rate peaks as Λ is increased and then decreases towards zero as Λ is further increased so that the instability vanishes in the diffusionless limit. This requirement for finite diffusivity indicates these modes are resistive, the mechanism for instability being the reconnection of field lines allowed to move relative to the fluid. Typically Λ_c is lower for resistive instability than ideal instability and the preference for $m = 1$ modes is less marked.

Resistive instability is usually associated with the presence of a critical level $\mathbf{k}.\mathbf{B}=0$ where $\mathbf{k}$ is a wavevector. For a toroidal field of the form (1.3) this condition reduces to $F(s) = 0$. However, Fearn and Weiglhofer (1992) and Fearn and Kuang (1993) have found resistive instability in the absence of critical levels. Although the necessary conditions for this 'new' resistive instability are not yet fully understood they found no instability unless $B''/B < 0$ near an insulating boundary (the prime denotes differentiation with respect to radius). Another feature of this instability was its absence when the boundaries were perfect conductors. Unlike ideal instability field curvature is not a necessary ingredient; Kuang and Roberts (1990,1991,1992) have extensively investigated resistive instability in a plane layer geometry with straight field lines.

Both ideal and resistive instability have also been investigated in the more realistic spherical geometry by Fearn and Weiglhofer (1991a,1991b). They found the constricting effects of the geometry to be a stabilising effect on the field gradient instabilities although the effect was less marked on resistive instability. Their work confirmed that these types of instability could have an important role to play in the dynamics of the Earth's core.

In addition to the two types of instability described above, which are now well established as being relevant to study of the geodynamo, magnetically driven instabilities destabilised by other effects have been found. Fearn (1988) showed these arise when some effect acts to counter the stabilising influence of rotation on ideal instability, eg. inertia and magnetic diffusion (Roberts and Loper, 1979), stratification (Roberts and Loper, 1979; Soward, 1979; Acheson, 1980), viscosity

(Fearn, 1988). In a non-rotating system the condition (1.6) is modified to

$$\Delta > m^2 - 4. \tag{1.12}$$

Rotation is therefore clearly a stabilising effect. If, in a rotating system, some mechanism acts to overcome this stabilising effect instability, not otherwise present in the rotating system, may become possible for $m^2 - 4 < \Delta < m^2$.

The investigations mentioned briefly above (and many others not mentioned) have assumed the mantle and inner core to be either perfectly insulating or perfectly conducting. However, the boundary conditions have a significant influence on certain instabilities, in some cases excluding them altogether, and although the inner core conductivity is not known with certainty it is likely to closely resemble that of the fluid outer core (Jeanloz, 1990). This provides our motivation in Chapter 2 in which we examine the effect of an inner core of uniform finite conductivity on magnetically driven instability in a cylindrical geometry.

The effect of a finitely conducting layer in the mantle whose conductivity depends on radius (i.e., the layer conductivity $\sigma_m = \sigma_m(s)$) is investigated in Chapter 3. In recent years our knowledge of this part of the Earth's interior has improved greatly from both seismology and laboratory experiments on minerals at high temperatures and pressures. The conductivity of the bulk of the mantle, which extends from 3485km from the Earth's centre to just below the surface at 6371km (Gubbins and Roberts, 1987) is not well determined but is very small in comparison with the outer core. It is now generally believed that a layer of thickness 200–300km exists at the base of the mantle, the D// layer, whose conductivity is considerably greater than the bulk of the material above it. This increased conductivity is due to iron enrichment from the fluid outer core.

Chapters 2 and 3 are extensions of the model employed by Fearn (1983,1988) to investigate the linear stability of planetary magnetic fields. In Chapter 4 we return to this model and take both the inner core and mantle to be insulating. Our aim here is to extend the linear analysis to a weakly nonlinear analysis to

determine whether the instabilities of interest described above, the ideal and resistive instabilities, are sub- or supercritical. While linear analyses can tell us about the necessary geometry and field strength for instability to arise it is only by extending this to the nonlinear regime that we can obtain information about the parameter ranges in which steady finite amplitude solutions to the equations exist. It is these solutions we are most likely to observe. This is particularly relevant to the possibility that internal fluid instabilities trigger polarity reversals and to the westward drift.

CHAPTER 2

Magnetic Instability With A Finitely Conducting Inner Core

2.1 INTRODUCTION

Our model of the Earth's interior comprises a cylindrical annulus of electrically conducting fluid rotating rapidly about its axis with angular velocity $\mathbf{\Omega}_0 = \Omega_0 \hat{\mathbf{z}}$ and confined between two solid regions rotating with the system. The fluid, with an azimuthal shear flow $\mathbf{U} = U(s^*)\hat{\phi}$, is permeated by an azimuthal magnetic field $\mathbf{B} = B(s^*)\hat{\phi}$. In this chapter the mantle, represented in our model by the region exterior to the annulus, is taken to be a perfect electrical conductor or insulator and we investigate the influence of an inner core, the region within the annulus, of arbitrary prescribed uniform electrical conductivity on linear magnetic instability of the above state.

Previous investigations of the most relevant types of instability, the ideal and resistive instability, have assumed the mantle and inner core to be either insulating or perfectly conducting. The effect of finitely conducting boundaries on thermally driven instabilities has been investigated [eg. Sparrow *et al.* (1963)] and in this Chapter we examine the effect of a finitely conducting inner core on magnetically driven instability. The effect of a finitely conducting layer in the mantle (with conductivity a function of radius) is investigated in the next Chapter. Although the inner core conductivity is not known precisely it is likely to be comparable with that of the fluid outer core. This provides the motivation for our model.

The work of Fearn (1983b,84,88) is extended to include a solution of the induction equation in an inner core of finite conductivity. As a reasonable representation of the magnetic field in the Earth's fluid core, the basic state we consider is, in

cylindrical polar coordinates (s^*, ϕ, z^*),

$$\mathbf{B}_0 = B_0(s^*)\hat{\phi}, \qquad \mathbf{U}_0 = U_0(s^*)\hat{\phi}, \tag{2.1}$$

incorporating field curvature but neglecting buoyancy effects. The parameter of interest is $\eta_i = \eta_i^*/\eta_o$ where η_i^* is the magnetic diffusivity of the inner core and η_o that of the fluid. The limits $\eta_i \to 0$ and $\eta_i \to \infty$ correspond to a perfectly conducting and an insulating inner core respectively. Basic states were chosen to permit comparison with earlier work and enable the study of field gradient and resistive (with and without a critical level) instabilities.

For both classes of instability the behaviour in the $\eta_i \to \infty$ limit was as expected. In each case the modes found approached those of a perfect insulator irrespective of the basic state. A new feature of this model was found in the $\eta_i \to 0$ limit. In this limit the expected modes approaching those of the perfectly conducting case were found (with one exception) and, in some cases, a new mode of instability was also present. Typically, these new modes of instability are low frequency modes penetrating deep into the inner core and requiring lower Λ_c's than the expected modes mentioned above. Both ideal and resistive cases of this new mode were found.

Perhaps the most significant result was found when η_i was varied over finite values. In almost all instances we found instability was most readily promoted when η_i was close to what is believed to be the the geophysical value of $\eta \approx 1$. This, together with the above, suggests that a perfectly conducting boundary condition may not provide the best guide to the results and the inclusion of a finitely conducting inner core is worthwhile in future studies of magnetic instability.

2.2 THE MODEL

2.2.1 Governing Equations

The model we adopt, combining simplicity with the essential features of the problem, is an infinite cylindrical annulus of electrically conducting incompressible fluid with an inner radius of s_i and outer radius s_o. The regions $0 \leq s^* \leq s_i$ and $s_o \leq s^*$ are rigid solids, the inner one having arbitrarily prescribed finite magnetic diffusivity η_i^*, the outer either insulating or perfectly conducting. The whole system rotates about its axis with angular velocity $\mathbf{\Omega}_0 = \Omega_0 \hat{\mathbf{z}}$. The fluid, with constant magnetic diffusivity η_o, magnetic permeability μ, kinematic viscosity ν and density ρ_0 moves relative to this system with velocity $\mathbf{U}$ and is permeated by a toroidal magnetic field $\mathbf{B}$. The equations governing the motion of the fluid and evolution of the magnetic field are

$$\frac{\partial \mathbf{U}}{\partial t} + \mathbf{U}.\nabla\mathbf{U} + 2\mathbf{\Omega}_0 \times \mathbf{U} = -\frac{\nabla P}{\rho_0} + \frac{1}{\mu\rho_0}(\nabla \times \mathbf{B}) \times \mathbf{B} + \nu\nabla^2\mathbf{U}, \tag{2.2}$$

$$\frac{\partial \mathbf{B}}{\partial t} = \nabla \times (\mathbf{U} \times \mathbf{B}) + \eta_o \nabla^2 \mathbf{B}, \tag{2.3}$$

$$\nabla.\mathbf{B} = \nabla.\mathbf{U} = 0, \tag{2.4a,b}$$

where P is the fluid pressure. In the inner core ($s^* \leq s_i$) there is no flow and the appropriate magnetic diffusion equation is

$$\frac{\partial \mathbf{B}}{\partial t} = \eta_i^* \nabla^2 \mathbf{B}. \tag{2.5}$$

Small perturbations $\mathbf{b}$ and $\mathbf{u}$ are then applied to an ambient state $\mathbf{B} = \mathbf{B}_0$, $\mathbf{U} = \mathbf{0}$ so that

$$\mathbf{B} = \mathbf{B}_0 + \mathbf{b}, \qquad \mathbf{U} = \mathbf{u}, \tag{2.6}$$

where

$$\mathbf{b} = (b_s, b_\phi, b_z), \qquad \mathbf{u} = (u_s, u_\phi, u_z). \tag{2.7}$$

Equations (2.2)–(2.5) are non-dimensionalised using the lengthscale s_o, the slow magnetohydrodynamic timescale τ_s [defined in (1.8)] and the magnetic field

B_M. The coordinates are then (s, ϕ, z) with the inner boundary at $s = s_{ib}$, where $s_{ib} = s_i/s_o$. Unless otherwise stated we take $s_{ib} = 0.35$ in our calculations which is representative of the Earth's inner/outer core ratio. After linearising, the equations governing the stability of the basic state are

$$\Lambda E_\eta \frac{\partial \mathbf{u}}{\partial t} + \hat{\mathbf{z}} \times \mathbf{u} = -\nabla p + (\nabla \times \mathbf{B}_0) \times \mathbf{b} + (\nabla \times \mathbf{b}) \times \mathbf{B}_0 + E\nabla^2 \mathbf{u}, \tag{2.8}$$

$$\frac{\partial \mathbf{b}}{\partial t} = \nabla \times (\mathbf{u} \times \mathbf{B}_0) + \Lambda^{-1}\nabla^2 \mathbf{b}, \tag{2.9}$$

$$\nabla.\mathbf{b} = \nabla.\mathbf{u} = 0, \tag{2.10a,b}$$

in the fluid and

$$\frac{\partial \mathbf{b}}{\partial t} = \Lambda^{-1}\eta_i \nabla^2 \mathbf{b}, \tag{2.11}$$

in the solid inner core. The coefficients of $\mathbf{b}$ and $\mathbf{u}$ in the equations (2.8)–(2.11) together with the boundary conditions (detailed in §2.2.2 below) are independent of ϕ, z and t permitting us to use a modal expansion of the form

$$f(s, \phi, z, t) = f(s) exp[i(m\phi + nz - \omega t)], \tag{2.12}$$

where f is any of the components of $\mathbf{b}$ or $\mathbf{u}$.

The parameters E and E_η, the Ekman and magnetic Ekman numbers, are non-dimensional measures of viscous and inertial effects respectively and are defined by

$$E = \frac{\nu}{2\Omega_0 s_o^2}, \qquad E_\eta = \frac{\eta_o}{2\Omega_0 s_o^2}, \tag{2.13}$$

where for the calculations in Chapters 2 and 3 of this thesis we take $E = E_\eta = 10^{-5}$ (unless otherwise stated). Although in the Earth these parameters are likely to be considerably smaller than this (possibly as small as $E = 10^{-15}$ and $E_\eta = 10^{-9}$) choosing realistic values would entail boundary layers too narrow to be resolved numerically. The main parameter of interest in this chapter is η_i where

$$\eta_i = \eta_i^*/\eta_o \tag{2.14}$$

is the ratio of magnetic diffusivity in the inner core to that of the fluid. The limits $\eta_i \to 0$ and $\eta_i \to \infty$ correspond to a perfectly conducting and a perfectly insulating inner core respectively.

2.2.2 Boundary Conditions

The boundary conditions on the velocity are simply the no slip condition and no normal component, i.e.,

$$\mathbf{u} = \mathbf{0}, \qquad s = s_{ib}, 1. \tag{2.15}$$

The magnetic field must be continuous everywhere. On the axis of rotation this implies

$$\left.\begin{aligned} Db_s = b_z = 0 \qquad & m = 1 \\ b_s = b_z = 0 \qquad & m > 1 \end{aligned}\right\} \qquad s = 0, \tag{2.16a,b}$$

where $D \equiv d/ds$.

In this Chapter, the mantle, $s \geq 1$, is taken to be either perfectly conducting or insulating. In the case of an insulator the condition is that the current normal to the boundary vanishes and the field matches to some external potential field $\mathbf{b}^{(e)} = -\nabla V$. The first of these gives

$$s^2 Db_s + sb_s + i(m^2 + n^2 s^2)b_z/n = 0, \qquad s = 1, \tag{2.17}$$

The external potential field V must satisfy

$$\nabla^2 V = 0, \tag{2.18}$$

with general solution

$$V = AI_m(ns) + CK_m(ns), \tag{2.19}$$

where A and C are constants and I_m and K_m are modified Bessel functions [see Abramowitz and Stegun (1965)]. For the magnetic field to remain bounded as $s \to \infty$ we require $A = 0$. Then, matching the field at the boundary $s = 1$ to eliminate the constant so that $\mathbf{b} = \mathbf{b}^{(e)}$ we get

$$b_s = \gamma b_z, \tag{2.20}$$

where

$$\gamma = i[K_{m+1}(n)/K_m(n) - m/n], \qquad s = 1, \tag{2.21}$$

In the perfectly conducting case the condition is that the tangential electric field is zero, i.e., $\mathbf{n} \times \mathbf{e} = \mathbf{0}$, where $\mathbf{n}$ is a vector normal to the boundary. This leads to

$$b_s = Db_z = 0, \qquad s = 1, \tag{2.22}$$

(see Fearn 1983a).

At the boundary between the fluid and the region of finite conductivity at $s = s_{ib}$ the magnetic field must remain continuous and the equations in solid and fluid regions are coupled. One possibility that was tried is simply to solve the induction equation at the boundary itself, utilising the continuity of $\mathbf{b}$ and coupling the equations across $s = s_{ib}$ (numerically, when the equations are solved at discrete points, this means defining derivatives solely in terms of points in a given region up to and including the boundary point with an equation at the boundary defined in terms of points of either region). An alternative is to use the continuity of $\mathbf{b}$ with (2.10a) and the z-components of (2.8) and (2.9). This leads to continuity conditions involving derivatives of b_s and b_z. However, we found that neither of these two alternatives is enough to ensure that our numerical solution of the system of equations is the one consistent with the physical conditions we are trying to model. The problem lies in the $\eta_i \to \infty$ limit.

As η_i becomes large we approach the case of an insulating inner core and (2.11) becomes

$$\nabla \times (\nabla \times \mathbf{b}) = \mathbf{0}. \tag{2.23}$$

The solution of (2.23).$\hat{\mathbf{z}}$ is

$$b_z = AI_m(ns) + CK_m(ns), \tag{2.24}$$

where A and C are constants and I_m and K_m are modified Bessel functions. The boundary condition at $s = 0$ ensures $C = 0$ and substitution of (2.24) into (2.23).$\hat{\mathbf{s}}$ then yields, after solving for b_s

$$b_s = [GI_m(ns) + HK_m(ns)]/s + ADI_m(ns)/in, \tag{2.25}$$

where G and H are constants. As before the condition at $s = 0$ implies $H = 0$. Physically however, the condition that should be satisfied in the inner core as $\eta_i \to \infty$ is

$$\nabla \times \mathbf{b} = \mathbf{0}. \tag{2.26}$$

i.e., the current in an insulator vanishes. The solutions (2.24) and (2.25) do not satisfy this condition, giving upon substitution

$$(\nabla \times \mathbf{b}).\hat{\mathbf{s}} = D(GnI_m(ns)/ms). \tag{2.27}$$

The condition that ensures the solution to (2.23) satisfies (2.26) is continuity of the tangential electric field, i.e.,

$$[\mathbf{n} \times \mathbf{e}] = \mathbf{0}, \tag{2.28}$$

where $[f] = (f)^i - (f)^o$ and the superscripts i and o refer to the inner core and outer core respectively. This can be expressed as

$$[\mathbf{n} \times \eta \mathbf{j}] = \mathbf{0}.$$

where η is the appropriate magnetic diffusivity for the inner core or the fluid. The z-component of this is

$$[\eta(inb_s - Db_z)] = 0, \tag{2.29}$$

or

$$(inb_s - Db_z)^i - \frac{1}{\eta_i}(inb_s - Db_z)^o = 0.$$

We approach the case of an insulating inner core by letting $\eta_i \to \infty$ so this gives

$$(inb_s - Db_z)^i = 0. \tag{2.30}$$

Substitution of (2.24),(2.25) (with C=H=0) into (2.30) then yields

$$(inGI_m(ns)/s)^i = 0, \tag{2.31}$$

and so, $G = 0$ and the solution (2.25) of (2.23) will satisfy (2.26). Finally, the continuity of $\mathbf{b}$ together with (2.10a) give

$$[Db_s] = 0, \tag{2.32}$$

which together with (2.29) form the magnetic boundary conditions at the inner core boundary (ICB).

2.2.3 Method of Solution

After substitution of the modal expansion (2.12) into equations (2.8)–(2.11) we can eliminate b_ϕ, u_ϕ and π using (2.10a), (2.10b) and (2.8).$\hat{\phi}$ respectively to leave a tenth order system of linear ordinary differential equations in s.

To solve these equations the regions $s < s_{ib}$ and $s_{ib} < s < 1$ are divided into N_1 and N_2 intervals respectively and differential operators replaced by fourth order finite difference operators. The resulting system of discretised equations can then be expressed as a matrix eigenvalue problem of the form

$$A\mathbf{v} = -i\omega C\mathbf{v}, \tag{2.33}$$

where

$$\mathbf{v} = [b_s^1, b_z^1, u_s^1, u_z^1, \ldots, b_s^{N-2}, b_z^{N-2}, u_s^{N-2}, u_z^{N-2}]^T, \tag{2.34}$$

where $N = N_1 + N_2$.

Two independent methods were employed to solve this eigenvalue problem. The first was the LR algorithm [Peters and Wilkinson (1971a)]. This method finds all the eigenvalues and eigenvectors of a given matrix but requires a large amount of storage and CPU time. For this reason a second method is used, the method of inverse iteration [Peters and Wilkinson (1971b), Fearn (1991a)]. Taking a particular eigenvalue found by the LR algorithm as a starting value, this second method iterates to the eigenvalue closest to it and also outputs the eigenvector associated with it. Much greater resolution can be achieved with this method since it can work with only the band of the matrix containing non-zero entries. It

can therefore utilise the banded structure of the matrix which arises as a natural consequence of the finite difference approximations to make considerable savings in storage and CPU time and output more accurate approximation to the eigenvector and eigenvalue.

2.3 RESULTS

2.3.1 Numerical Procedure

The code we used is one employed by Fearn (1988) modified to allow either a perfectly conducting or insulating boundary condition to be used at the CMB and to incorporate a solution of the induction equation in the inner core. The first step is to determine if instability is present for a given set of parameters and basic state. A value of Λ is chosen and the LR algorithm used to find all of the eigenvalues. If none are found with a positive growth rate, i.e., with

$$p = \Re(-i\omega) > 0 \tag{2.35}$$

then Λ is increased and the process is repeated until one is found. This eigenvalue, the most unstable mode (in the sense that it is the first growing mode, there may be other modes at larger field strengths which grow faster), is then used as input for the method of inverse iteration which yields both the eigenvalue closest to the initial value and its corresponding eigenvector and can be used with considerably higher resolution than the LR algorithm. Newton-Raphson iteration is then used to iterate from this eigenvalue to find the point of marginal stability, i.e., to find the value of Λ, Λ_c where $p = 0$.

In most of the calculations in this thesis the first part of this process was unnecessary. In the majority of cases results of Fearn (1983b,88) or Fearn and Weiglhofer (1991a) were used as a starting point. Most of their results were obtained with $E = E_\eta = 0$ and in these cases values of E and E_η smaller than the standard were chosen (in general $E = E_\eta = 10^{-8}$ was small enough to accurately approximate the $E = E_\eta = 0$ case) and the mode followed as E and E_η were

increased to $E = E_\eta = 10^{-5}$. The parameter under consideration was then incremented by some small amount and the inverse iteration process repeated with the previous critical parameters used as the required initial estimate.

2.3.2 Plotting Eigenfunctions

Our code produces as output b_s, b_z, u_s and u_z and from these b_ϕ and u_ϕ could be calculated using (2.10a) and (2.10b) if desired. The eigenfunctions have been normalised so that $max|b_z| = 1$ and real parts plotted as full lines, imaginary parts as broken lines. Throughout this chapter we use $N_1 = N_2 = 1000$ grid points. In most cases this is more than sufficient but ensures adequate resolution of viscous and magnetic boundary layers for the full range of parameters values we consider.

2.3.3 Basic States

The basic states we have elected to investigate are chosen to permit direct comparison with previous work and to allow study of ideal, resistive and exceptional instability. The first field is unstable to ideal and exceptional instability

$$F = s^\alpha. \tag{2.36}$$

The second is unstable to ideal, resistive and exceptional instability and, with appropriate parameters, can be chosen with or without critical levels

$$F = \left(\frac{1}{1+\alpha}\right)\left(\frac{4(1-s^\beta)(s^\beta - s_{ib}^\beta)}{(1-s_{ib}^\beta)^2} + \alpha\right). \tag{2.37}$$

The factor $1/(1+\alpha)$ is a normalisation factor chosen so that the maximum of $F = 1$. The non-monotonic field (2.37) is likely to be more geophysically realistic than the field (2.36) since it vanishes at the boundaries. With $\alpha > 0$ there are no critical levels in $s_{ib} \leq s \leq 1$, with $\alpha = 0$ the field is zero at both boundaries. The gradient of field (2.37) is positive in the inner part of the annulus so that we expect ideal instabilities to be concentrated in that region.

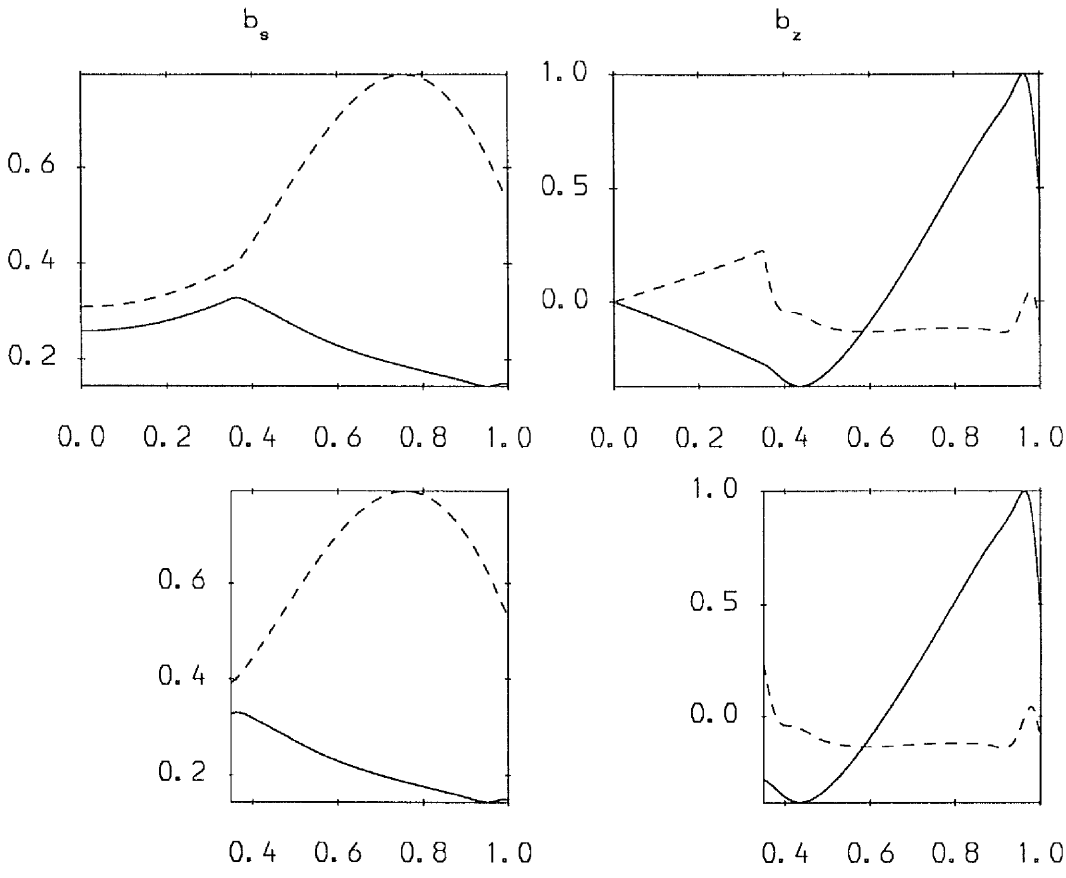

Figure 2.1 Comparison of ideal modes of field (2.36) with $m = 1, \alpha = 1$. The top figure includes a solution in the inner core with $\eta_i = 10^3$ and the bottom with an insulating boundary condition applied at the ICB. Critical parameters are given in (2.38a,b).

2.3.4. A Check On The Results

As a test of the code, we compare results with some obtained using the code employed by Fearn (1983b,88), modified to allow any combination of perfectly conducting/insulating inner and outer boundaries to be chosen [in Fearn (1983b,88) both boundaries were perfectly conducting (1983b) or insulating (1988)] and incorporating viscosity. Here the outer boundary is taken to be insulating. We also examine the consistency of our results with an analytic consideration.

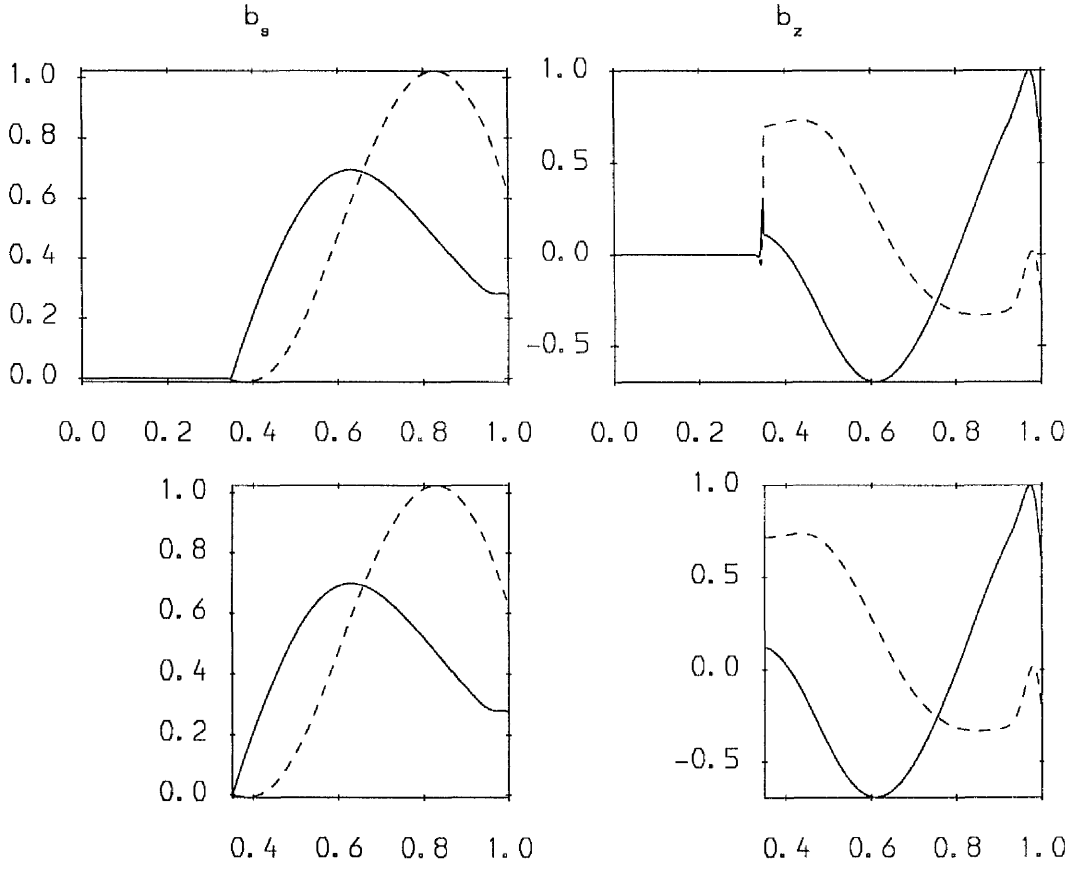

Figure 2.2 Comparison of ideal modes of field (2.36) with $m = 1, \alpha = 1$. The top figure includes a solution in the inner core with $\eta_i = 10^{-3}$ and the bottom with a perfectly conducting boundary condition applied at the ICB. Critical parameters are given in (2.38c,d).

Figures 2.1–2.2 show eigenfunctions b_s, b_z for an ideal instability of the basic state (2.36) with $\alpha = 1$ and an insulating outer boundary. Figure 2.1 is a comparison between the eigenfunctions with solution in the inner and outer cores and $\eta_i = 10^3$ (top) and a solution in the fluid only with an insulating inner boundary (bottom). The agreement in the fluid region is excellent and in the inner core region in the top figure the solution can be seen slowly decaying as would be expected. A comparison of the critical parameters for the $\eta_i = 10^3$ case and an

insulating inner boundary is shown in (2.38a) and (2.38b) respectively with the parameters for the $\eta_i = 10^{-3}$ case and a perfectly conducting boundary in (2.38c) and (2.38d).

$$\Lambda_c = 192.42, \qquad n_c = 2.370, \qquad \omega_c = -0.5052. \tag{2.38a}$$

$$\Lambda_c = 192.49, \qquad n_c = 2.374, \qquad \omega_c = -0.5069. \tag{2.38b}$$

$$\Lambda_c = 210.43, \qquad n_c = 4.508, \qquad \omega_c = -0.9800. \tag{2.38c}$$

$$\Lambda_c = 210.21, \qquad n_c = 4.514, \qquad \omega_c = -0.9814. \tag{2.38d}$$

Figure 2.2 compares the solution in the whole core with $\eta_i = 10^{-3}$ with the case of a perfectly conducting inner boundary. Again the agreement in the fluid region is excellent. In the inner core, b_z can be seen adjusting rapidly in a thin layer (so that $b_s, b_z = 0$ throughout the bulk of the inner core as would normally be expected in a perfect conductor). This is considered further below.

2.3.5 The Limit $\eta_i \to 0$

Consider (2.11).$\hat{\mathbf{z}}$, the equation determining b_z in the inner core.

$$-i\omega b_z = \Lambda^{-1}\eta_i(D^2 + s^{-1}D - s^{-2}(m^2 + n^2 s^2))b_z,$$

which may be rewritten as

$$[s^2D^2 + sD - m^2 - (n^2 - \frac{i\omega\Lambda}{\eta_i})s^2]b_z = 0, \tag{2.39}$$

with solution

$$b_z = AI_m(ks) + CK_m(ks), \tag{2.40}$$

where

$$k = (n^2 - \frac{i\omega\Lambda}{\eta_i})^{1/2}. \tag{2.41}$$

Condition (2.16) implies $C = 0$ and if we choose to normalise b_z so that $b_z(s = s_{ib}) = 1$ we obtain

$$b_z = I_m(ks)/I_m(ks_{ib}). \tag{2.42}$$

As we increase the conductivity of the inner core, $\eta_i \to 0$ and we have

$$k \approx \left(\frac{-i\omega\Lambda}{\eta_i}\right)^{1/2}. \tag{2.43}$$

At marginal stability, ω is real and we can write this as

$$k = (1 \pm i)\left(\frac{|\omega_c|\Lambda_c}{2\eta_i}\right)^{1/2}. \tag{2.44}$$

The $\pm$ sign in this expression is $+$ if $\omega_c < 0$, $-$ if $\omega_c > 0$. (It should be noted here we are assuming that as $\eta_i \to 0$, $\eta_i << \omega\Lambda$. This is not always the case; solutions for which $\omega\Lambda \to 0$ as $\eta_i \to 0$ were found for some fields [basic state (2.37)]. The analysis in this section does not apply to these low frequency modes which will be discussed further in §2.3.9).

To leading order (see Abramowitz and Stegun), then, in the limit $\eta \to 0$ (such that $|ks| >> 1$)

$$I_m(ks)/I_m(ks_{ib}) \sim \left(\frac{1}{(2\pi ks)^{1/2}}\right) exp[ks] \left(\frac{1}{(2\pi ks_{ib})^{1/2}}\right)^{-1} exp[-ks_{ib}], \tag{2.45}$$

which, with (2.43) at marginal stability, can be written

$$I_m(ks)/I_m(ks_{ib}) = \left(\frac{s_{ib}}{s}\right)^{1/2} exp[(1 \pm i)\left(\frac{|\omega_c|\Lambda_c}{2\eta_i}\right)^{1/2}(s - s_{ib})]. \tag{2.46}$$

There are two points to be made from consideration of (2.46). The first is that when η_i is very small the real part of the exponential will decay very rapidly to zero as s is decreased from $s = s_{ib}$. This can be clearly seen in Figures 2.2 and 2.3, in particular the latter which shows blow-ups of the eigenfunctions b_s, b_z at the boundary $s = s_{ib}$ for decreasing values of η_i. A narrow boundary-layer structure can be seen developing as $\eta_i \to 0$ and the field is expelled from the inner core. Secondly, the imaginary part of this same exponential will give rise to oscillations with a length scale $\sim (\eta_i/\omega\Lambda)^{1/2}$ placing a limit on how small η_i can be whilst retaining sufficient numerical resolution. In practice we found $\eta_i \approx 10^{-3}$ was in most cases small enough to accurately approximate the perfectly conducting case.

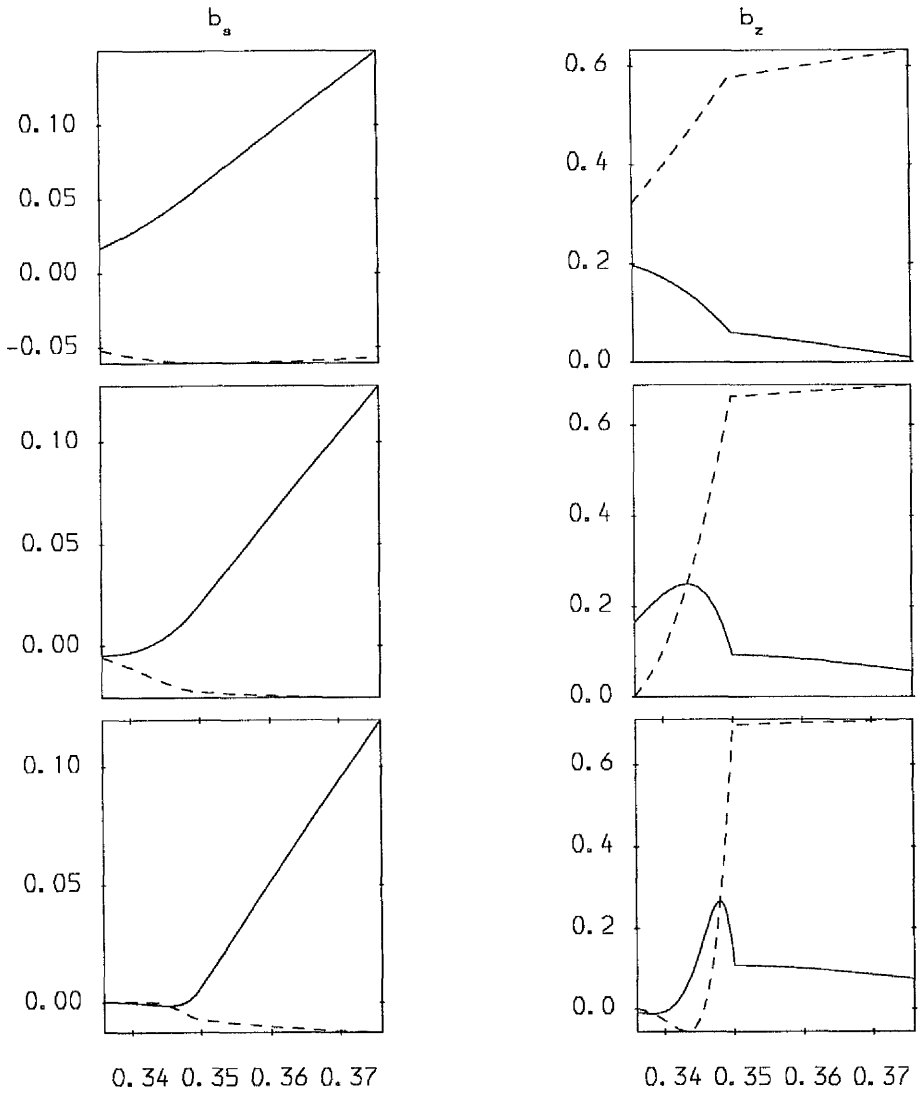

Figure 2.3 Blow ups of the eigenfunctions of an ideal mode of field (2.36) at the ICB with $m = 1, \alpha = 1$ and, from top to bottom, $\eta_i = 10^{-1}, 10^{-2}, 10^{-3}$.

2.3.6 Field Gradient Instabilities

In the previous section we considered the limits $\eta_i \to \infty$ and $\eta_i \to 0$ for the purposes of comparison with earlier work. In the rest of this chapter we examine the effect of varying η_i on the instabilities.

The first type of instability we consider is the field gradient instability. For completeness we consider first the field (2.36) before proceeding to the more real-

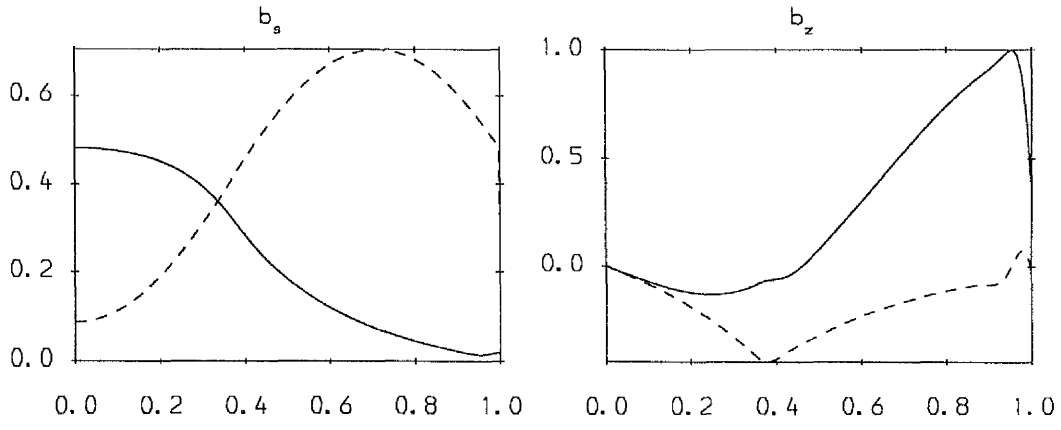

Figure 2.4 As in Figures 2.1 and 2.2 but with $\eta_i = 1$. Critical parameters are given in (2.47).

istic case of (2.37). Figure 2.4 is the eigenfunction for this field with $\eta_i = 1, \alpha = 1$ and with critical parameters

$$\Lambda_c = 188, \qquad n_c = 1.69, \qquad \omega_c = -0.198. \tag{2.47}$$

Comparison with Figures 2.1 and 2.2 shows the mode evolves in a manner that would be expected, the field being expelled from the inner core as η_i is decreased. The variation of Λ_c with η_i is shown in Figure 2.5. The discontinuity in the gradient of the curve is due to Λ being minimised over n. The curve represents the *global* minimum over n, but local minimums can also occur and at the point of discontinuity the global minimum 'jumps' from one local minimum to another. This is clarified in Figure 2.6, which shows plots of Λ_c versus n for $\eta_i = 0.1$ (full line) and $\eta_i = 1$ (dashed line). The change of global minimum from one local minimum to the other is clearly illustrated and, away from these minima, Λ_c can be seen increasing as n is sufficiently increased or decreased. The circles on the vertical axes of Figure 2.5 represent the critical Λ's with a perfectly conducting or insulating boundary condition applied indicating (together with Figures 2.1 and 2.2) a good match with the appropriate solutions.

The second basic state we consider, field (2.37), is of greater interest. With

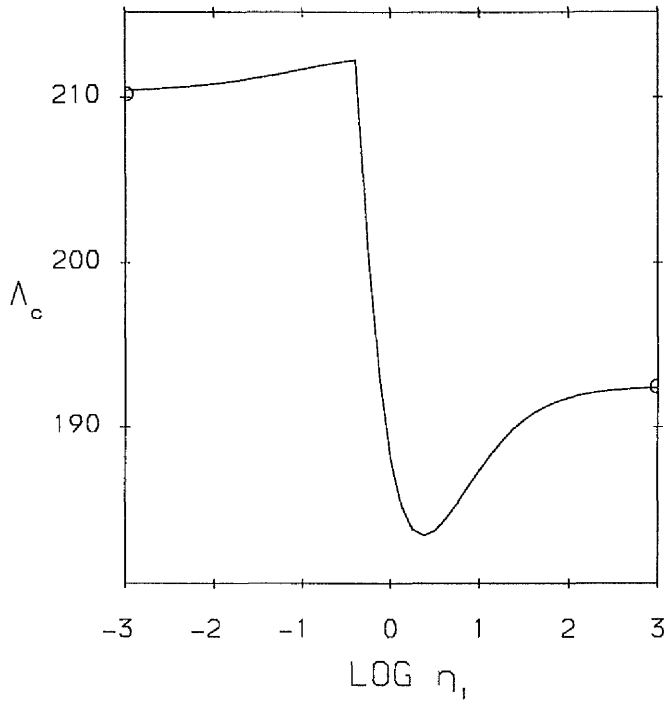

Figure 2.5 Critical Elsasser number versus $\log_{10}\eta_i$ for ideal modes of field (2.36) with $m = 1, \alpha = 1$. The circles indicate the values with a perfectly conducting or insulating boundary condition applied.

this field geometry $m = 1$ modes are not easily categorised as ideal or resistive with individual modes exhibiting some of the characteristics of both (see Table 1, Fearn 1988) so that we restrict attention to $m = 2$. In Figures 2.7 and 2.8 the full line represents the 'expected' modes, i.e., those that approach the perfectly conducting and insulating solutions in the limits $\eta_i \to 0$ and $\eta_i \to \infty$ respectively.

However, at some η_i a second local minimum develops (of Λ with respect to n) which becomes the global minimum as η_i is further decreased (this curve, the dashed line, is only plotted when it becomes the global minimum; this should not be interpreted as modes converging or vanishing). Figure 2.9 clearly illustrates this point which shows that the global minimum of Λ over n is an order of magnitude lower for very small but finite η_i modes than for the perfectly conducting case.

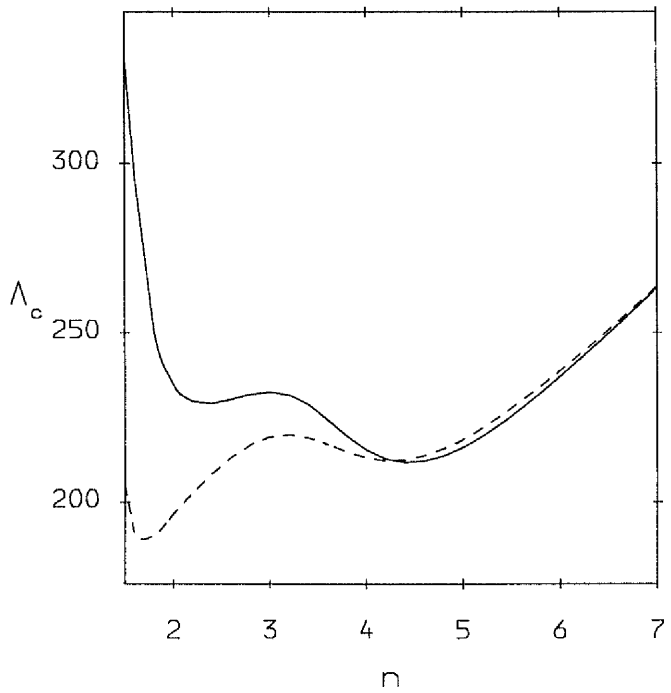

Figure 2.6 Critical Elsasser number versus n for the ideal modes of Figure 2.5. The lines are $\eta_i = 0.1$ (full line) and $\eta_i = 1$ (dashed line) illustrating how the global minimum 'jumps' from one local minimum to another.

The frequency of these modes, corresponding to Figure 2.7, is plotted in Figure 2.8. For the 'new' slow modes the frequency scales with η_i and is $O(\eta_i/\Lambda)$ so that $\omega_c \to 0$ as $\eta_i \to 0$. This is discussed further in §2.2.9. The frequency of the faster modes remains $O(1)$. In both cases the frequency is negative, i.e., the modes travel westward. Figures 2.10 and 2.11 illustrate eigenfunctions for the expected and low frequency instabilities. The lower middle and bottom parts of Figure 2.10 are eigenfunctions at $\eta_i = 10^{-3}$ for both minima of Figure 2.9. The former matches closely the eigenfunction for a perfectly conducting boundary and is confined to the outer core but the latter low frequency solution occupies the whole core. This behaviour is explained by differing timescales; the timescale of the slow (low frequency) mode is the diffusive timescale of the inner core so that on this timescale it can penetrate into the inner core (this is discussed further in

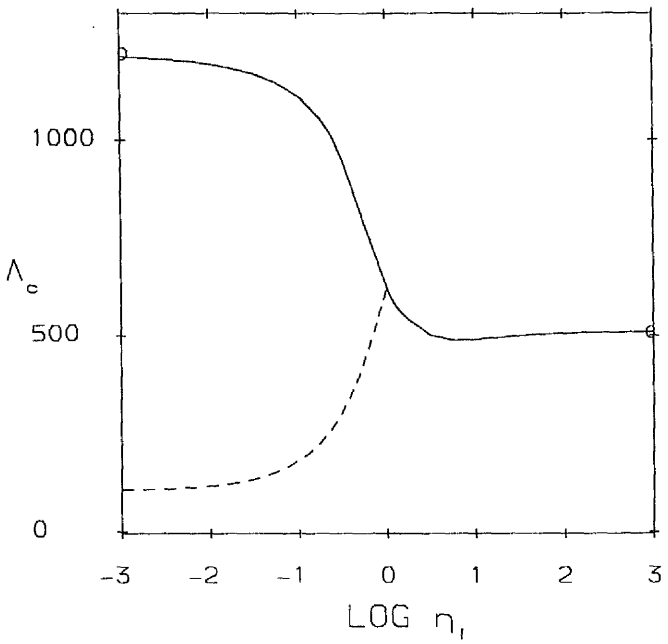

Figure 2.7 Critical Elsasser number versus $\log_{10}\eta_i$ for ideal modes of field (2.37) with $m = 2, \beta = 1, \alpha = 0$.

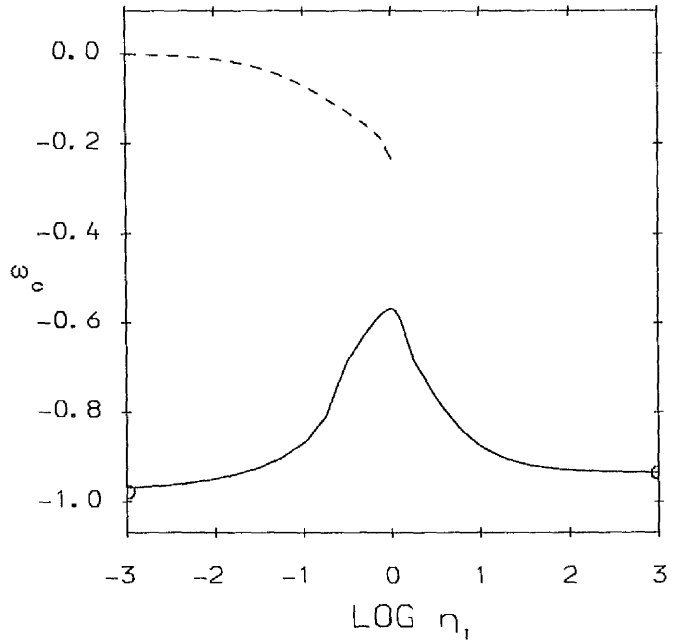

Figure 2.8 Graph of ω_c versus η_i for the ideal modes of Figure 2.7.

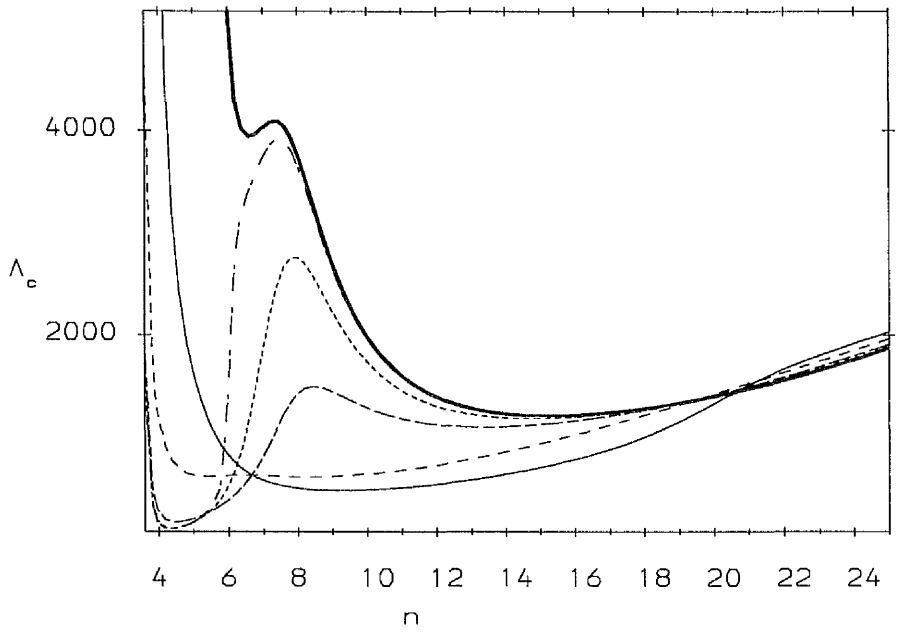

Figure 2.9 Critical Elsasser number versus n for the ideal modes of Figure 2.7. The curves are $\eta_i = 10$, (thin full line), 1, (dashed), 10^{-1}, (long-short dash), 10^{-2}, (short dash), 10^{-3}, (dash dot) and with perfectly conducting inner boundary (thick full).

§2.2.9) while the faster (higher frequency) mode operating on a shorter timescale can only penetrate a very short distance (see Figure 2.2 or 2.3).

The critical parameters for these two modes [Figure 2.10 & 2.11 (lower middle) and Figure 2.10 & 2.11 (bottom)] together with the cases $\eta_i = 10^3$ and $\eta_i = 1$, are

$$\Lambda_c = 508, \quad n_c = 9.61, \quad \omega_c = -0.934, \quad \eta_i = 10^3, \quad (2.48a)$$

$$\Lambda_c = 623, \quad n_c = 8.25, \quad \omega_c = -0.568, \quad \eta_i = 1, \quad (2.48b)$$

$$\Lambda_c = 1213, \quad n_c = 15.1, \quad \omega_c = -0.969, \quad \eta_i = 10^{-3}, \quad (2.48c)$$

$$\Lambda_c = 106, \quad n_c = 4.30, \quad \omega_c = -0.131 \times 10^{-2}, \quad \eta_i = 10^{-3}, \quad (2.48d)$$

illustrating the dramatic decrease in field strength required for these new low frequency instabilities. The unrealistically large value of Λ_c in (2.48c) is attributable

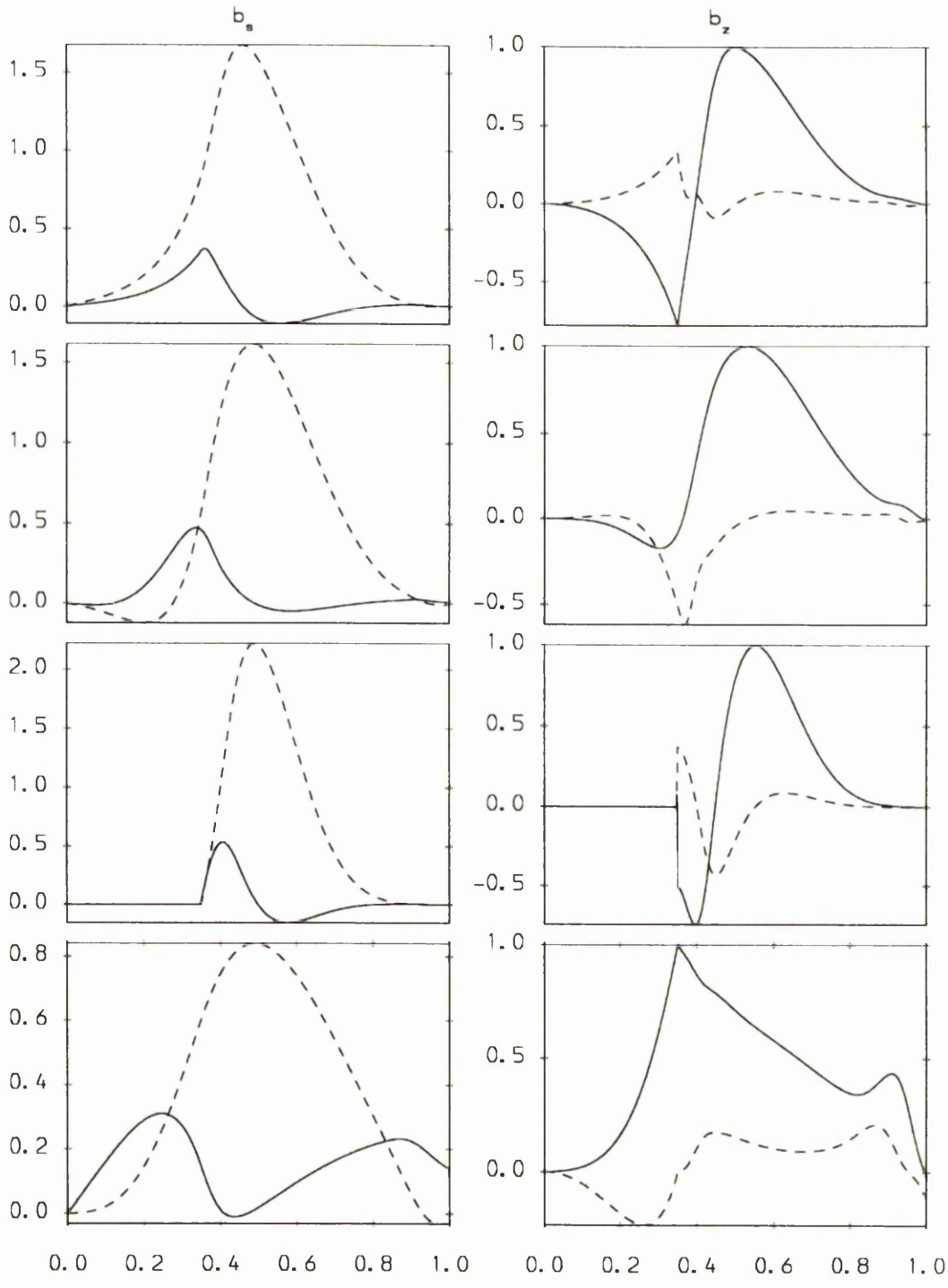

Figure 2.10 Eigenfunctions for b_s, b_z of ideal modes of Figure 2.7 with, from top to bottom, $\eta_i = 10^3, 1, 10^{-3}$ (full line Figure 2.7), 10^{-3} (dashed line Figure 2.7). Critical parameters are in (2.48).

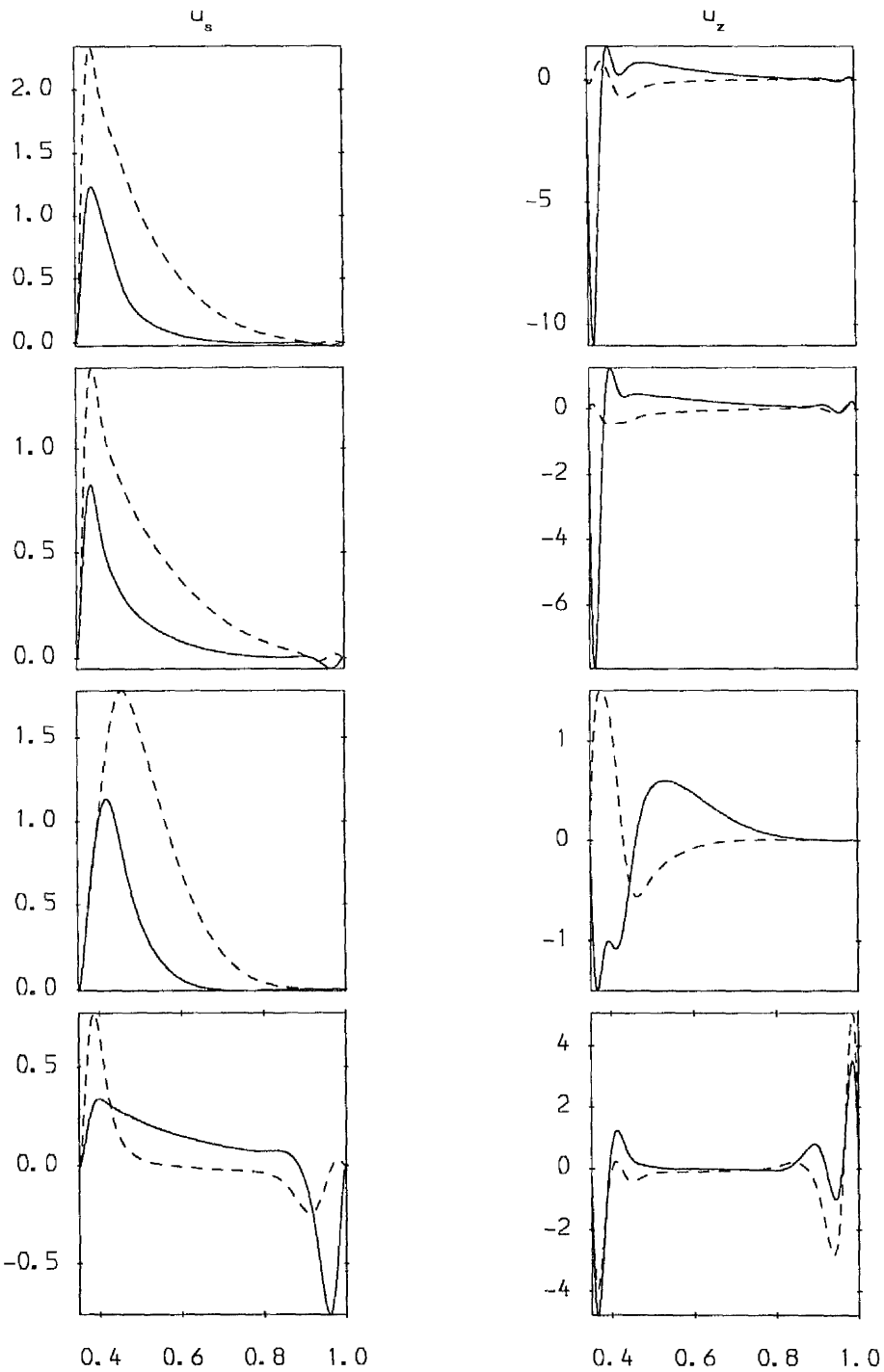

Figure 2.11 As in Figure 2.10 but for eigenfunctions of u_s, u_z.

to the choice of $m = 2$.

2.3.7 Resistive Instability With A Critical Level ($\alpha = 0$)

Typically, resistive instability requires significantly lower field strengths than an ideal instability and although less influenced by the geometry of the container there are features which depend on the particular basic state. In the case of field (2.37) with $\alpha = 0$, $\Lambda \to 0$ as $n \to 0$ so that we choose n to be fixed at $n = 3$ (see Fearn 1988).

The interesting behaviour again occurs when $\eta_i < 1$. Figures 2.12 and 2.13 plot the critical Elsasser number and frequency against η_i for resistive modes of field (2.37) with $\alpha = 0$. The dashed line in Figure 2.12 encloses a region of low frequency instability occupying the whole core in a similar way to that described above but clearly resistive in nature since the growth rate p vanishes when $\Lambda \to \infty$. The full line converges to the higher frequency modes of an insulating or perfectly conducting boundary indicated by the circles on the vertical axes. The rapidly changing part of this line is magnified in Figure 2.14 showing the line is a smooth one and these high frequency modes have three critical states in a very narrow range of η_i. It should be made clear that while the full and broken lines cross, the eigenvalues and eigenfunctions are in fact very different. The behaviour $\omega_c \to 0$ as $\eta_i \to 0$ is clearly illustrated in Figure 2.13 and discussed further in §2.3.9.

To more clearly illustrate what is going on, growth rate versus Λ curves are shown in Figure 2.15. These can be understood in relation to Figure 2.12 by imagining vertical lines of constant η_i in Figure 2.12. In Figure 2.15 both the full line and dash-dot lines are plots with $\eta_i = 2 \times 10^{-2}$ demonstrating the existence of three critical states when η_i is small. The dash-dot line, cutting $p = 0$ twice in Figure 2.15 (this is more easily seen in Figure 2.16 in which part of Figure 2.15 is magnified) corresponds to the dashed line of Figure 2.12 while the full line, cutting $p = 0$ only once in Figure 2.15 (at higher Λ $p \to 0$ for this mode) corresponds to the full line of Figure 2.12. The remaining three lines in Figure 2.15 correspond

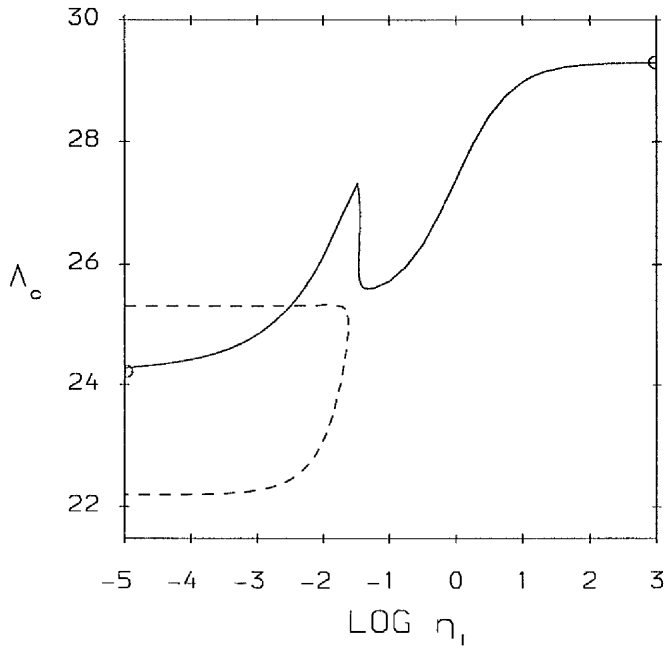

Figure 2.12 Critical Elsasser number versus $\log_{10}\eta_i$ for resistive modes of field (2.37) with $m = 2, \beta = 1, \alpha = 0$.

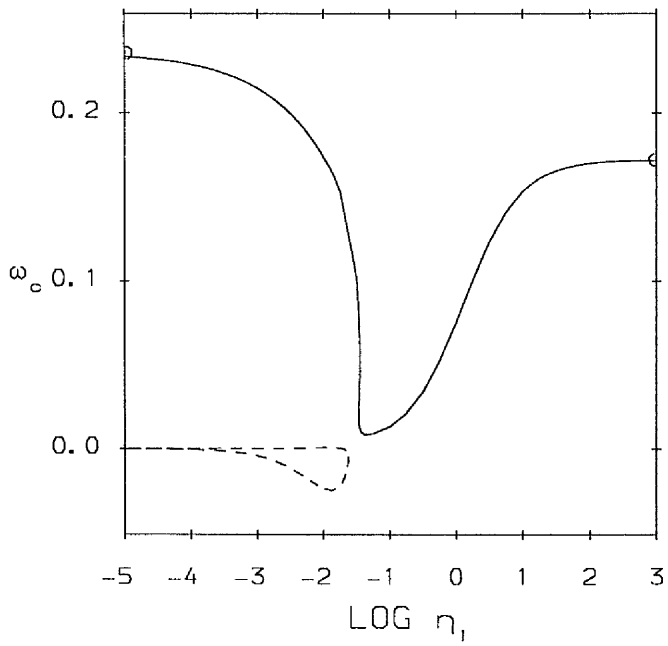

Figure 2.13 Graph of ω_c versus η_i for the resistive modes of Figure 2.12.

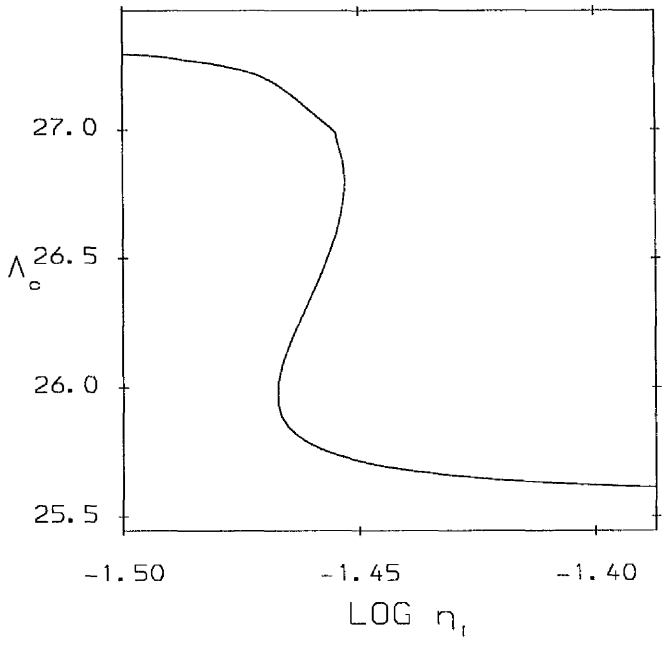

Figure 2.14 Blow up of rapidly changing part of full line of Figure 2.12 showing the curve is a smooth one.

to the full line of Figure 2.12; the short dashed line ($\eta_i = 3 \times 10^{-2}$) lies just to the left of the region magnified in Figure 2.14 cutting $p = 0$ once, the long-dash short-dash line ($\eta_i = 3.5 \times 10^{-2}$) passes through this region and cuts $p = 0$ three times while the dashed line, ($\eta_i = 4 \times 10^{-2}$), passes to the right of this region and cuts $p = 0$ once. In contrast to the ideal modes however, there is very little difference in field strengths between slow and fast modes as shown by these results with $\eta_i = 10^{-3}$

$$\Lambda_c = 25.3, \qquad \omega_c = 0.870 \times 10^{-4}, \tag{2.49a}$$

$$\Lambda_c = 22.3, \qquad \omega_c = -0.428 \times 10^{-2}, \tag{2.49b}$$

$$\Lambda_c = 24.8, \qquad \omega_c = 0.215, \tag{2.49c}$$

where (2.49a) and (2.49b) correspond to the same mode (full line of Figure 2.12). In general, Λ_c for these modes is not strongly dependent on η_i, critical parameters at $\eta_i = 10^3$ and 1 respectively given by

$$\Lambda_c = 29.3, \qquad \omega_c = 0.172, \tag{2.50a}$$

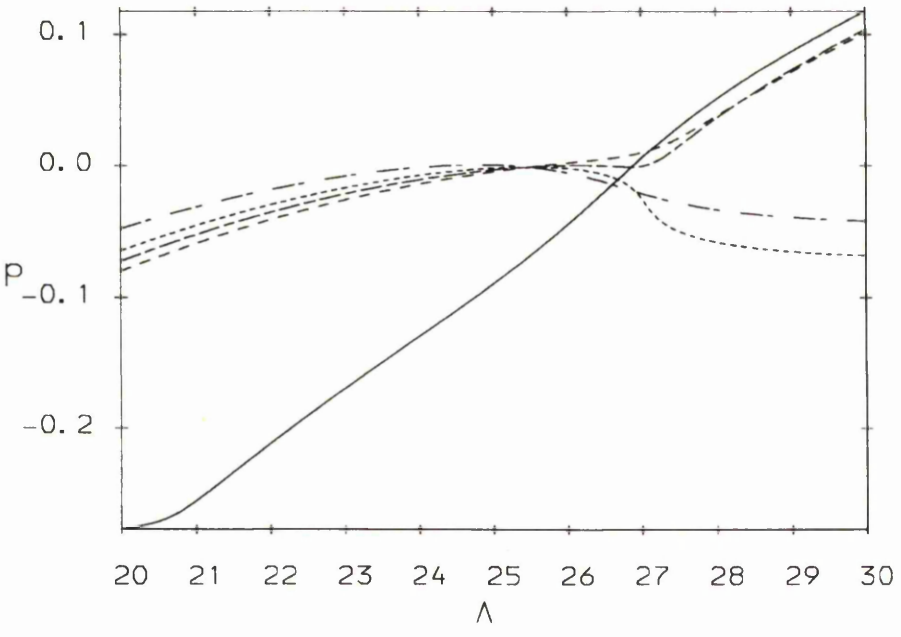

Figure 2.15 Growth rate versus Λ for resistive modes of field (2.37) with $\alpha = 0, \beta = 1, m = 2$. The curves are $\eta_i = 2 \times 10^{-2}$ (dash-dot and full) 3×10^{-2} (short dash) 3.5×10^{-2} (long-short dash) and 4×10^{-2} (dashed).

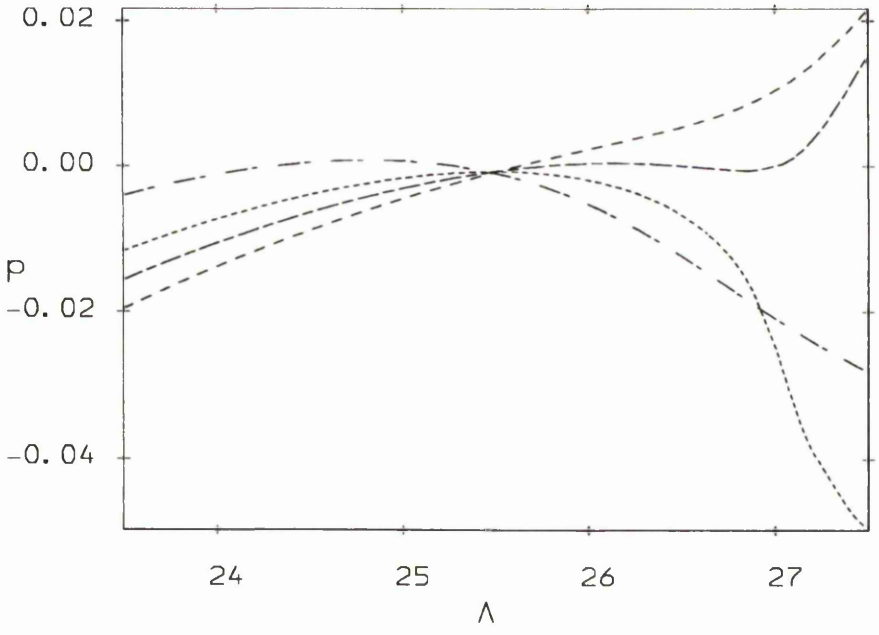

Figure 2.16 Magnified part of Figure 2.15 showing where lines cross $p = 0$ (the full line of Figure 2.15 has been omitted).

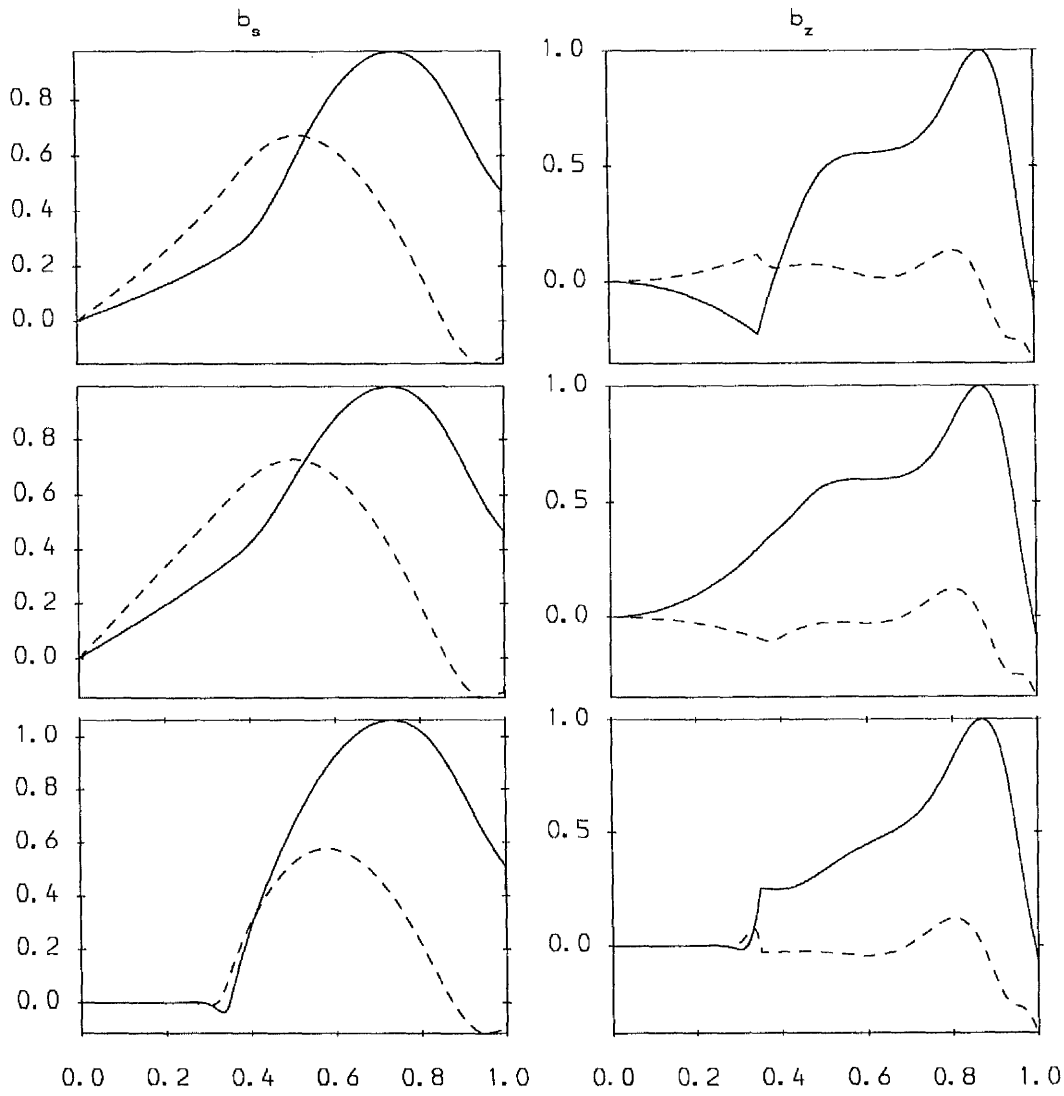

Figure 2.17 Eigenfunctions for b_s, b_z of resistive modes of Figure 2.12 with, from top to bottom, $\eta_i = 10^3, 1, 10^{-3}$ (full line Figure 2.12). Critical parameters are in (2.50a), (2.50b) and (2.49c) respectively.

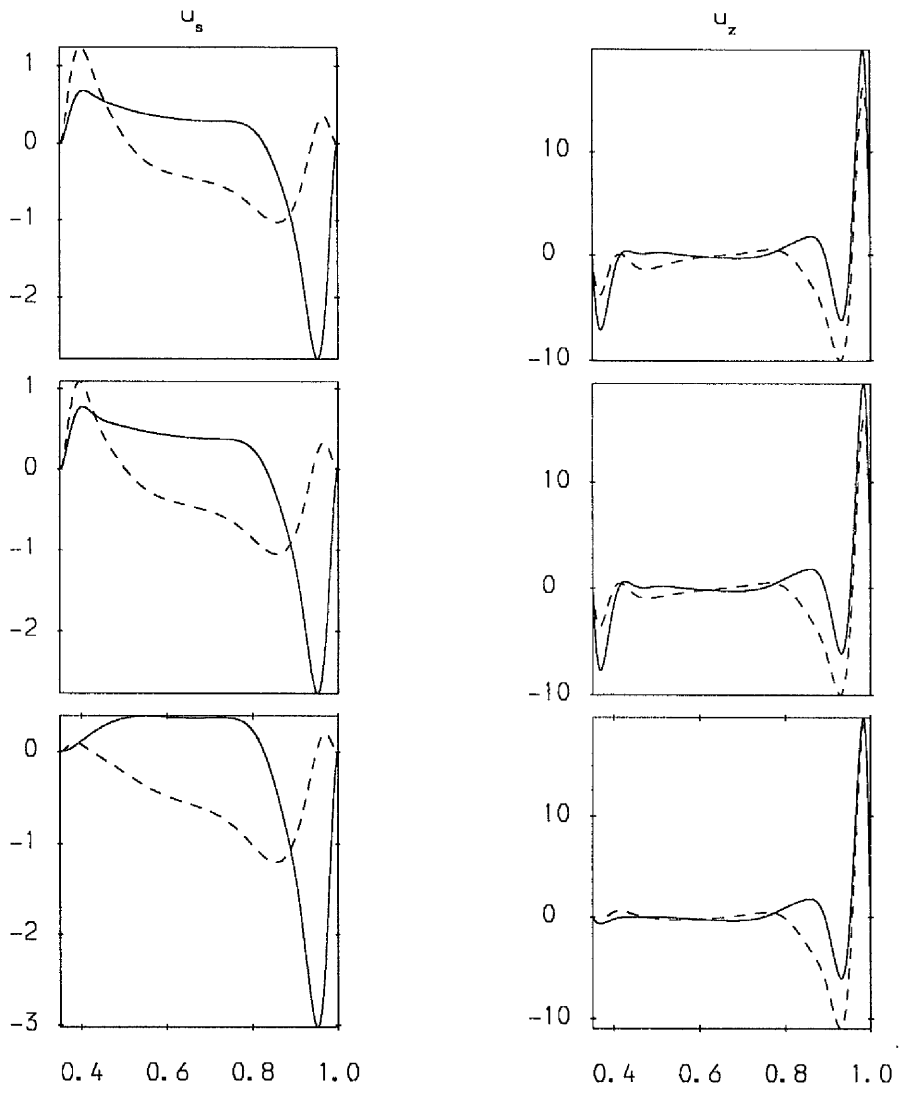

Figure 2.18 As in Figure 2.17 but for eigenfunctions of u_s, u_z.

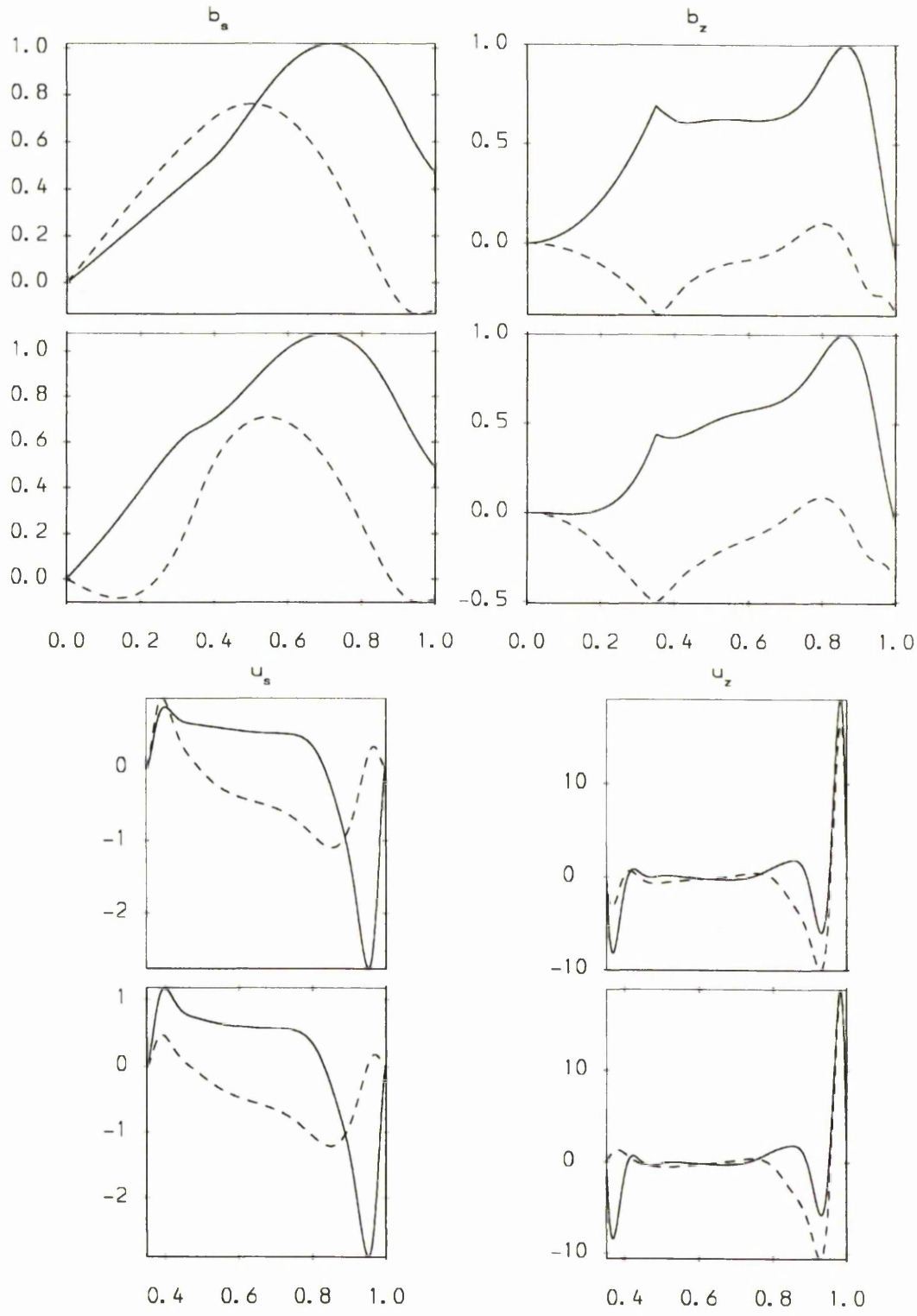

Figure 2.19 As in Figure 2.17 & 2.18 but for resistive slow modes. Critical parameters are given in (2.49a) (1st and 3rd Figures) and (2.49b) (2nd and 4th).

$$\Lambda_c = 27.4, \qquad \omega_c = 0.075, \tag{2.50b}$$

Eigenfunctions of the modes in (2.49) and (2.50) are illustrated in Figures 2.17–2.19 showing again the deeper penetration of the slow modes at very low η_i permitted by their longer timescale.

2.3.8 Resistive Instability Without A Critical Level ($\alpha > 0$)

Fearn and Weiglhofer (1992) investigated resistive instability of the field (2.37) in a cylindrical geometry and found that with insulating boundaries the instability persisted as α was increased through zero up to $\alpha \approx 0.2$, i.e., even in the absence of a critical level. However they did not find this behaviour with both boundaries perfectly conducting. To investigate this further we wish to choose the parameters such that the field has no zero within the outer core. The conditions for this instability are not yet fully understood but Fearn and Kuang (1993) have gone some way towards this and found the instability was absent unless $B_0''/B_0 < 0$ (the prime, in our case, means derivative with respect to s) near an insulating boundary. To allow us to satisfy this condition at both boundaries and therefore permit investigation of these modes with an insulating or perfectly conducting outer boundary we increase the inner radius to $s_{ib} = 0.7$ and take $\alpha = 0.5$ and $\beta = 2$.

It might be anticipated that with a perfectly conducting outer boundary Λ_c would increase as η_i is decreased until the instability vanishes. However Figures 2.20 and 2.21 show that instability continues to exist as the conductivity of the inner core is increased. Indeed Λ_c decreased to around a third of its value at large η_i . Figure 2.22 shows that the modes are evolving into slow modes of the kind we have already seen in §2.2.6 and §2.2.7. Typical eigenfunctions are illustrated in Figures 2.22–2.23 with critical parameters

$$\Lambda_c = 33.99, \qquad \omega_c = -1.950, \qquad \eta_i = 10^3, \tag{2.51a}$$

$$\Lambda_c = 12.88, \qquad \omega_c = -0.679, \qquad \eta_i = 1, \tag{2.51b}$$

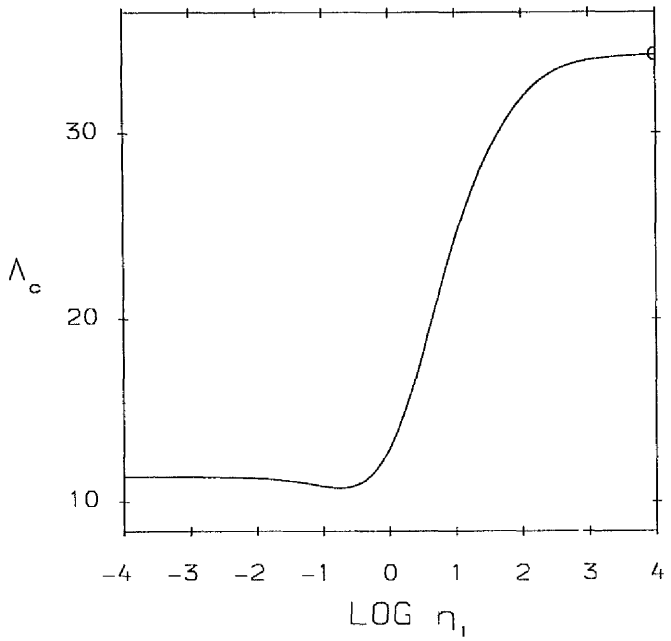

Figure 2.20 Critical Elsasser number versus $\log_{10}\eta_i$ for resistive modes of field 2.37 with $m = 1, n = 1, \beta = 2, \alpha = 0.5, s_{ib} = 0.7$ and a perfectly conducting outer boundary.

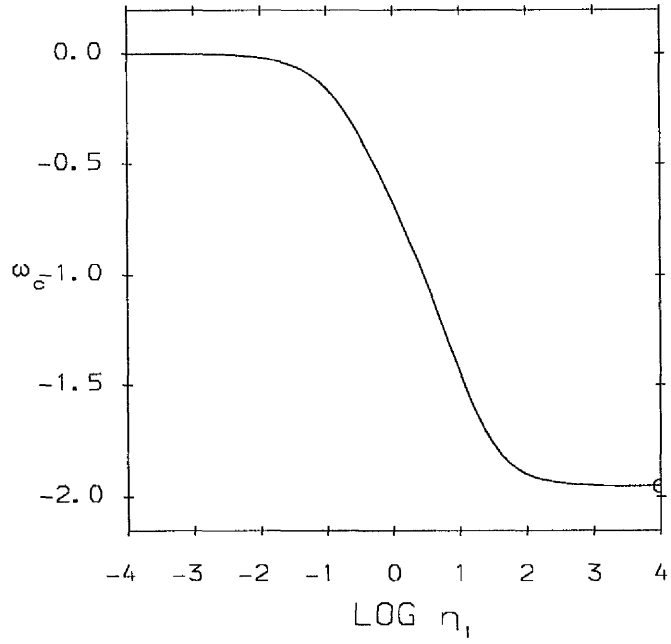

Figure 2.21 Frequency versus $\log_{10}\eta_i$ for modes of Figure 2.20.

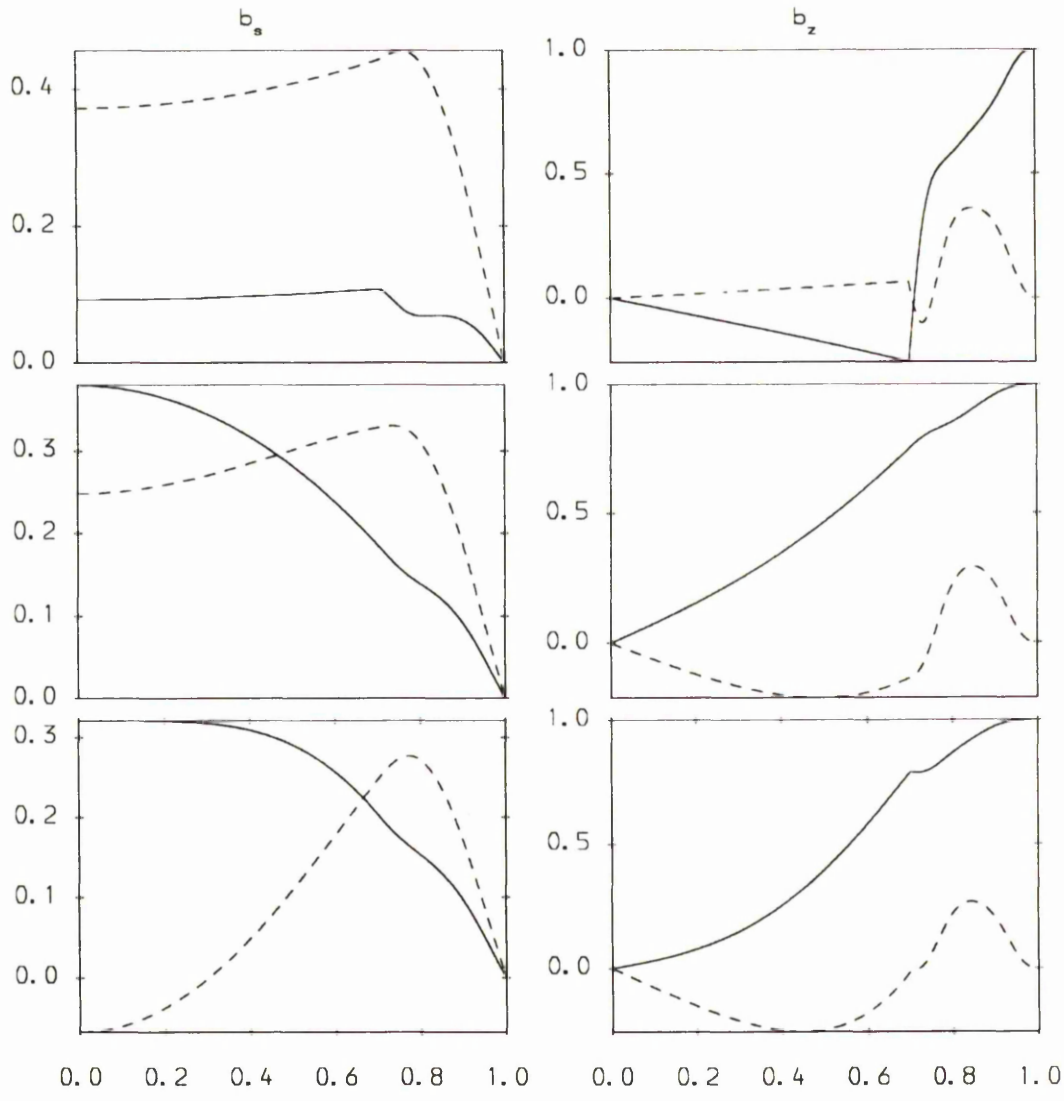

Figure 2.22 Eigenfunctions b_s, b_z for resistive modes of Figure 2.20 with, from top to bottom, $\eta_i = 10^3, 1, 10^{-3}$. Critical parameters are given in (2.51a)–(2.51c) respectively.

$$\Lambda_c = 11.34, \qquad \omega_c = -0.186 \times 10^{-2}, \qquad \eta_i = 10^{-3}, \tag{2.51c}$$

In each case $m = 1$ and $n = 1$.

Nearly identical behaviour is found when the outer boundary is insulating. Figures 2.24–2.27 are equivalent to 2.20–2.23 but with an insulating outer boundary. Differences are quantitative rather than qualitative, the equivalent parameters

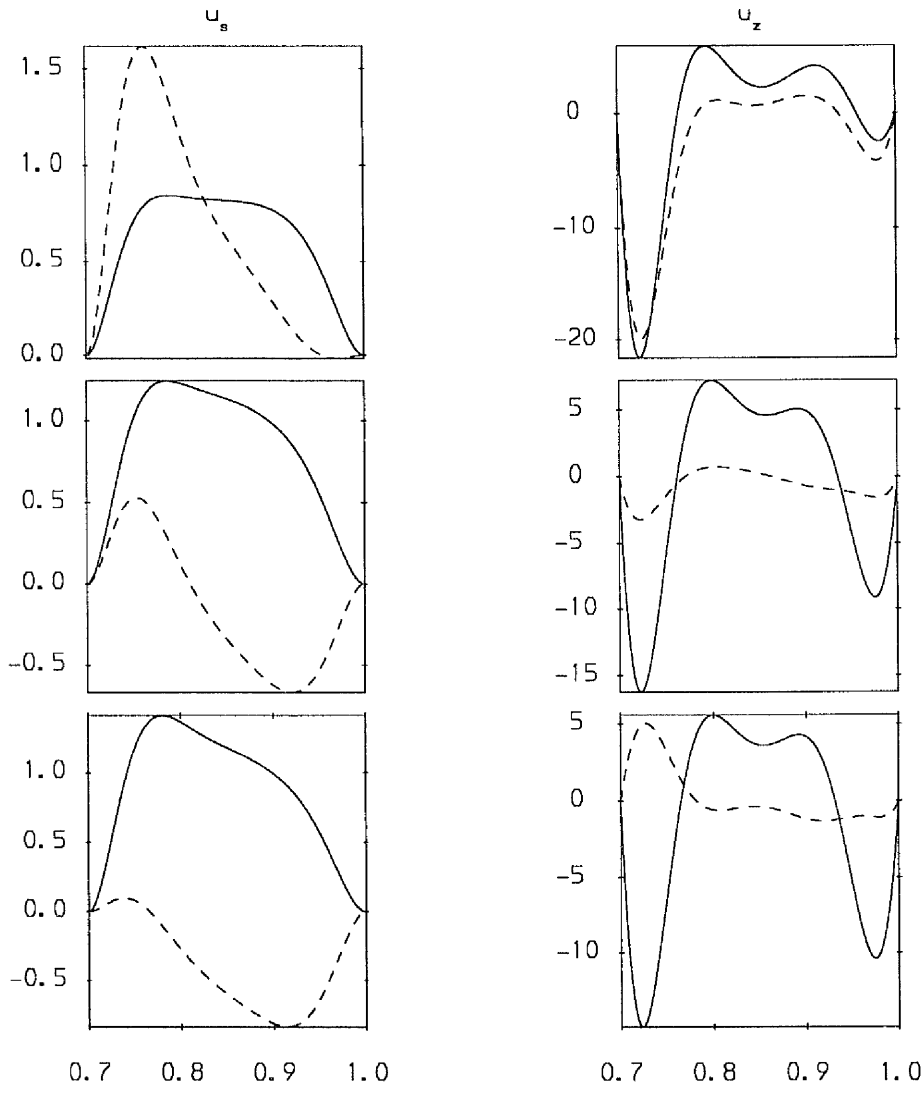

Figure 2.23 As in 2.22 but for eigenfunctions u_s, u_z.

to (2.51) being

$$\Lambda_c = 6.86, \qquad \omega_c = -1.367, \qquad \eta_i = 10^3, \tag{2.52a}$$

$$\Lambda_c = 4.21, \qquad \omega_c = -1.080, \qquad \eta_i = 1, \tag{2.52b}$$

$$\Lambda_c = 4.17, \qquad \omega_c = -0.445 \times 10^{-2}, \qquad \eta_i = 10^{-3}, \tag{2.52c}$$

This might have been expected since we chose the basic state to satisfy $B_0''/B_0 < 0$ at both boundaries. However, the instabilities we have found with

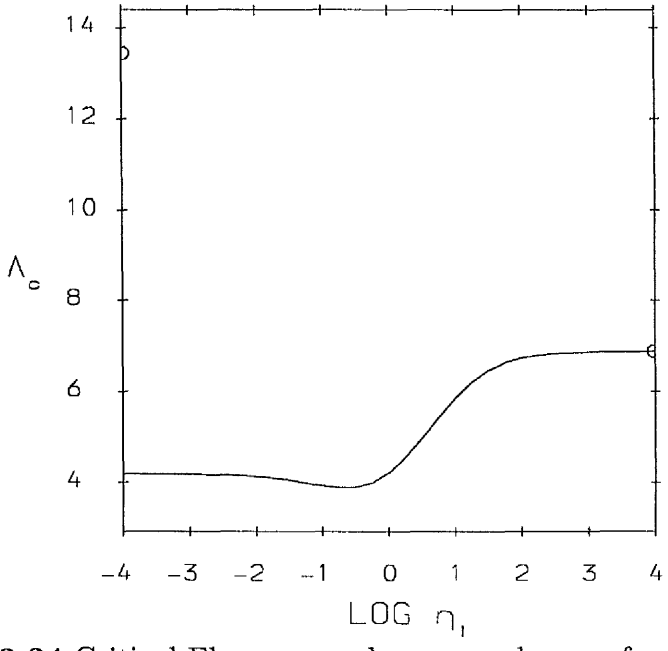

Figure 2.24 Critical Elsasser number versus $\log_{10}\eta_i$ for resistive modes of field 2.37 with $m = 1, n = 1, \beta = 2, \alpha = 0.5, s_{ib} = 0.7$ and an insulating outer boundary.

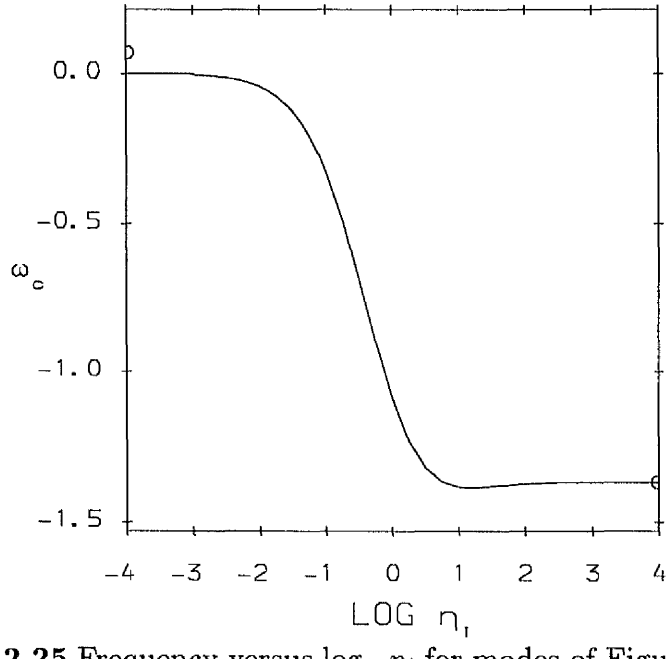

Figure 2.25 Frequency versus $\log_{10}\eta_i$ for modes of Figure 2.24.

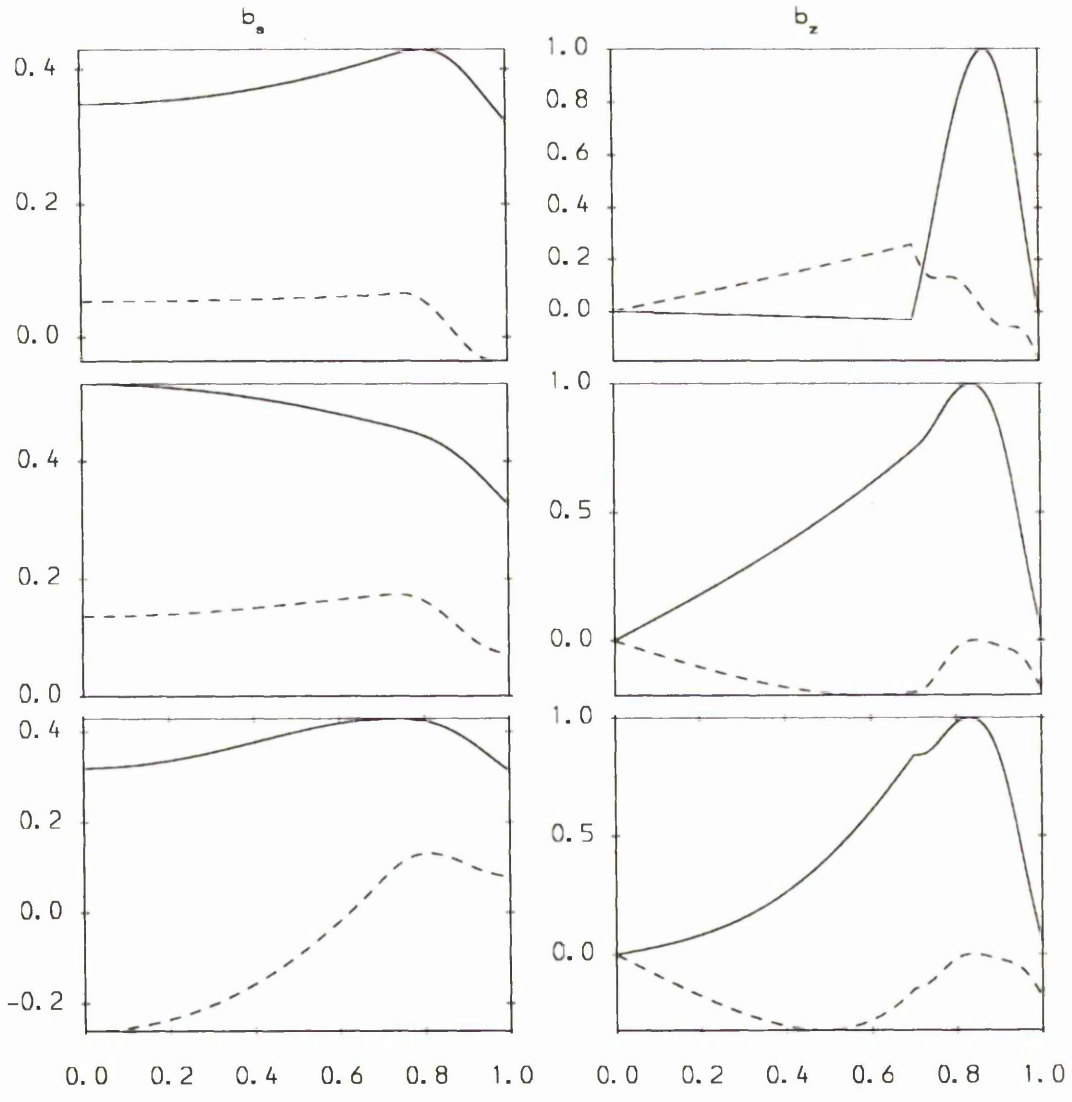

Figure 2.26 Eigenfunctions b_s, b_z for resistive modes of Figure 2.24 with from top to bottom $\eta_i = 10^3, 1, 10^{-3}$. Critical parameters are given in (2.52a)–(2.52c) respectively.

small η_i are low frequency modes that do not correspond to the case of a perfectly conducting inner boundary where Λ_c was found to be 13.43 with $\omega_c = 0.07$. The corresponding modes to this case could not be found and we have no explanation for this. We have found all the eigenvalues for this case at Λ's greater than 13.43 and only one with a positive growth rate was found, corresponding to the low frequency mode we have found with much lower Λ_c. One possible problem was

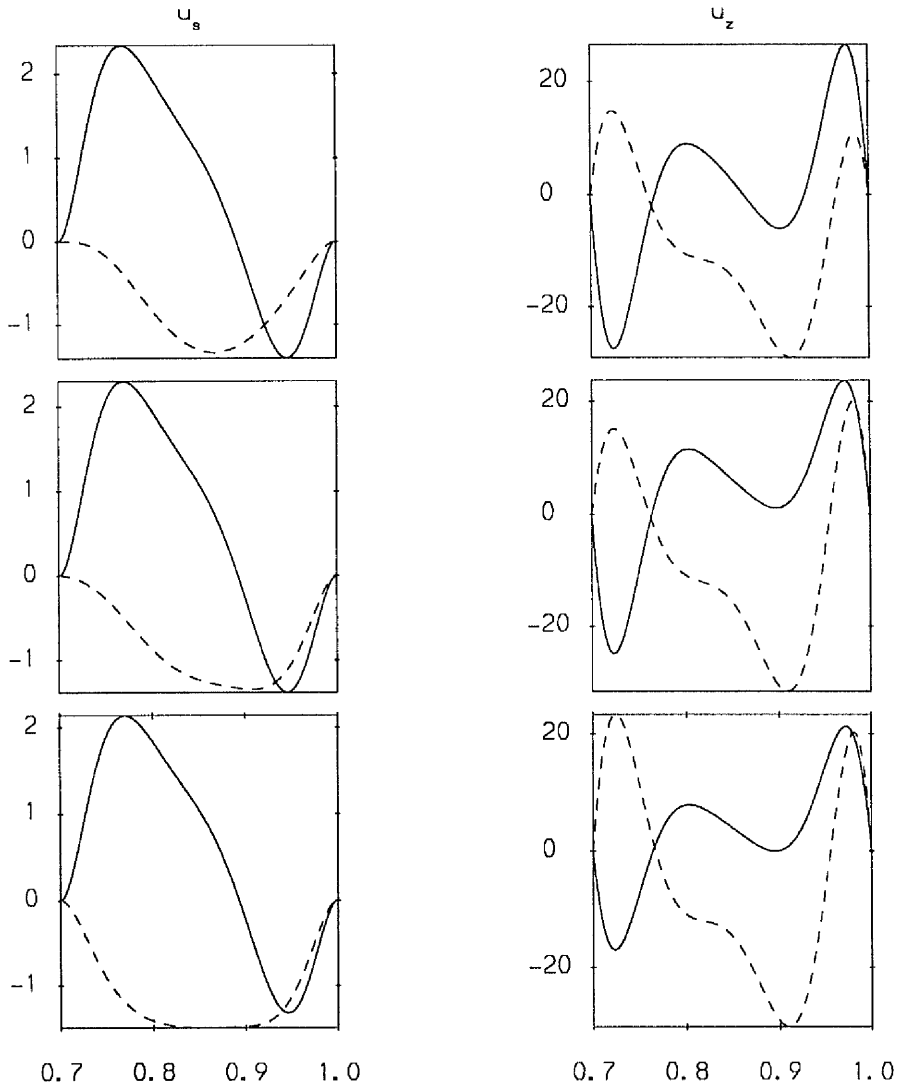

Figure 2.27 As in 2.26 but for eigenfunctions u_s, u_z.

that in the perfectly conducting case, the frequency passed through a zero close to the Ekman number we have used but we were unable to find the modes at higher or lower Ekman numbers and this remains unexplained.

2.3.9 The Low Frequency Instabilities

In §2.3.5 an analysis of the equations in the inner core was made in the limit $\eta_i \to 0$ applicable *only* if $|\omega|\Lambda >> \eta_i$ as $\eta_i \to 0$. However, we have found instability when $\eta_i \to 0$ for which this condition does not hold and we consider these modes further here.

Consider the induction equation in the inner core

$$\frac{\partial \mathbf{b}}{\partial t} = -\eta_i \Lambda^{-1} \nabla \times (\nabla \times \mathbf{b}), \tag{2.53}$$

or

$$\mathbf{b} = -\frac{i\eta}{\omega\Lambda} \nabla \times (\nabla \times \mathbf{b}). \tag{2.54}$$

If $|\omega|$ remains $O(1)$ as $\eta_i \to 0$ (our fast modes) then clearly $\mathbf{b} \to 0$ in the limit $\eta_i \to 0$ (see, for example Figure 2.2) and, with the condition (2.28) we would recover the boundary conditions (2.22) for a perfect conductor.

However, an alternative possibility is $|\omega| \to 0$ as $\eta_i \to 0$. This is found to be the case for our slow modes, both the growth rate and frequency ω_i where

$$\omega_i = \Re(\omega), \tag{2.55}$$

scaling with η_i as $\eta_i \to 0$. This is illustrated in Figures 2.29 and 2.30 in which Λ is fixed and supercritical [$|\omega_i|\Lambda$ and $|p|\Lambda$ are plotted since it is the quantity $\omega\Lambda$ which appears in the induction equation (2.54)]. The instability timescale is then the diffusion timescale of the inner core so that on this timescale significant penetration into the inner core is possible. In the limit $\eta_i = 0$ both $p = 0$ and $\omega_i = 0$, the timescale on which the instability grows will become infinitely long and no field lines will then cross into the inner core from the fluid. This explains why modes of this type are not observed when a perfectly conducting boundary condition is applied, eg. by Fearn and Weiglhofer (1992). In reality of course $\eta_i \neq 0$, the diffusion timescale of the inner core is $O(10^4)$ years, and it is conceivable that these modes will be present although probably not preferred (in Figure 2.7 the slow modes (dashed line) are preferred to the fast modes (full line) for $\eta_i \lesssim 1.0$).

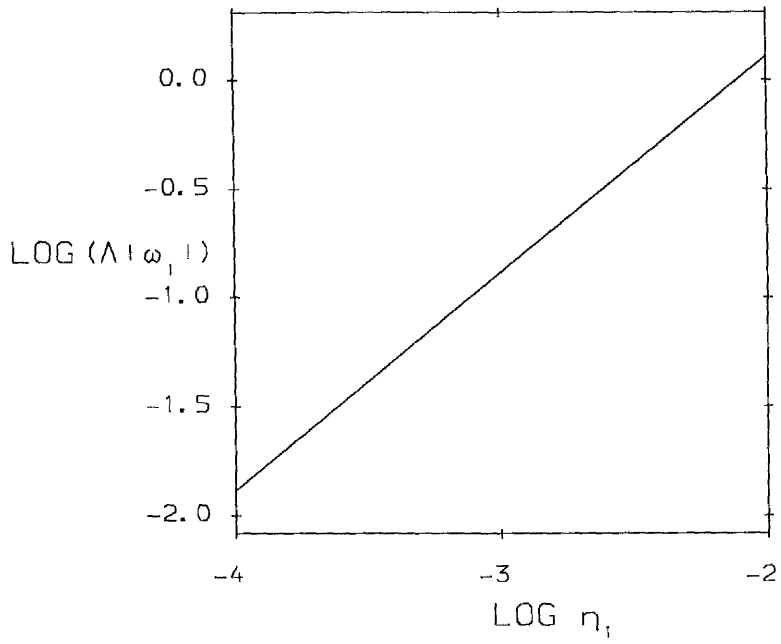

Figure 2.28 Plot of $\log_{10}|\omega_i|\Lambda$ versus $\log_{10}\eta_i$ with Λ and n fixed at $\Lambda = 200, n = 4.3$ showing how the frequency scales with η_i for slow modes. The mode is the equivalent of (2.48d) but supercritical.

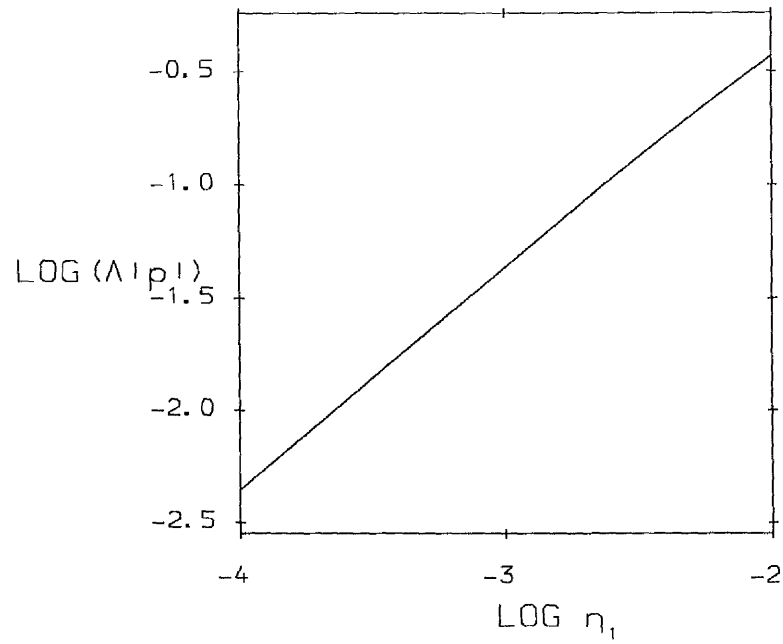

Figure 2.29 As in Figure 2.28 but for $\log_{10}|p|\Lambda$ versus $\log_{10}\eta_i$ showing how the growth rate scales with η_i for the slow modes.

2.4 CONCLUSIONS

We have investigated the effect of finite conductivity in the inner core on ideal and resistive instability of a toroidal magnetic field both of which have been established as relevant to parameter regimes appropriate to the Earth. We were able to reproduce (with one exception) solutions found with an insulating or perfectly conducting boundary condition applied at the ICB and found that in general a given basic state was most prone to magnetic instability when η_i was close to the geophysical value of $\eta \approx 1$. Some interesting and unexpected behaviour was found when $\eta_i \lesssim 1$. This took the form of low frequency modes of instability penetrating deep into the inner core at small η_i and was found to occur for both ideal and resistive instability. Both the growth rate and frequency of these low frequency modes scaled with η_i so that in the limit $\eta_i \to 0$, the perfectly conducting limit, the timescale of growth and oscillation for the modes tends to infinity and no instability would be observed. That it should occur when the field is zero at the boundaries is unsurprising. Ideal modes are concentrated where the field gradient is positive and the zero of the field is an important influence on the resistive modes. Both of these features are present at or near the ICB so the conductivity of the inner core might be expected to play a role.

In terms of the critical Elsasser number, a measure of the field strength, the difference between the 'high' and low frequency resistive modes was minimal, the big difference being in the structure of the eigenfunctions. However, for ideal modes the difference became dramatic as η_i was reduced, the lower frequency modes occurring at Λ_c's an order of magnitude lower and at smaller axial wave numbers. In this sense they are therefore the modes that would appear first although it must be noted that at more geophysical values of η_i the differences were much less marked.

It had been previously thought that resistive instability depended on the presence of a critical level. Fearn and Weiglhofer (1992) then found resistive instability with a zero of the field outwith the fluid, but not in the presence of perfectly con-

ducting boundaries. In Figure 2.20 we have found that instability persists when $\eta_i \rightarrow 0$. One worrying feature was our inability to find the equivalent mode to Fearn and Weiglhofer with an insulating outer boundary and perfectly conducting inner boundary. We have found, as yet, no reason why this should be the case. Instability was found, at lower Λ_c than expected and this difference clearly warrants further attention.

What then of the significance to the Earth? Although, as mentioned above, the low frequency mode would not be observed in the limit of perfect conductivity the Earth's inner core is not, of course, a perfect conductor and if, as thought, the conductivity of the inner core is comparable with that of the outer then it is feasible these modes have a role to play, at least in the case of ideal instabilities (see Figure 2.7). For the high frequency instability $\eta_i = 1$, the geophysically realistic value, is in most cases at, or close to, the minimum of Λ_c over η_i i.e., the most unstable case (see Figures 2.5,2.7,2.20,2.24). For these reasons the choice of perfectly conducting boundaries may not provide the fullest and most accurate picture of magnetic instabilities in the core and the inclusion of finite conductivity in the inner core in future models would be desirable and worthwhile as the results here underline the relevance of these types of instability to studies of the geomagnetic field.

CHAPTER 3

The Effect Of A Finitely Conducting Layer In The Mantle On Magnetic Instability In The Core

3.1 INTRODUCTION

Having examined the effect of inner core conductivity on magnetic instability in the core in Chapter 2, in this Chapter we turn our attention to the influence of mantle conductivity. Our model is similar to that of Chapter 2, a rapidly rotating cylindrical annulus of electrically conducting fluid permeated by a toroidal magnetic field, with the addition of a layer at the base of the mantle of arbitrary conductivity and thickness. Unless otherwise stated we take the inner core conductivity to be the same as that of the fluid and allow the mantle layer conductivity to depend on the radius.

Understanding of the conditions under which planetary magnetic fields, in particular the Earth's, become unstable has by now developed considerably. Many of the important features have been investigated, eg. field geometry and differential rotation but in the investigations of magnetic instability to date, the mantle has been treated as a perfect electrical conductor or insulator. Such an assumption is made for reasons of simplicity but in light of recent improvements in our knowledge of the structure of the Earth's interior it is appropriate to investigate the possible effects of a region of finite conductivity in the mantle.

Our increased understanding of the Earth's interior has stemmed from two sources. Firstly, improved seismic data has allowed greater resolution of features within the Earth. They have confirmed the existence of a layer at the bottom of the mantle, the D'' layer, of thickness 200–300km [Young and Lay (1987)], although considerable variations in this thickness are known to exist. Lateral heterogeneities

of the order of 10km in length have also been established from measurements of wave speed changes [Bataille and Flatté (1988)]. Secondly, advances in technology have allowed high pressure and temperature experiments to be conducted in the laboratory to mimic conditions at the solid-liquid interface of the core-mantle boundary (CMB). The molten (mainly) iron of the outer core will react rapidly with the minerals of the mantle. The products of these reactions will be lifted away from the reaction zone by mantle convection. However, this convection occurs on timescales much longer than the reaction timescales, tens or hundreds of millions of years for mantle convection compared with less than a million years for the reactions, and the relatively dense reaction products will sink back towards the CMB forming a layer at the bottom of the mantle - the D'' layer. The iron content in this region will be further enhanced by penetration of core material along the mineral grains in the mantle [see, eg., Young and Lay (1987), Jeanloz and Lay (1993)].

Estimates of the conductivity of the lower mantle derived from such experiments vary considerably; Li and Jeanloz (1987) give an upper bound of $10^{-2}\mathrm{Sm}^{-1}$ at a depth of about 1900km while Peyronneau and Poirier (1989) estimate the conductivity to be 4–40Sm^{-1} in the lower mantle, extrapolated to a lower bound of 70Sm^{-1} at the CMB. Whichever figure is correct, it is small in comparison with the more widely accepted figure of $10^{4}\mathrm{Sm}^{-1}$ for the D'' layer [Li and Jeanloz (1987)]. This appreciable conductivity (for comparison, the outer core conductivity is $\sim 5 \times 10^{5}\mathrm{Sm}^{-1}$) is due to an enriched iron content from the outer core and may vary considerably because of lateral heterogeneities. For a general review of features of the Earth's interior see Jeanloz (1990).

Here, our aim is to examine what effect this conducting layer might have on linear magnetic instability. Of primary interest are the two types of instability already discussed in some detail which have been established as being of significance to the Earth and possibly responsible for secular variation and field reversals [McFadden and Merrill (1993)]: field gradient (or ideal) instability and resistive

instability. One other type of instability, the so called 'exceptional' instability of Roberts and Loper (1979), is thought to be of more theoretical than geophysical interest since with insulating boundaries in the limit of vanishing viscosity ($E \to 0$) the critical field strength required for instability $\to \infty$ and with geophysical values of E the critical field strength far exceeds estimates of the Earth's field strength. We investigate this further with finitely conducting boundaries.

In previous investigations the mantle has been assumed to be perfectly conducting or insulating because the boundary conditions are comparatively simple and the need to solve equations in the mantle is avoided. Here we extend the model of Chapter 2 to include a layer at the base of the mantle with conductivity a function of radius. The ratio of magnetic diffusivity in the mantle layer to that of the fluid is denoted by η_m, where $\eta_m \to \infty$ corresponds to an insulating layer and $\eta_m \to 0$ to a perfectly conducting one. The inner core diffusivity is in most instances assumed to equal that of the fluid, i.e., $\eta_i = 1$. Previous studies incorporating a conducting mantle have involved layers of constant conductivity or conductivity decreasing as some power of the radius, eg. Ducruix, Courtillot and Le Mouël (1980); Benton and Whaler (1983); Drew (1993); Fearn and Proctor (1992). Diffusivity profiles similar to Fearn and Proctor (1992) are adopted in a single layer of finite conductivity; above this layer the mantle is assumed to be insulating. No attempt has been made to model the lateral heterogeneities.

The addition of a conducting layer was found to be a destabilising influence for each type of instability considered. Solutions were found to match with the insulating mantle case in the limit $\eta_m \to \infty$ but when η_m was varied, Λ_c decreased as η_m was decreased towards more geophysical values ($\eta_m \approx 50$). Not surprisingly, increasing the thickness of the layer also had the effect of decreasing Λ_c. A particularly interesting feature was the dependence of the direction of propagation of fast resistive modes, the direction changing from east to west as η_m was decreased through $\eta_m \approx 10$. The Roberts-Loper exceptional mode was investigated and found to persist when $\eta_i, \eta_m \to 0$ but with growth rate and frequency scaling

with η_i ($= \eta_m$ in this case). The behaviour of Λ_c as E and E_η [defined in (2.13)] were reduced was also found to depend on η_i and η_m. When $\eta_i, \eta_m \lesssim 1$ we find Λ_c remains finite as $E, E_\eta \to 0$ but $\Lambda_c \to \infty$ as $E, E_\eta \to 0$ otherwise.

3.2 THE MODEL

3.2.1 Governing Equations

Our model is identical to that explained in detail in Chapter 2, a cylindrical annulus of electrically conducting fluid permeated by a toroidal magnetic field $\mathbf{B}$ and rotating rapidly about the z axis with a solid inner core of uniform relative magnetic diffusivity η_i (i.e., the inner core magnetic diffusivity has been non-dimensionalised using the outer core magnetic diffusivity). To this we add an outer layer of thickness ϵ and relative magnetic diffusivity $\eta_m(s)$ (all variables here are dimensionless) at the base of the mantle, i.e., in $1 \leq s \leq 1+\epsilon$. Above this the mantle is taken to be insulating. The appropriate equations for the fluid outer core and solid inner core are given in (2.7)–(2.10). In the mantle layer the induction equation is

$$\frac{\partial \mathbf{b}}{\partial t} = -\Lambda^{-1} \nabla \times (\eta_m \nabla \times \mathbf{b}), \qquad 1 \leq s \leq 1+\epsilon \tag{3.1}$$

The linear analysis then proceeds as before. The basic state is $\mathbf{B} = B_0 \hat{\phi}$, $\mathbf{U} = \mathbf{0}$ where $B_0 = B_M s F(s)$ and F takes one of the forms (2.35) or (2.36). Unless otherwise stated the parameters E, E_η and s_{ib} take the values $E = 10^{-5}, E_\eta = 10^{-5}$ and $s_{ib} = 0.35$.

3.2.2 Boundary Conditions

The formulation of the boundary conditions applied is given in Chapter 1. Here, the conditions on the axis of rotation and at the ICB are as before. With a finitely conducting layer at the base of the mantle the condition at the CMB is now the same as that at the ICB, i.e., continuity of magnetic field and tangential electric field. Above this layer the mantle is taken to be insulating and the appropriate condition for an insulator applied at $s = 1+\epsilon$.

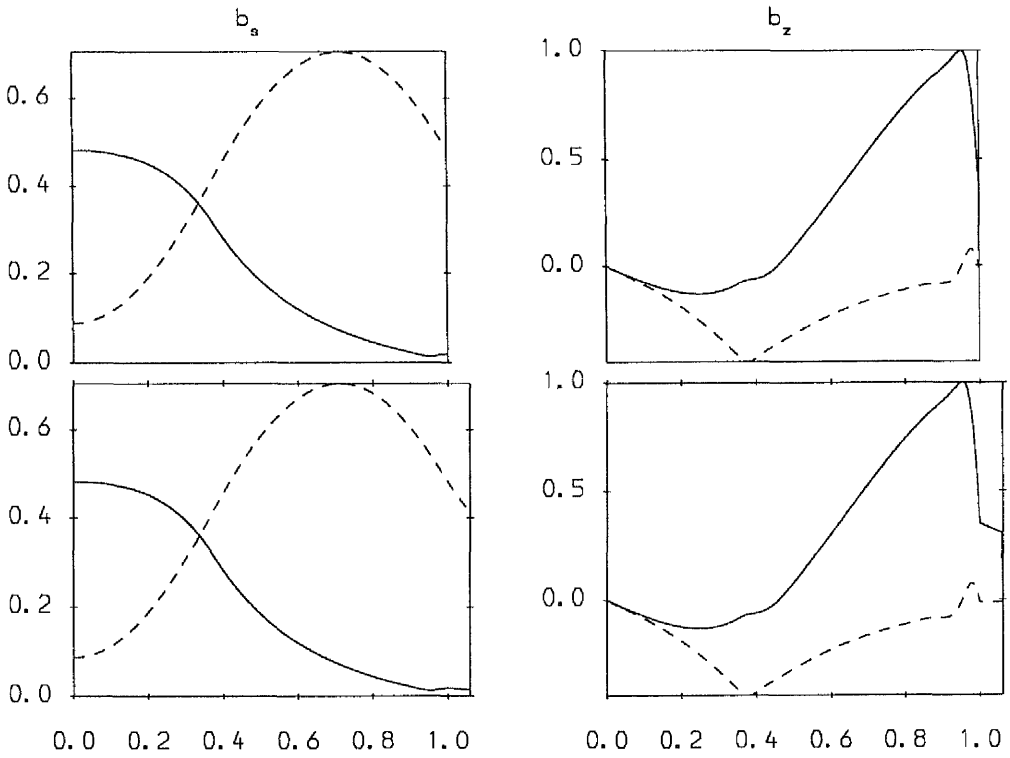

Figure 3.1 Comparison of ideal modes of field (2.36) with $m = 1, \alpha = 1$ and $\eta_i = 1$. The top figure has an insulating boundary condition applied at the CMB, the lower figure includes a conducting layer of uniform diffusivity $\eta_m = 10^4$ and depth $\epsilon = 0.06$. Critical parameters are given in (3.2a) (top) and (3.2b) (bottom).

3.3 A LAYER OF UNIFORM DIFFUSIVITY

We consider initially a layer of uniform diffusivity. Unless otherwise stated (i.e., except in §3.3.2) we take the depth to be $\epsilon = 0.06$ which in our model corresponds to $\sim 209km$, approximately the depth inferred from seismic measurements for the D'' layer and $\eta_i = 1$ which is probably appropriate to the Earth.

3.3.1 A Check On The Results

Before proceeding to investigate the effect of varying η_m we make a comparison with a result of the previous Chapter [results of which were, in turn, compared with those of Fearn (1988)]. The same code has been used, modified to incorporate

the conducting mantle layer.

Figure 3.1 is a comparison of eigenfunctions b_s, b_z of an ideal instability of the field (2.36) with $\alpha = 1$ and $m = 1$. In each case $\eta_i = 1$. The top figure has an insulating boundary condition applied at the CMB and the bottom figure a layer of uniform diffusivity $\eta_m = 10^4$ and depth $\epsilon = 0.06$. The agreement in the core is excellent and critical parameters corresponding to the top and bottom parts of Figure 3.1 are, respectively,

$$\Lambda_c = 188.11, \qquad n_c = 1.691, \qquad \omega_c = -0.1983. \tag{3.2a}$$

$$\Lambda_c = 188.05, \qquad n_c = 1.691, \qquad \omega_c = -0.1983. \tag{3.2b}$$

Having found good agreement between the $\eta_m \to \infty$ solution and an insulating boundary solution we can proceed with confidence to examine the effect of varying η_m.

3.3.2 Layer Thickness

In Chapter 2 we found that in general Λ_c decreased as η_i was decreased towards 1. We might anticipate therefore that similar behaviour would be found as η_m was decreased and that this effect would be more marked with a thicker layer. This was found to be the case. Figure 3.2 illustrates the destabilising effect of increased layer thickness on ideal instabilities of field (2.36) with $\alpha = 1$ and uniform diffusivity. For a given value of η_m, Λ_c clearly decreases as ϵ is increased, this being more marked the more conducting the layer becomes. As would be expected, Λ_c becomes independent of ϵ as $\eta_m \to \infty$.

3.3.3 Field Gradient Instability

As in Chapter 2, for field gradient, or ideal instability Λ_c is minimised over n since $\Lambda_c \to \infty$ as $n \to 0$ or $n \to \infty$. Figure 3.2 also illustrates the behaviour of Λ_c as η_m is varied for the field (2.36). The conducting layer is clearly destabilising but the effect is only significant when $\eta_m < O(10^2)$ when Λ_c changes rapidly as

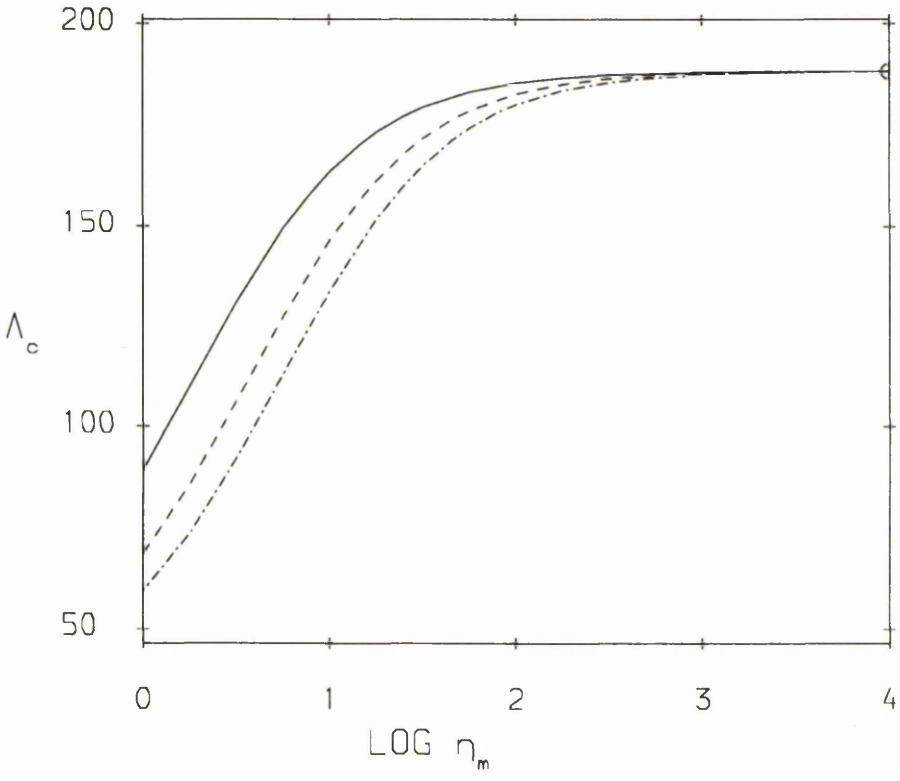

Figure 3.2 Critical Elsasser number versus $\log_{10}\eta_m$ for ideal modes of field (2.36) with $m = 1, \alpha = 1$, and $\eta_i = 1$. The lines correspond to $\epsilon = 0.03$ (full line) $\epsilon = 0.06$ (dashed line) and $\epsilon = 0.09$ (dash-dot line) [$\epsilon = 0.03$ corresponds to about 105km]. The circle on the vertical axis represents a solution with an insulating boundary condition applied at the CMB.

indicated by the following sample modes whose eigenfunctions are illustrated in Figures 3.3 and 3.4.

$$\Lambda_c = 182, \quad n_c = 1.70, \quad \omega_c = -0.201, \quad \eta_m = 10^2, \tag{3.3a}$$

$$\Lambda_c = 146, \quad n_c = 1.73, \quad \omega_c = -0.222, \quad \eta_m = 10, \tag{3.3b}$$

$$\Lambda_c = 68.6, \quad n_c = 1.79, \quad \omega_c = -0.254, \quad \eta_m = 1, \tag{3.3c}$$

Of more geophysical interest is the field (2.37). When this field was considered

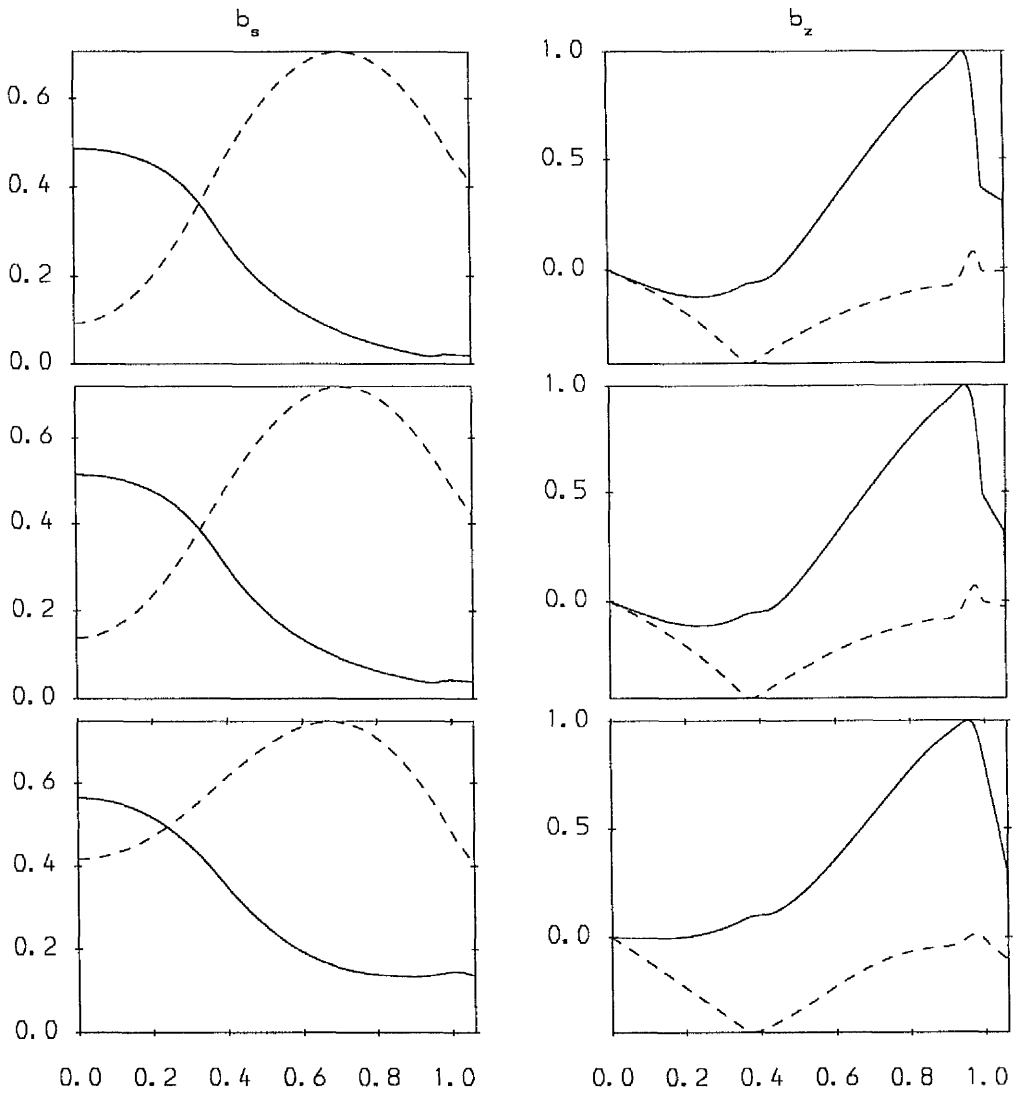

Figure 3.3 Eigenfunctions of b_s, b_z for ideal modes of field (2.36) with $m = 1, \alpha = 1$, $\eta_i = 1$ and, from top to bottom, $\eta_m = 10^2, 10, 1$. The critical parameters are given in (3.3a)–(3.3c) respectively.

in the previous Chapter it was found that as η_i was reduced, both a slow and a fast mode developed, the slow mode being preferred when η_i was sufficiently small. We have chosen $\eta_i = 0.1$ in this case so that the contrast between fast and slow modes is large and the effect of varying η_m on each may be compared. The ideal modes of this field are concentrated in the inner part of the annulus where the field gradient

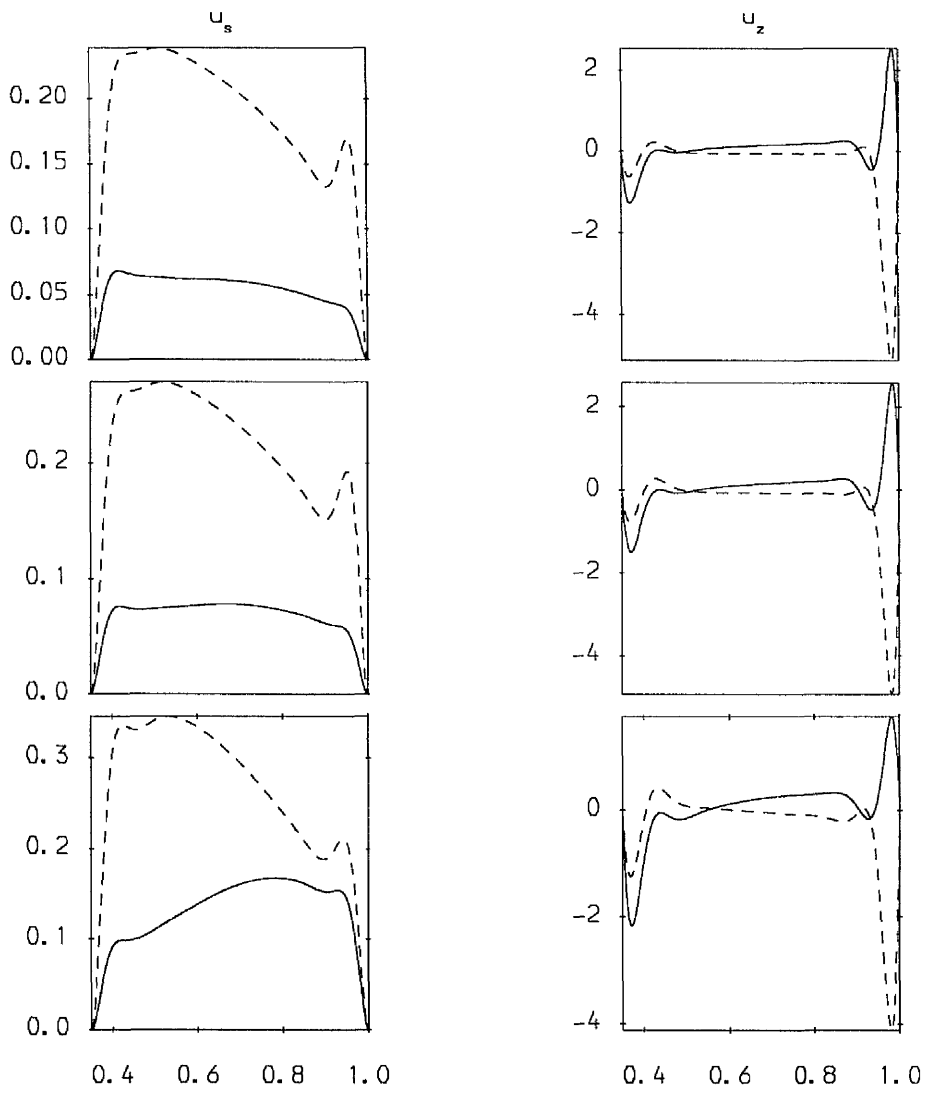

Figure 3.4 Eigenfunctions of u_s, u_z for the ideal modes of Figure 3.3.

is positive so that we might expect the influence of the mantle conductivity to be small. This is found to be the case for the fast modes where the influence of the layer conductivity was almost negligible (particularly when η_i was small). This is illustrated by the sample modes, for which $m = 2, \alpha = 0, \beta = 1$ and $\eta_i = 0.1$,

$$\Lambda_c = 1112.87, \qquad n_c = 13.34, \qquad \omega_c = -0.8678, \qquad \eta_m = 10^3, \qquad (3.4a)$$

$$\Lambda_c = 1112.86, \qquad n_c = 13.35, \qquad \omega_c = -0.8680, \qquad \eta_m = 1, \qquad (3.4b)$$

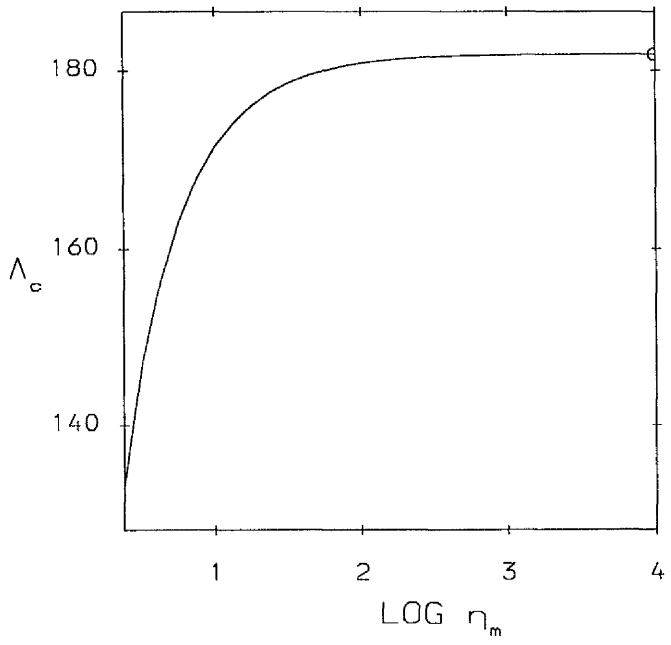

Figure 3.5 Critical Elsasser number versus $\log_{10}\eta_m$ for ideal slow modes of field (2.37) with $m = 2, \alpha = 0, \beta = 1$ and $\eta_i = 0.1$.

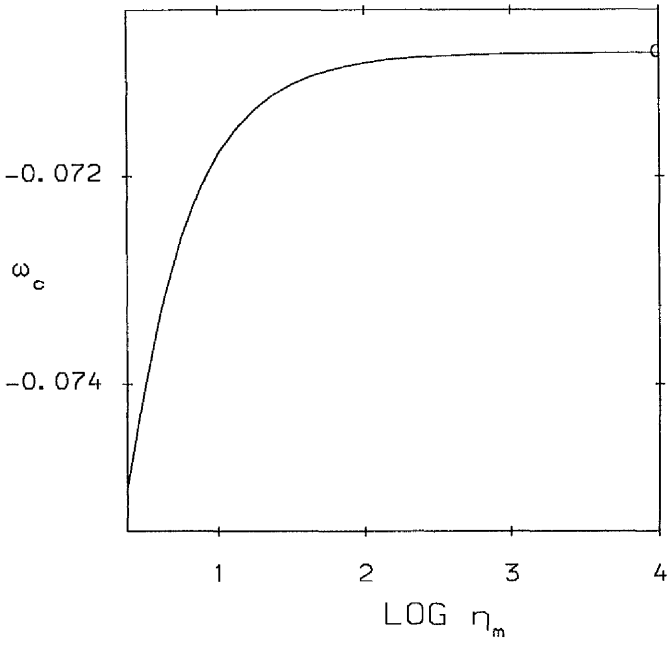

Figure 3.6 Frequency versus $\log_{10}\eta_m$ for ideal slow modes of Figure 3.5.

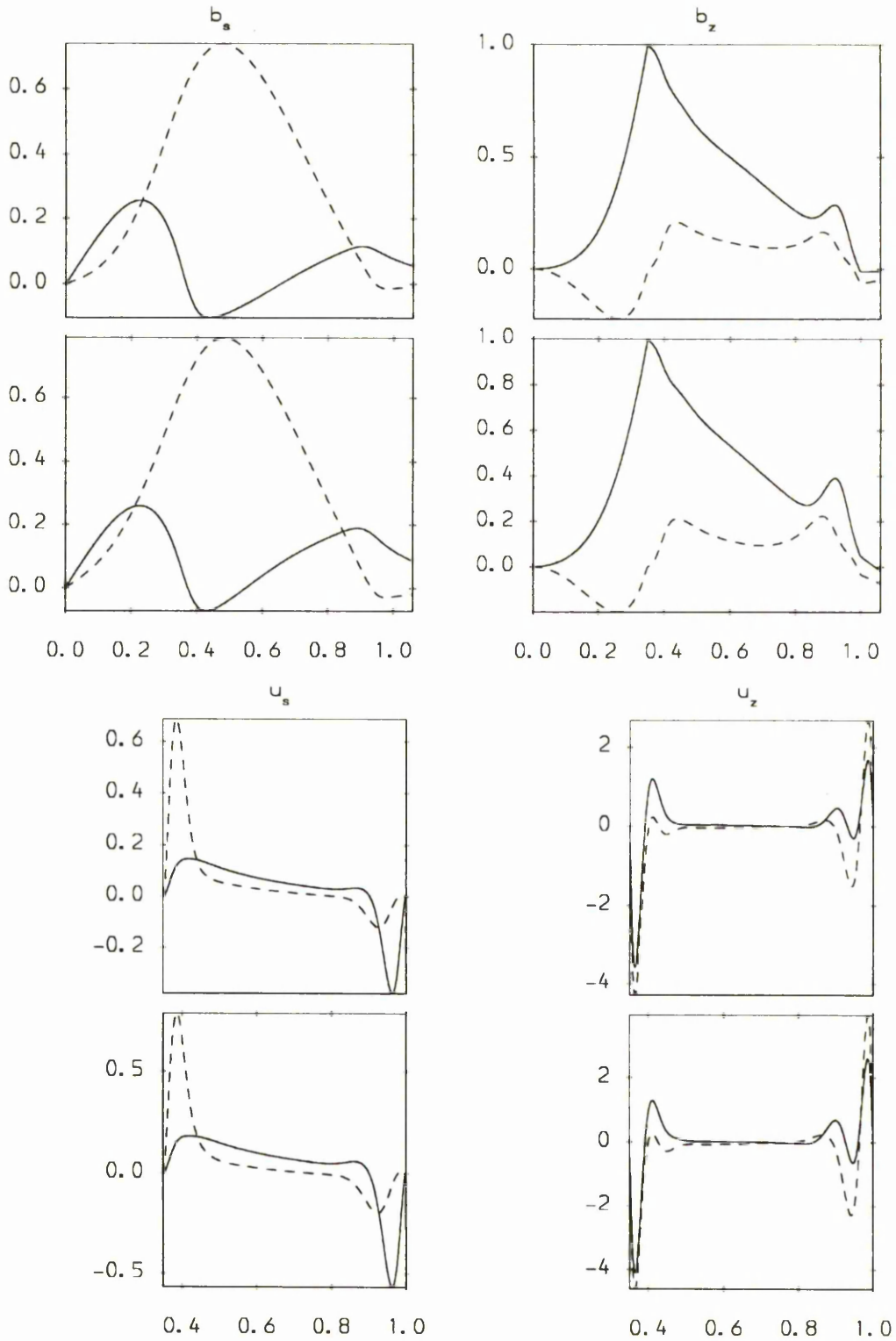

Figure 3.7 Eigenfunctions of b_s, b_z, u_s, u_z for ideal slow modes of Figure 3.5 with parameters in (3.5a) (1st and 3rd Figures.) and (3.5b) (2nd and 4th).

[for field (2.37) $m = 1$ modes show characteristics of both ideal and resistive instability [Fearn (1988)] so we have chosen $m = 2$ here with the result that Λ_c is much higher than a geophysical value]. The slow ideal modes are more strongly influenced by the conductivity of the layer, indicated in Figures 3.5 and 3.6. We have here only taken η_m as low as $10^{1/2}$ (this is still smaller than a likely value for the D'' layer in the Earth); lower than this Λ_c continues to decrease but ideal and resistive modes become harder to separate. Slow modes typically penetrate the whole of the core and this may account for a greater influence from the conductivity of the mantle. Eigenfunctions of these slow modes are shown in Figure 3.7 with critical parameters

$$\Lambda_c = 182, \quad n_c = 4.45, \quad \omega_c = -0.708 \times 10^{-1}, \quad \eta_m = 10^3, \quad (3.5a)$$

$$\Lambda_c = 147, \quad n_c = 4.43, \quad \omega_c = -0.740 \times 10^{-1}, \quad \eta_m = 10^{1/2}, \quad (3.5b)$$

3.3.4 Resistive Instabilities

The field (2.37) is also unstable to resistive instability. Although resistive instability has been found in the absence of critical levels [Fearn and Weiglhofer (1992), Fearn and Kuang (1993)] we here consider only instability in the presence of critical levels. In this case n is fixed since $\Lambda_c \to 0$ as $n \to 0$. In Chapter 2 it was found that when η_i was sufficiently small both slow and fast modes occurred for a given value of η_i with the slow modes having slightly smaller Λ_c's but a growth rate scaling with η_i.

Since $\mathbf{k}.\mathbf{B} = 0$ on the boundaries we expected to find that resistive instability was more influenced by the conductivity of the mantle layer than ideal instabilities of this field, particularly the fast modes which in the case of ideal instability are concentrated near the ICB. Our predictions were confirmed. Figures 3.8 and 3.9 show the effect of varying η_m on fast resistive modes, with eigenfunctions shown in Figure 3.10. Again a difference in Λ_c is noticeable only when $\eta_m < O(10^2)$ and the decrease is not a large one. However, a more significant effect of the conducting layer can be seen in Figure 3.9 in which ω_c changes sign, i.e., the direction of

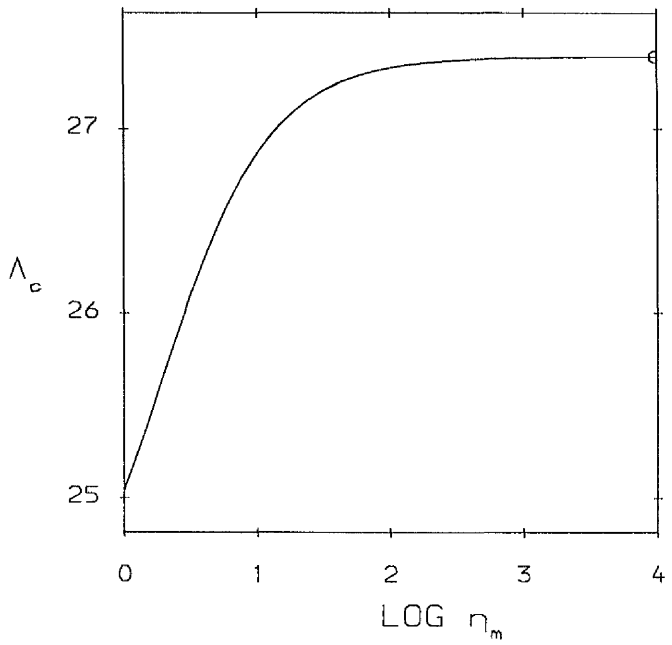

Figure 3.8 Critical Elsasser number versus $\log_{10}\eta_m$ for resistive fast modes of field (2.37) with $m = 2, \alpha = 0, \beta = 1$ and $\eta_i = 1$.

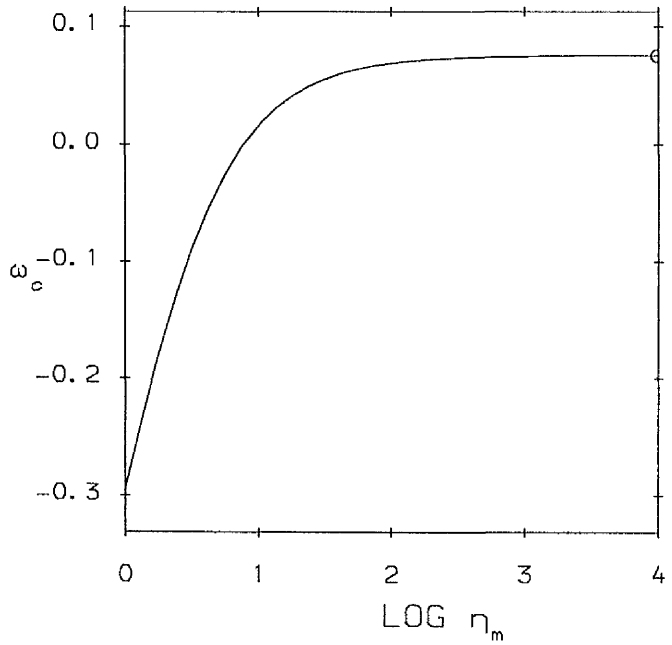

Figure 3.9 Frequency versus $\log_{10}\eta_m$ for resistive fast modes of Figure 3.8.

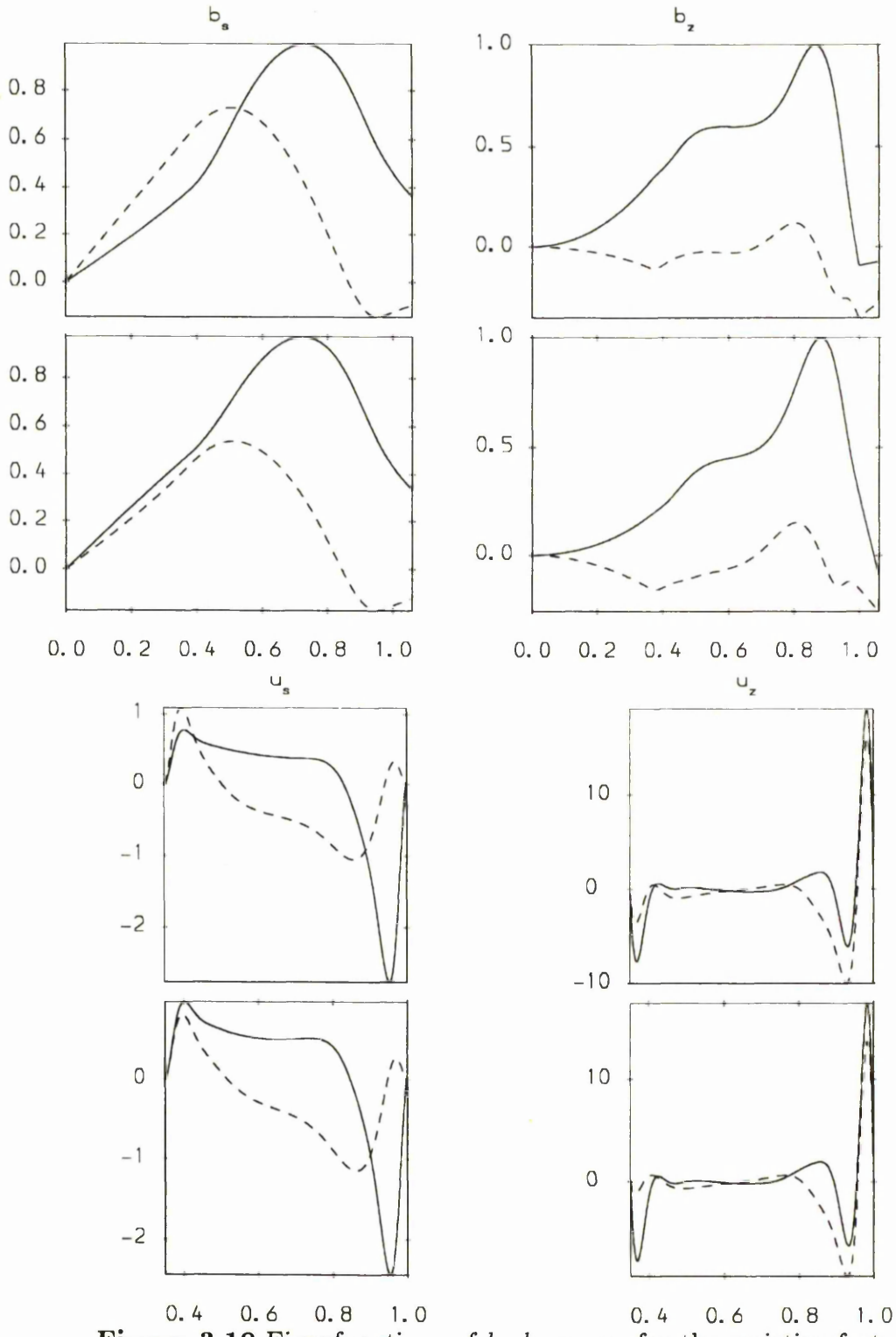

Figure 3.10 Eigenfunctions of b_s, b_z, u_s, u_z for the resistive fast modes of Figure 3.8 with $\eta_m = 10^3$, 1, $\Lambda_c = 27.4$, 25.0, $\omega_c = 0.075$, -0.294 (top and bottom Figures respectively).

propagation of these modes depends on the conductivity of the layer. This was an unexpected feature not found in the other cases considered (ideal modes, as mentioned in Chapter 1, *always* propagate westwards) and may be of importance to the observed westward drift.

For the slow resistive modes of field (2.37) the effect was a more marked one when η_m became $O(1)$. Since the resistive slow modes were found only when $\eta_i \lesssim 10^{-2}$ we have taken a mode with $\eta_i = 10^{-3}$ [mode (2.48b) of Chapter 2)] and decreased η_m. When η_m was decreased below ~ 10 a rapid change occurred, both the critical Elsasser number (plotted against η_m in Figure 3.11) and frequency (plotted in Figure 3.12) increasing with the result that the mode was no longer able to penetrate into the inner core [this can only happen if $|\omega|\Lambda = O(\eta_i)$]. Eigenfunctions are illustrated in Figures 3.13 and 3.14, the former showing the field being expelled from the inner core as η_m is decreased and the mode appears to evolve into a fast mode (cf. Figure 3.13 and bottom Figure 2.16). Critical parameters for these modes are

$$\Lambda_c = 21.8, \qquad \omega_c = -0.751 \times 10^{-2}, \qquad \eta_m = 10, \tag{3.6a}$$

$$\Lambda_c = 22.2, \qquad \omega_c = -0.211 \times 10^{-1}, \qquad \eta_m = 10^{1/2}, \tag{3.6b}$$

$$\Lambda_c = 23.5, \qquad \omega_c = -0.156, \qquad \eta_m = 1, \tag{3.6c}$$

3.3.5 Roberts-Loper Exceptional Instability

Roberts and Loper (1979) found instability of a field of the form (2.36) with $\alpha = 0$ [and therefore stable to ideal and resistive modes] present only when $-1 < \omega < 0$ and $m = 1$ and hence termed 'exceptional'. Their analysis was valid for small fluid magnetic diffusivity. They show that their instability is due to a combination of inertia and diffusivity in the narrow magnetic boundary layers present in the limit of small magnetic diffusivity. The mode was absent in the presence of perfectly conducting boundaries. Fearn (1988) investigated these modes further, adding viscosity to Roberts and Loper's analysis and found it could play a destabilising role similar to the combination of inertia and magnetic diffusivity.

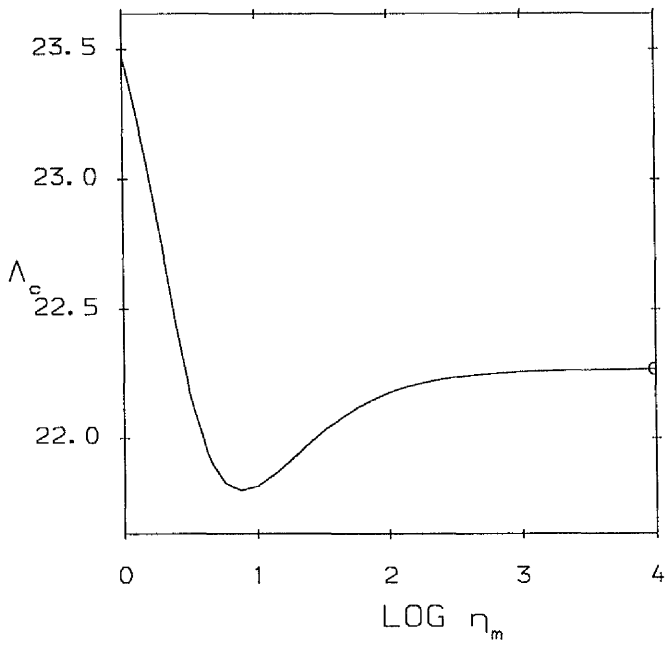

Figure 3.11 Critical Elsasser number versus $\log_{10}\eta_m$ for resistive slow modes of field (2.37) with $m = 2, \alpha = 0, \beta = 1$ and $\eta_i = 10^{-3}$.

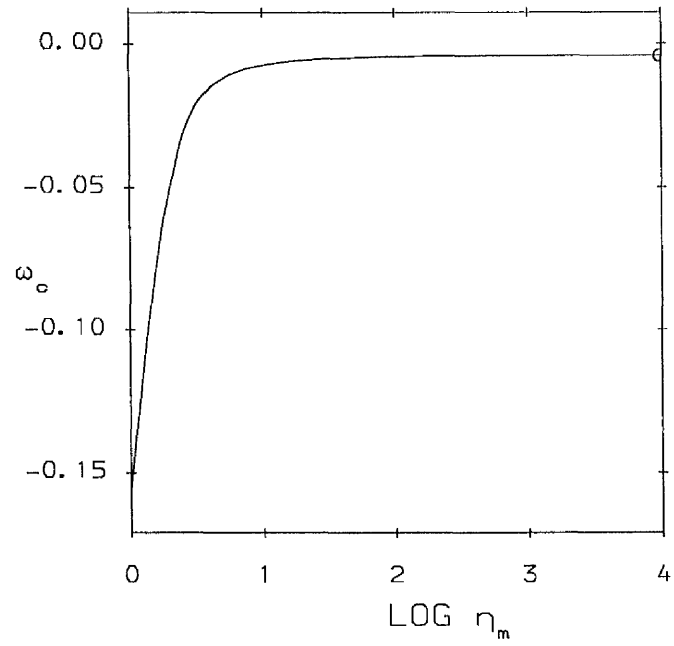

Figure 3.12 Frequency versus $\log_{10}\eta_m$ for resistive slow modes of Figure 3.11.

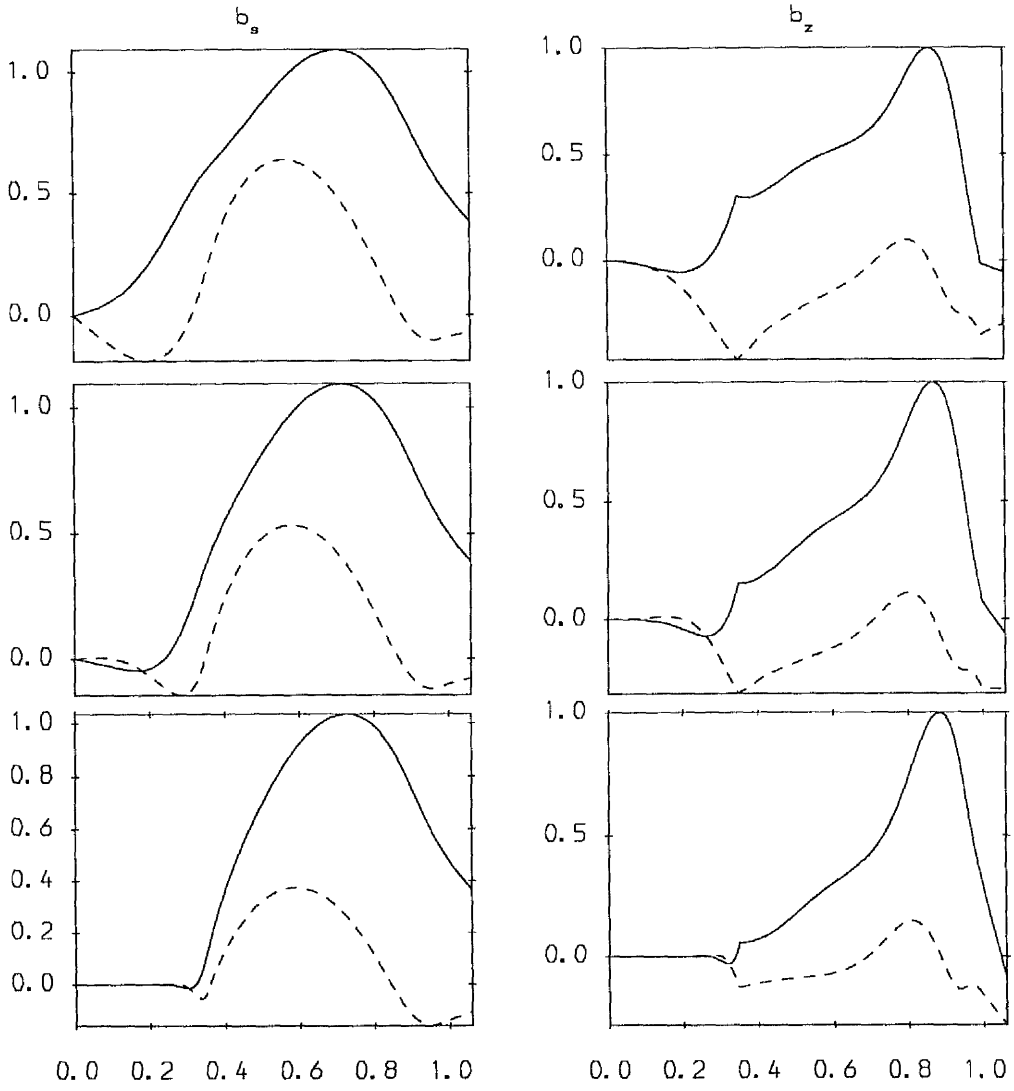

Figure 3.13 Eigenfunctions of b_s, b_z for the resistive slow modes of Figure 3.11 with critical parameters in (3.6a)–(3.6c) respectively.

His calculations were performed with perfectly insulating boundaries and he found that when $E, E_\eta \to 0$ (making the magnetostrophic approximation) $\Lambda_c \to \infty$. He also examined finite diffusivity and other fields and found the conditions for instability to be less exceptional; eg. for the field (2.36) with $\alpha = 3$ he found instability with $m = 2$ and $\omega < -1$.

Starting with a mode from Fearn (1988) [see Figure 6a of that paper] of field

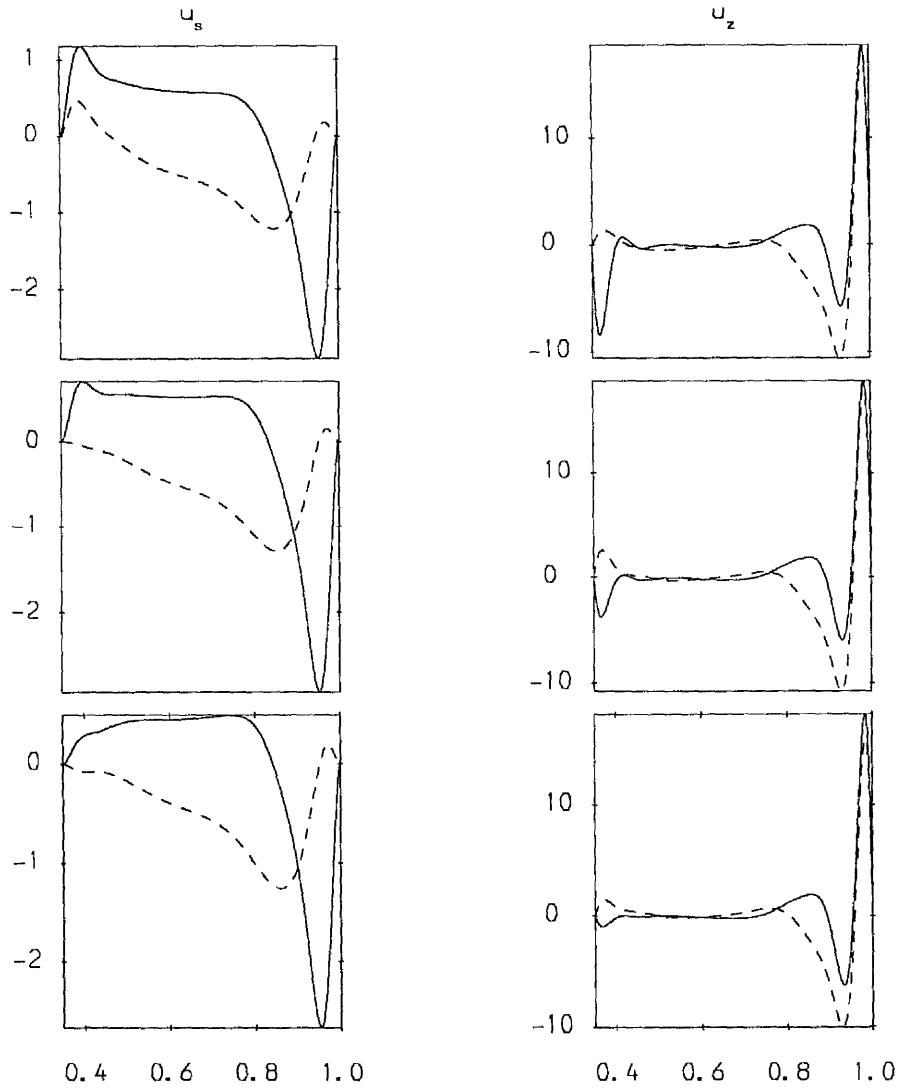

Figure 3.14 Eigenfunctions of u_s, u_z for the resistive slow modes of Figure 3.13.

(2.36) with $\alpha = 0$ we decreased the conductivity of the inner core and mantle to examine the effect on the critical parameters. Figures 3.15 and 3.16 show the variation in Λ_c and ω_c respectively. As $\eta_i, \eta_m \to 0$ we find that Λ_c remains finite tending towards a constant (≈ 317) and both the growth rate and frequency scale with $\eta_i = \eta_m$ so that there will be no instability in the limit $\eta_i, \eta_m \to 0$. Sample eigenfunctions are shown in Figures 3.17 and 3.18. It should be noted that in the boundary layer analysis of Section 4 in Roberts and Loper (1979) they make the

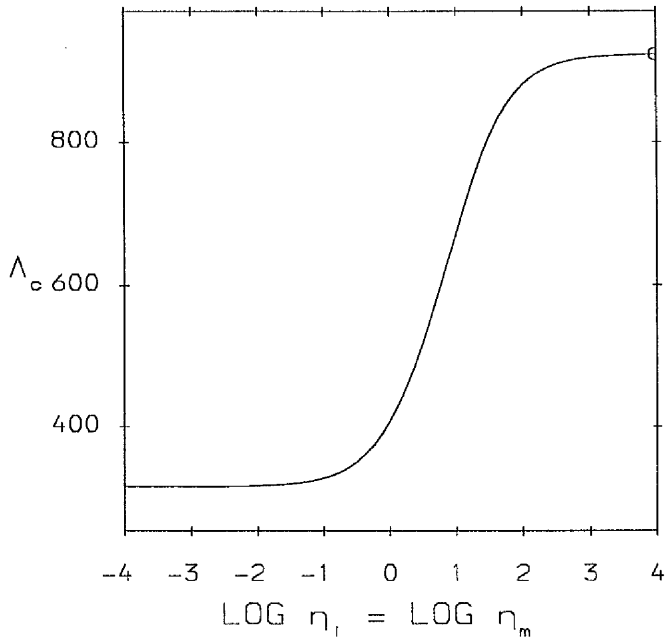

Figure 3.15 Critical Elsasser number versus $\log_{10}\eta_i = \log_{10}\eta_m$ for exceptional modes of field (2.36) with $m = 1, n = 1$ and $\alpha = 0$.

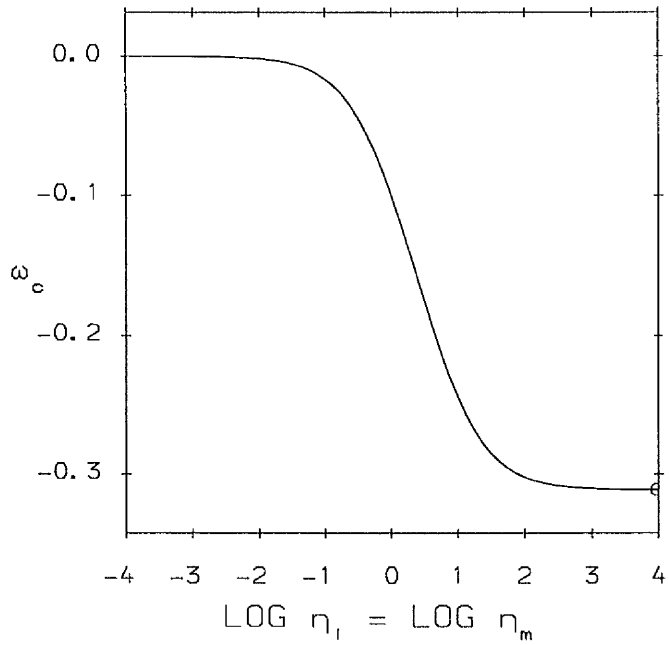

Figure 3.16 Frequency versus $\log_{10}\eta_i = \log_{10}\eta_m$ for exceptional modes of Figure 3.15.

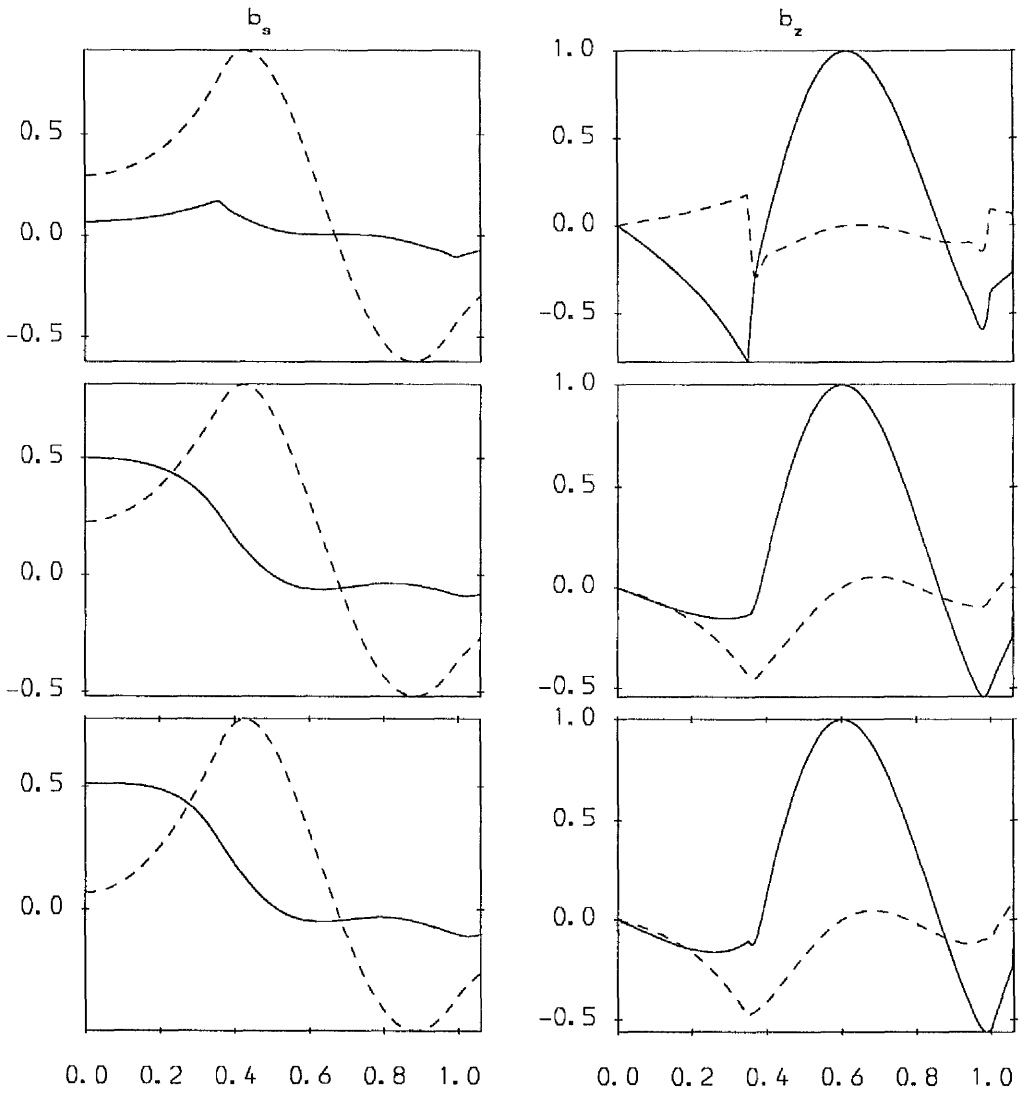

Figure 3.17 Eigenfunctions of b_s, b_z for exceptional modes of field (2.36) with $m = 1$ and $\alpha = 0$. The critical parameters are, from top to bottom, $\Lambda_c = 920, 408, 317$, $\omega_c = -0.310, -0.999 \times 10^{-1}, -0.181 \times 10^{-3}$, $n_c = 5.13, 4.25, 4.01$ and $\eta_i = \eta_m = 10^3, 1, 10^{-3}$.

simplifying assumption that $\Lambda|\omega| >> \eta_m$ (in their notation $|\omega| >> \Gamma\Lambda$) but the modes we have found by decreasing η_i, η_m do not satisfy this when $\eta_i, \eta_m \to 0$.

The conductivity of the boundaries also had a marked effect on the behaviour of Λ_c as viscous and fluid inertia effects were reduced, i.e., as $E, E_\eta \to 0$. This is

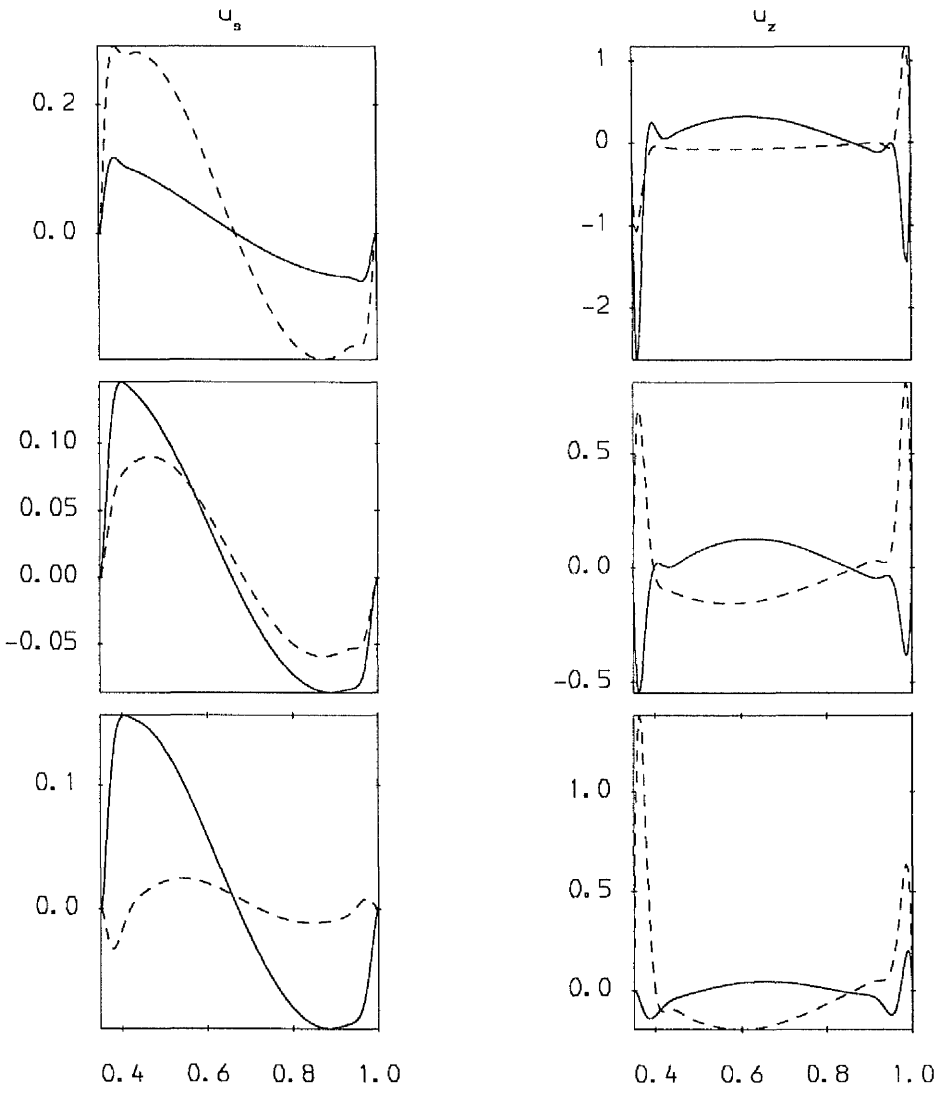

Figure 3.18 Eigenfunctions of u_s, u_z for the exceptional modes of Figure 3.17.

demonstrated in Figure 3.19 in which Λ_c versus $\log E = \log E_\eta$ for several values of $\eta_i = \eta_m$ as well as the most geophysically realistic case of $\eta_i = 1, \eta_m = 50$. We find $\Lambda_c \to$ constant as $E = E_\eta \to 0$ when $\eta_i = \eta_m \lesssim 1$ but $\Lambda_c \to \infty$ for more realistic values of η_i, η_m [over the range considered the frequency was essentially independent of E, E_η for each of the curves in Figure 3.19)] making it unlikely this type of instability will be important in the Earth's core.

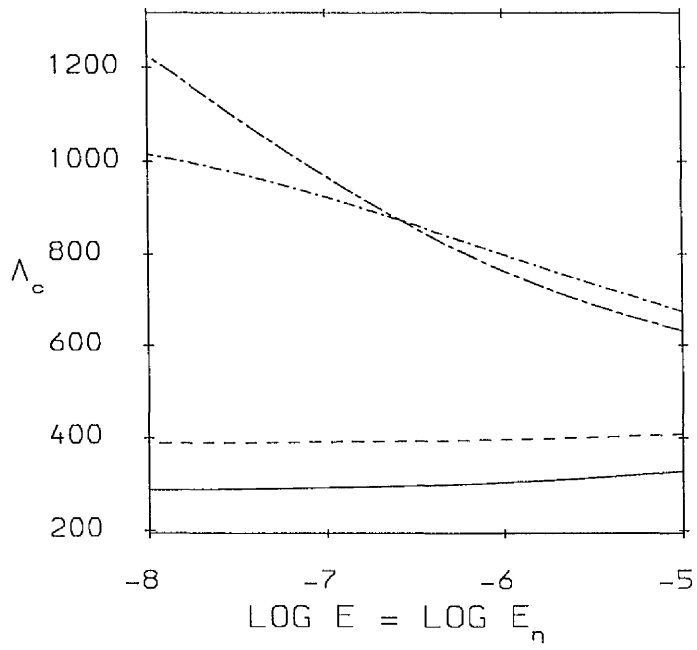

Figure 3.19 Critical Elsasser number versus $\log_{10}E = \log_{10}E_\eta$ for exceptional modes of field (2.36) with $m = 1$ and $\alpha = 0$. The lines correspond to $\eta_i = \eta_m = 0.1$ (full line), $\eta_i = \eta_m = 1$ (dashed line), $\eta_i = \eta_m = 10$ (dash-dot line) and (probably geophysically realistic) $\eta_i = 1$, $\eta_m = 50$ (long-dash short-dash line).

3.4 A LAYER WITH NON-UNIFORM DIFFUSIVITY

So far we have assumed the layer to have uniform diffusivity. Here we consider diffusivity as a function of radius i.e., we take

$$\eta_m(s) = \lambda s^\beta. \tag{3.7}$$

If $\lambda = 1$ the diffusivity is then continuous across the CMB. We investigated ideal modes of field (2.36) with $\alpha = 1$ and $\lambda = 1$. No significant differences were found from the case of uniform diffusivity. Sample modes, for comparison with (3.3), are

$$\Lambda_c = 183, \quad n_c = 1.70, \quad \omega_c = -0.202, \quad \beta = 10^3, \tag{3.8a}$$

$$\Lambda_c = 142, \quad n_c = 1.74, \quad \omega_c = -0.223, \quad \beta = 10^2, \tag{3.8b}$$

$$\Lambda_c = 80.8, \quad n_c = 1.78, \quad \omega_c = -0.247, \quad \beta = 10, \tag{3.8c}$$

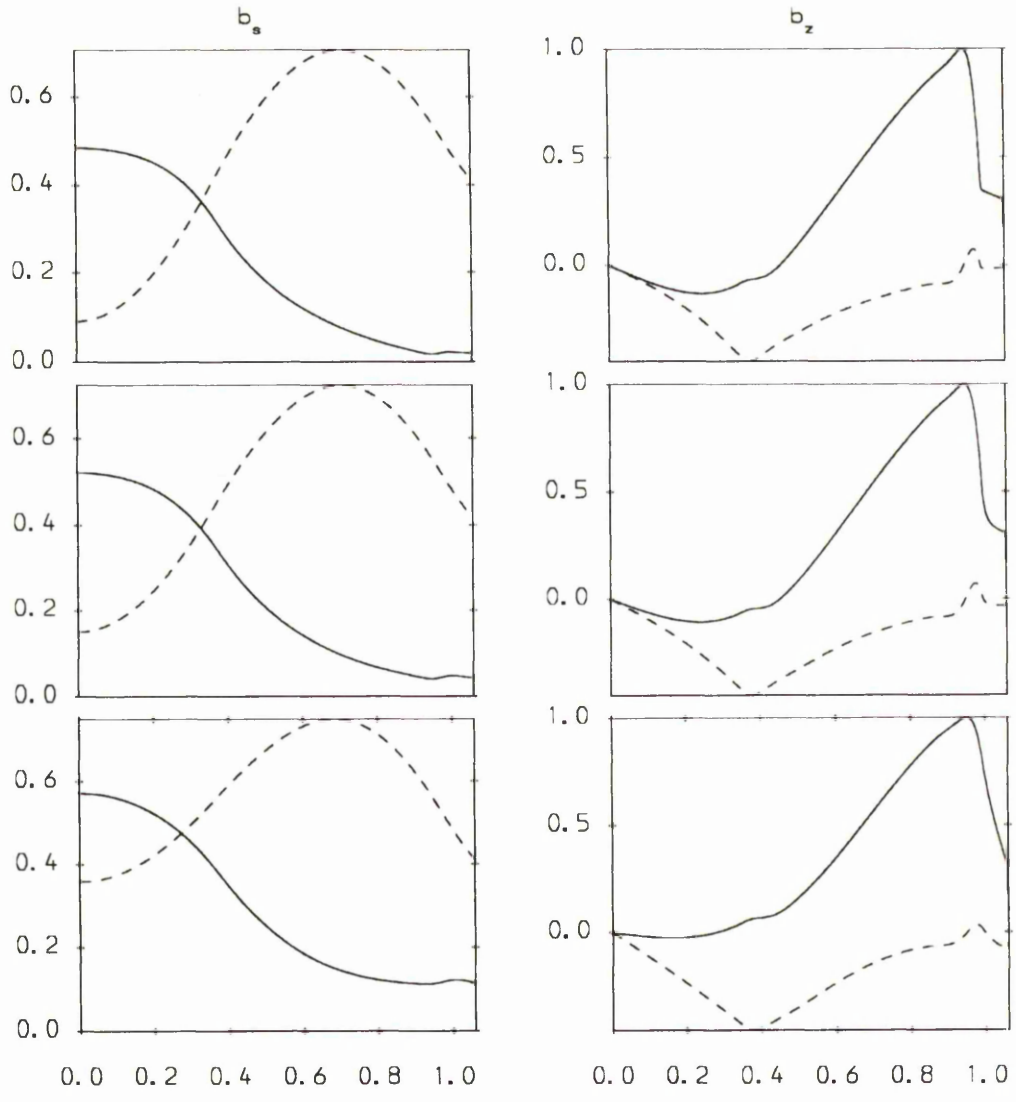

Figure 3.20 Eigenfunctions for b_s, b_z of ideal modes of field 2.35 and diffusivity profile 3.7. In each case $\lambda = 1$. The critical parameters are given in, from top to bottom, (3.8a)–(3.8c) with $\beta = 10^3, 10^2$ and 10 respectively.

Eigenfunctions for these modes are shown in Figures 3.20 and 3.21.

When $\lambda \neq 1$ the diffusivity is discontinuous across the CMB. Figure 3.22 illustrates the mode of (3.5b) with $\lambda = 100$ (top) and $\lambda = 0.01$ (bottom). The critical parameters, given below, changed in the way one would expect with $\lambda < 1$

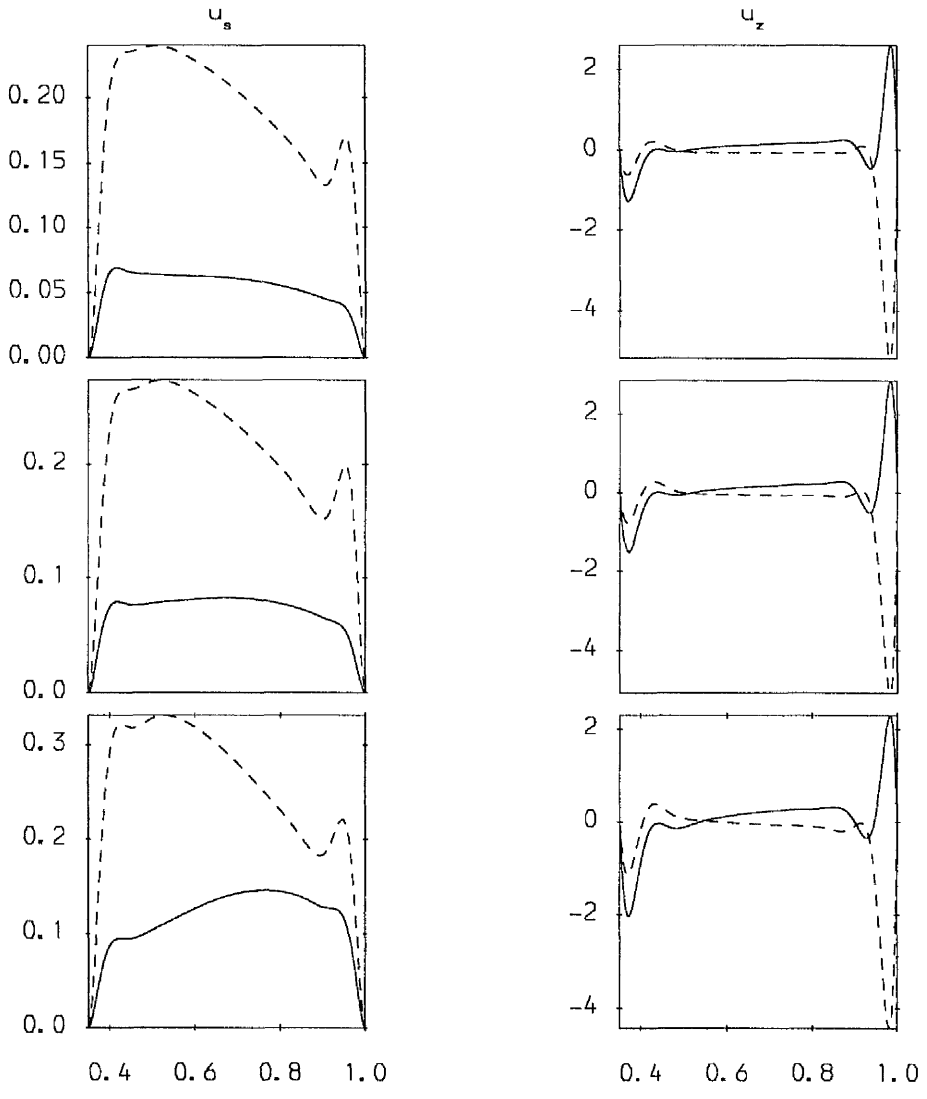

Figure 3.21 As in Figure 3.20 but for eigenfunctions of u_s, u_z.

having a destabilising effect.

$$\Lambda_c = 187, \qquad n_c = 1.69, \qquad \omega_c = -0.199, \qquad \lambda = 10^2, \tag{3.9a}$$

$$\Lambda_c = 82.3, \qquad n_c = 1.58, \qquad \omega_c = -0.044, \qquad \lambda = 10^{-2}, \tag{3.9b}$$

3.5 CONCLUSIONS

We have added a finitely conducting layer at the base of the mantle to a model representative of planetary magnetic fields and investigated its effect on

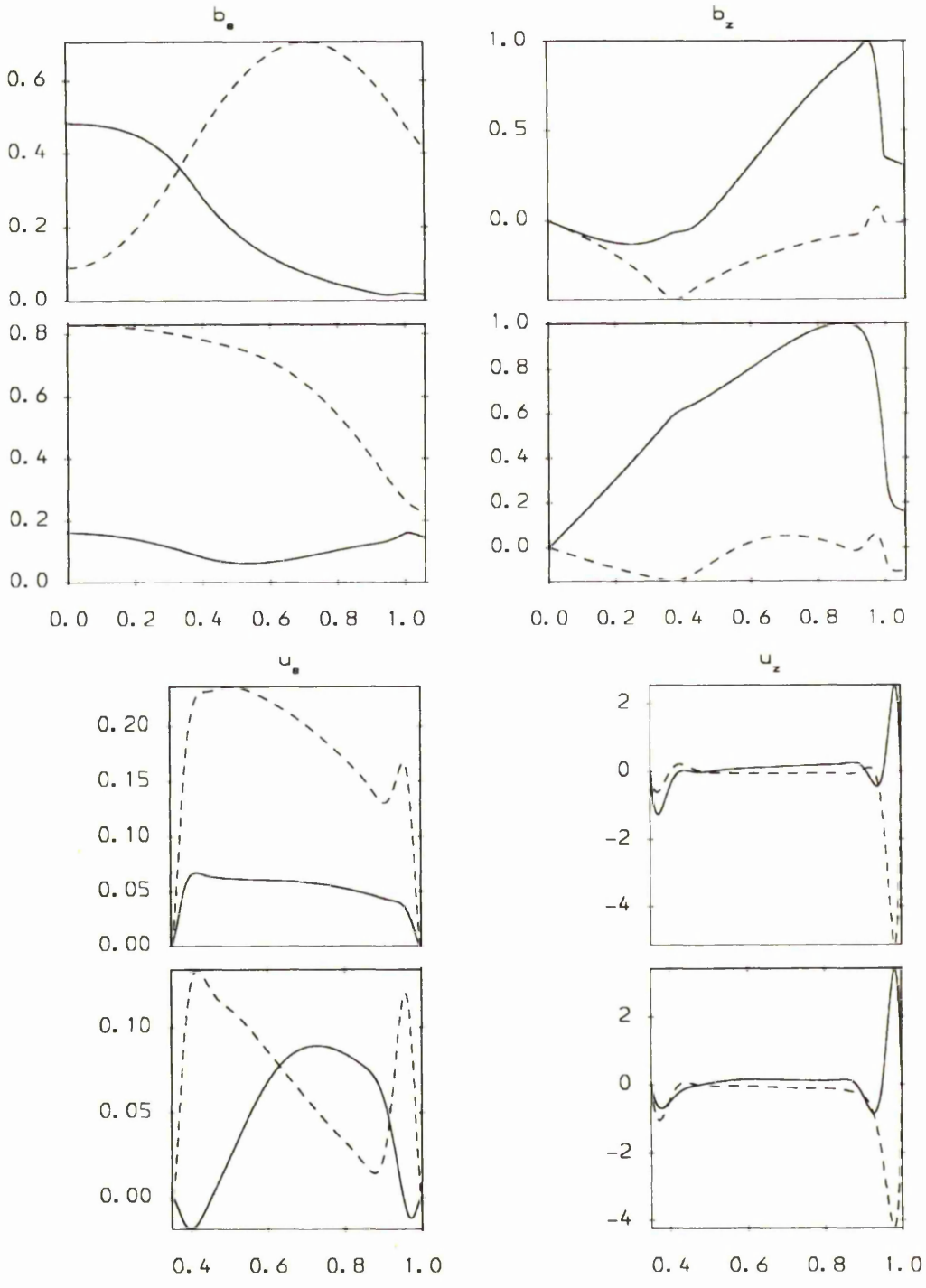

Figure 3.22 Eigenfunctions for b_s, b_z, u_s, u_z of ideal modes of field 2.36 with diffusivity profile 3.7 and $\beta = 10^2$. The critical parameters are given in (3.9a) (1st and 3rd Figures) and (3.9b) (2nd and 4th).

magnetic instabilities of relevance to the Earth. Our model also incorporated a finitely conducting inner core which, in general, was assumed to have the same electrical conductivity as the fluid outer core as is believed to be the case in the Earth. The layer was, in most cases, chosen to have a thickness $\epsilon = 0.06$ to reflect the D'' layer which seismic evidence suggests has a depth of $200km$. Three types of instability were investigated, each well known from previous work; ideal and resistive instability, already firmly established as being of significance to the Earth, and the Roberts-Loper exceptional mode which requires field strengths larger than those likely to be encountered in the Earth and is therefore probably only of theoretical interest. In each case we were able to recover the solution with an insulating mantle in the limit $\eta_m \to \infty$.

The addition of the layer was in almost all cases a destabilising influence. The critical Elsasser number Λ_c above which instability occurs was further reduced by increasing the layer depth, this effect being greatest when the diffusivity of the layer was small. However, for ideal and resistive instability, the type of instability of primary interest here, the change in Λ_c was negligible, particularly for the fast modes [see (3.4) and Figure 3.8]. The conductivity of the layer did however exert an important influence on the direction of propagation of fast resistive modes (see Figure 3.9). When η_m was large the modes travelled east; when it was decreased below $\eta_m \approx 10$ they travelled west. The Λ_c's for slow modes of both type were more strongly influenced, especially the resistive modes for which Λ_c increased when $\eta_m \lesssim 10$. The frequency in this case also increased with the result that $|\omega|\Lambda$ was no longer of the same order as η_i and the mode could not penetrate into the inner core. It was not surprising therefore that allowing the diffusivity in the layer to vary with radius had only a minimal effect, in keeping with the slightly destabilising influence of a conducting layer outlined above.

The Roberts-Loper exceptional instability has not previously been investigated in the presence of finitely conducting boundaries and is not found when both boundaries are perfectly conducting. Starting from a mode from Fearn (1988) with

insulating boundaries we decreased both η_i and η_m with $\eta_i = \eta_m$ and found the mode evolved to a low frequency mode with growth rate and frequency scaling with $\eta_i (= \eta_m)$ which penetrated into both the inner core and conducting mantle layer. The field strength required for instability was also considerably reduced, Λ_c falling to around a third its value with insulating boundaries when $\eta_i = \eta_m = 10^{-3}$. A common approximation in models of the Earth is the neglect of viscous and inertial effects. In the presence of insulating boundaries this has the effect of filtering out the exceptional instability since $\Lambda_c \rightarrow \infty$ as $E, E_\eta \rightarrow 0$. However, with η_i and $\eta_m \leq 1$ this was no longer the case, $\Lambda_c \rightarrow$ *constant* as $E, E_\eta \rightarrow 0$ and the mode would no longer be filtered out by the magnetostrophic approximation.

While it is, of course, desirable to make our models as realistic as possible an important question is the appropriateness of the inclusion of any effect in future models of the Earth. The conductivity of the D'' layer is believed to be $10^4 Sm^{-1}$ and the outer core $5 \times 10^5 Sm{-}1$ which translates to $\eta_m = 50$ in our model. With regard to those instabilities likely to be geophysically relevant inspection of Figures 3.2, 3.5, 3.8 and 3.11 suggests that at realistic parameter values Λ_c shows no significant difference from the $\eta_m \rightarrow \infty$ case and the approximation of the mantle as a perfect insulator is a reasonable one. However, the dependence on η_m of the direction of propogation of fast resistive modes is interesting and may have a role to play in explaining the observed westward drift of certain persistent features of the Earth's field. Although the field strengths required for exceptional instabilities were significantly less than with both boundaries insulating this is largely attributable to the finite conductivity of the inner core and with realistic parameter values (long-dash short-dash line of Figure 3.19) Λ_c remains unrealistically high as $E, E_\eta \rightarrow 0$.

CHAPTER 4

Weakly Nonlinear Magnetic Instability

4.1 INTRODUCTION

Linear studies of magnetic instability in the Earth, such as those detailed in Chapters 2 and 3, are now well advanced and most of the important features, such as field geometry and differential rotation, have been investigated. These studies represent an essential first step; they tell us what type of instability we can expect to have a role in the dynamics of the Earth's core and the conditions required for the onset of instability. However, linear theory fails to tell us how these instabilities develop beyond the point of onset and whether stable finite amplitude solutions to the perturbation equations exist only for field strengths greater than that required for the onset of instability or whether they can be found at lower field strengths as well. Answers to these questions can only be found by extending the analysis into the nonlinear regime.

To begin to investigate the nonlinear development of instabilities in a cylindrical geometry we consider a parameter regime in which our dimensionless measure of magnetic field strength, Λ, is slightly greater than that required for instability, i.e.

$$0 < \frac{(\Lambda - \Lambda_c)}{\Lambda_c} \ll 1. \tag{4.1}$$

We make the common approximation of neglecting viscous and inertial effects assuming them to be small in comparison with the Coriolis, Lorentz and pressure forces, i.e., we make the magnetostrophic approximation. In the linear analyses of Chapters 2 and 3 the extra work involved in retaining these terms was relatively small. However, they would considerably complicate the lengthy algebraic expressions which arise in the nonlinear analysis so that we make the magnetostrophic approximation to simplify the problem. The penalty to be paid for this is that we

must then consider Taylor's constraint (this is discussed further in §4.2.3). In the parameter regime (4.1), the exponential growth of the perturbations is very slow but after some long time the nonlinear self-interaction modifies the growthrate so that the perturbations equilibrate at some finite amplitude thereby modifying the basic state and establishing some new nonlinear equilibrium. The parameter regime in which stable nonlinear finite amplitude equilibrium may exist can be determined from the coefficients of the amplitude equation

$$\frac{dA}{dt} = \alpha A + h|A|^2 A \tag{4.2}$$

where A is the complex amplitude and α the growth rate and frequency of the linear analysis. The criticality (the meaning of which is made clear below) of the instability is determined by h. If $h < 0$, stable finite amplitude solutions to the perturbation equations exist only for $\Lambda > \Lambda_c$, the instability is said to be supercritical and the nonlinear equilibrium state is described by (4.2). If $h > 0$, stable finite amplitude solutions may also exist for $\Lambda < \Lambda_c$. The instability is then said to be subcritical but the eventual stable nonlinear equilibrium cannot be described by (4.2) since an assumption made in its derivation (described in detail in §4.2.3) is that the amplitude of the perturbations is very small. It is envisaged, on physical grounds, that there will exist some $\Lambda_M < \Lambda_c$ below which no stable finite amplitude solutions can be found. This latter case of subcritical instability is of interest since it provides for the rapid evolution of the basic state (given a suitable disturbance) through the growth of the perturbation into a new stable finite amplitude equilibrium.

As mentioned above, establishing the criticality of the instabilities is achieved through the determination of the coefficient h in the amplitude equation (4.2). This equation is derived by a multiple scale method in which the perturbations are expanded as a power series in their amplitude. An application of this technique was made by Kuang (1992). Kuang considered resistive instability of a sheared force free horizontal field in a plane layer geometry. In his model the most unstable perturbations are single-roll type solutions, i.e. one dimensional and this simplifies

the problem considerably. In particular, he was able to solve the system of linear equations that results from the technique up to an order in the amplitude such that Taylor's constraint (discussed in §4.2.3) is satisfied. He found that for the most unstable modes the bifurcation at marginal Λ was supercritical.

The simplifications that Kuang could exploit in his model do not arise here. Instead, the nonlinear development of the perturbations gives rise to terms at second order in the series of linear equations that result from the method which are independent of the axial and azimuthal coordinates - they are the nonlinear modification to the basic state. In particular, a geostrophic flow U_G is generated which cannot be determined simply from the momentum equation since it is a function only of the radial coordinate s. To determine this flow viscous effects are reinstated but considered important only in the Ekman boundary layers. It can then be shown (eg. Fearn 1994) that the resulting modification to Taylor's constraint gives an expression for the determination of the geostrophic flow U_G. This is discussed further in §4.2.3.

Kuang considered both the parameter regime (4.1) and the case $\Lambda \to \infty$. The basic states we have chosen do not satisfy $\nabla^2 \mathbf{B} = 0$, but rather decay on a diffusion timescale based on the annulus radius. In order for the analysis to be valid we require the magnitude of the perturbations (proportional to $\Lambda - \Lambda_c$) to be small. However $\Lambda - \Lambda_c$ must be big enough for the instability to grow on a timescale faster than the decay timescale of the basic state. This will be true provided that Λ is large enough. This is most clearly the case in the limit $\Lambda \to \infty$ but this regime is physically much less interesting than the regime (4.1).

In §4.3.2 we investigate instabilities of a monotonic magnetic field and of a field with zeros at the boundaries (both fields are azimuthal) and determine if they are of sub- or supercritical type. In the case of the monotonic field only subcritical instability was found. For the case of a field with zeros at the boundaries and a maximum within the fluid instability was in general found to be subcritical, an exception being for $m = 1$ (m is the azimuthal wave number) modes when the

maximum of the field was close to the outer boundary. As a test we then consider the effect of the toroidal flow generated by the nonlinear effects on the measure of critical magnetic field strength Λ_c. Using the geostrophic flow U_G calculated for the case $\Re_m = 0$ (where $\Re_m$, defined in (1.5), is a measure of the strength of the differential rotation) as input into the linear problem Λ_c was calculated as $\Re_m$ was slightly increased. As expected we found Λ_c decreased for the case of subcritical instability and increased for the case of supercritical instability.

4.2 THE MODEL

4.2.1 Governing Equations

In this chapter we again consider a cylindrical annulus of conducting fluid but take the inner core ($s \leq s_{ib}$) and mantle ($s \geq 1$) to be insulating (this gives simple boundary conditions and removes the need to solve equations in the inner core and mantle). In addition, the annulus is bounded in the z-direction by perfectly conducting plates at $z = \pm d$ (in dimensionless coordinates). The presence of these perfectly conducting plates does not affect the solution of the linear stability problem (see below). It does however affect the nonlinear equations and introduces a more physically realistic closed container with, for a given d, discrete axial wavenumbers n (see 4.14). The simplicity of the boundary conditions for a perfect conductor allow the separation of the z-dependence of the perturbations in a simple way as $\cos[n(z+d)]$ or $\sin[n(z+d)]$. The appropriate non-dimensionalised equations governing the stability of the basic state are in essence the same as (2.7)–(2.9) but with two important differences. Naturally, in a nonlinear analysis we must retain squares and products of the perturbation quantities $\mathbf{b}$ and $\mathbf{u}$. We also make the magnetostrophic approximation in which viscous and inertial forces are neglected (although the importance of viscosity is considered in determining the geostrophic flow - see §4.2.3). The instability timescale is long compared with the inertial timescale and viscous forces are small compared with Coriolis and Lorentz forces so that it is a common approximation in geomagnetic studies to neglect these terms in (2.7), i.e., to take $E = E_\eta = 0$ (this has consequences for the boundary

conditions which are discussed in §4.2.2). The equations governing $\mathbf{b}$ and $\mathbf{u}$ are then

$$\hat{\mathbf{z}} \times \mathbf{u} = -\nabla p + (\nabla \times \mathbf{B}_o) \times \mathbf{b} + (\nabla \times \mathbf{b}) \times \mathbf{B}_o + (\nabla \times \mathbf{b}) \times \mathbf{b}, \tag{4.3}$$

$$\frac{\partial \mathbf{b}}{\partial t} = \Re_m \nabla \times (\mathbf{U}_o \times \mathbf{b}) + \nabla \times (\mathbf{u} \times \mathbf{B}_o) + \nabla \times (\mathbf{u} \times \mathbf{b}) + \Lambda^{-1} \nabla^2 \mathbf{b}, \tag{4.4}$$

$$\nabla . \mathbf{b} = \nabla . \mathbf{u} = 0, \tag{4.5a, b}$$

where $\Re_m$, the modified magnetic Reynolds's number, is defined in (1.5) and can be regarded as a measure of the strength of differential rotation.

The basic state takes the form

$$\mathbf{B}_0 = B_M s F(s) \hat{\phi}, \qquad \mathbf{U}_0 = U_M s \Omega(s) \hat{\phi}, \tag{4.6}$$

where F and Ω are chosen such that $\max|F| = \max|\Omega| = 1$.

We then proceed in a similar manner to the previous chapters, eliminating the variables p, u_s, u_ϕ, u_z and b_ϕ using (4.3).$\hat{\mathbf{z}}$, $\frac{\partial}{\partial z}$(4.3).$\hat{\phi}$, $\frac{\partial}{\partial z}$(4.3).$\hat{\mathbf{s}}$, (4.5a) and (4.5b). The resulting equations can be expressed in the form

$$L\Phi = \mathbf{N}, \tag{4.7}$$

where

$$\Phi = \begin{bmatrix} b_s \\ b_z \end{bmatrix}, \tag{4.8}$$

and L, a matrix of linear differential operators and N is the nonlinear interaction vector,

$L =$

$$\begin{bmatrix} [(F^2 + sFF' - sF^2\partial_s - \Re_m\Omega)\partial_\phi - \partial_t + \\ \Lambda^{-1}(3s^{-1}\partial_s + \partial_s^2 + s^{-2}(1+\partial_\phi^2) + \partial_z^2)]\partial_z & -F^2 s^{-1}(\partial_\phi^2 + s^2\partial_z^2)\partial_\phi \\ & +2s^{-1}\Lambda^{-1}\partial_z^2 \\ [Fs^{-1}(1+\partial_\phi^2) + F^2 s\partial_s^2 & [(F(sF\partial_s + 4F + sF') - \Re_m\Omega)\partial_\phi - \partial_t \\ +3F^2\partial_s - 3FF' - sFF'']\partial_\phi & +\Lambda^{-1}(s^{-1}\partial_s + \partial_s^2 + s^{-2}\partial_\phi^2 + \partial_z^2)]\partial_z \end{bmatrix} \tag{4.9}$$

$$N = \begin{bmatrix} -\partial_z[\nabla \times (\mathbf{u} \times \mathbf{b})]_s + Fs^{-1}\partial_\phi^2[(\nabla \times \mathbf{b}) \times \mathbf{b}]_z - Fs^{-1}\partial_\phi\partial_z[(\nabla \times \mathbf{b}) \times \mathbf{b}]_\phi \\ -\partial_z[\nabla \times (\mathbf{u} \times \mathbf{b})]_z + Fs^{-1}\partial_\phi\partial_s[s[(\nabla \times \mathbf{b}) \times \mathbf{b}]_\phi] - Fs^{-1}\partial_\phi^2[(\nabla \times \mathbf{b}) \times \mathbf{b}]_s \end{bmatrix} \tag{4.10}$$

where $\partial_z \equiv \frac{\partial}{\partial z}$. The linearised form of (4.6)

$$L\Phi = \mathbf{0}, \tag{4.11}$$

is the problem solved by Fearn (1988). The equations (4.11) admit solutions of the form

$$f(s, \phi, z) = f(s, z)\exp[i(m\phi - \omega t)], \tag{4.12}$$

where f is any of the perturbation variables.

4.2.2 Boundary conditions

In making the magnetostrophic approximation the order, in s, of our system of differential equations (4.7) drops from ten to four rather than six as would be expected. This is related to the cylindrical walls being parallel to the axis of rotation. Clearly, in neglecting viscosity, the no-slip condition cannot be applied but the question then arises of which of the remaining boundary conditions should be applied. Fearn (1983a), generalising work of Condi (1978), addressed this problem by reinstating viscous effects and considering the limit $E \to 0$. He showed that the contribution from the boundary layer was greater for u_s than for b_s and b_z so that it is the conditions on b_s and b_z (which must be satisfied by the mainstream) which are retained and the condition on u_s (which is accommodated by the boundary layer) that is dropped. This problem does not arise on the perfectly conducting horizontal plates since equations (4.7) are sixth order in z.

The plates at $z = \pm d$ are perfect conductors and the appropriate boundary conditions are that the normal velocity and tangential electric field are zero (the latter of these implies the normal magnetic field is zero) giving

$$b_z = \frac{\partial b_s}{\partial z} = 0. \tag{4.13}$$

Differentiating (4.5a) with respect to z then leads to

$$\frac{\partial^2 b_z}{\partial z^2} = 0. \tag{4.14}$$

The cylindrical walls of the container are insulating. Physically, the conditions that are applied are that the current normal to the boundary vanishes and the field matches to some external potential field (see §2.2.2). Here we give the conditions as they apply to the linear problem, the details for the nonlinear problem are given in Appendix C. With the perturbation variables in the linear problem written as

$$\begin{bmatrix} b_s \\ b_z \end{bmatrix} = \begin{bmatrix} b_{s1} \cos n(z+d) \\ i b_{z1} \sin n(z+d) \end{bmatrix} e^{im\phi}, \tag{4.15}$$

(see next section for more details) the condition that the normal current vanishes $s = s_{ib}$ and $s = 1$ is

$$s^2 D b_{s1} + s b_{s1} + (m^2 + n^2 s^2) b_{z1}/n = 0, \qquad s = s_{ib}, 1, \tag{4.16}$$

and matching to an external potential field leads to

$$b_s = \gamma b_z, \tag{4.17}$$

where

$$\gamma = \begin{cases} -i[I_{m+1}(n s_{ib})/I_m(n s_{ib}) + m/n s_{ib}] & s = s_{ib} \\ i[K_{m+1}(n)/K_m(n) - m/n] & s = 1 \end{cases} \tag{4.18}$$

(see §2.2.2).

4.2.3 Taylor's Constraint and the Magnetostrophic Approximation

A distinguishing feature of the geodynamo problem is the unusual force balance in the outer core. Generally, in rapidly rotating hydrodynamical systems the Coriolis force dominates and constrains motions to be two dimensional - this is the well known Taylor-Proudman theorem. In the Earth however, this constraint is relaxed since the Coriolis force is balanced by pressure and Lorentz forces. However, a remaining consequence of the rapid rotation is that the viscous and inertial forces (other than the Coriolis force) are, relatively, very small. In terms of the

dimensionless parameters E and E_η, the Ekman and magnetic Ekman numbers measuring viscous and inertial effects respectively and defined by

$$E = \frac{\nu}{2\Omega s_o^2}, \qquad E_\eta = \frac{\eta}{2\Omega s_o^2},$$

estimates are $O(10^{-15})$ and $O(10^{-9})$ (although it should be noted that the former of these is not well known). A common approximation therefore is to neglect these terms in the momentum equation, making it a diagnostic rather than predictive equation. This is known as the magnetostrophic approximation.

The consequences of making the magnetostrophic approximation, which has the effect of filtering out short timescale motions, on the geodynamo problem were first discussed by Taylor (1963). He considered the mass flux across cylinders of radius s, coaxial with the axis of rotation and contained within the outer core, i.e.

$$\int\int_{C(s)} U_s d\phi dz, \tag{4.19}$$

(in cylindrical coordinates) where $C(s)$ is the surface of the cylinder described above. If the magnetostrophic approximation is made, the cylinder $C(s)$ extends all the way to the boundary. There can, therefore, be no flow into the ends of the cylinder. For an incompressible fluid this implies that the integral (4.19) is zero. Taylor then showed that solutions to (4.3) can only be found if

$$\int\int_{C(s)} [(\nabla \times \mathbf{B}) \times \mathbf{B}]_\phi d\phi dz = 0, \tag{4.20}$$

[see, for example, Fearn (1994)]. This is known as Taylor's constraint and has been the subject of a great deal of attention particularly in the contexts of magnetoconvection (eg. Roberts and Stewartson, 1974,1975; Soward, 1980, 1986; Skinner and Soward, 1988) and dynamo models (eg. Soward and Jones, 1983; Braginsky and Roberts, 1988). If, in the framework of the magnetostrophic approximation, (4.20) is satisfied then solutions to (4.3) can be found up to an 'arbitrary' geostrophic flow $\mathbf{U}_G = U_G(s)\hat{\phi}$ [arbitrary in the sense that we can add any such flow to a solution of

(4.3)]. Taylor envisaged that this geostrophic flow would alter the magnetic field, via the induction equation, in such a way that (4.20) would be satisfied. However, one cannot be sure that (4.20) will be satisfied. Fearn and Proctor (1987) tried to determine U_G by choosing it to minimise the integral on the left hand side of (4.20) for a prescribed field and flow but with mixed results.

An alternative way of determining U_G is to include the effects of Ekman suction. Consider the division of the outer core into three regions comprising boundary layers at the ICB and CMB in which viscous effects are important and the interior in which they can be neglected. In this case the integral (4.19) is non-zero and it can be shown that (4.20) is modified to

$$U_G = \frac{1}{2\pi}(2E)^{-1/2} \int\int_{C(s)} [(\nabla \times \mathbf{B}) \times \mathbf{B}]_\phi d\phi dz. \tag{4.21}$$

Unlike (4.20), which was a constraint on the magnetic field $\mathbf{B}$, (4.21) is an expression which determines U_G at the outer edge of the boundary layer. Since U_G is independent of z (4.21) then prescribes U_G throughout the annulus. Other forms of coupling, topographic or electromagnetic coupling, may also be important but if these are included and viscous effects neglected (4.20) must still be satisfied. A much more detailed discussion of Taylor's constraint and the modifications to it when core-mantle coupling is introduced can be found in Fearn, Roberts and Soward (1988) and Fearn and Proctor (1992).

In the problem under investigation here we are interested in the nonlinear development of perturbations of the form (4.14). These perturbations are expanded as a power series in their complex amplitude (see §4.2.4) which, when substituted into the governing equations, give rise to a series of linear equations at ascending powers of the amplitude. At second order in this expansion terms arise which give rise to a toroidal flow U_G independent of the coordinates ϕ and z. This flow, which represents the nonlinear modification to the basic state by the perturbations, cannot be determined simply from the momentum equation [(4.3).ϕ] since this determines only the z-derivative of the velocity. To determine it we rein-

troduce viscous effects which are important in the Ekman boundary layers but considered negligible elsewhere. The geostrophic flow, U_G, is then determined by the expression (4.21) above.

4.2.4 Finite Amplitude Analysis

Here we present the analysis whereby the amplitude equation governing the nonlinear behaviour of the perturbations is derived. It is the coefficient of the nonlinear term in this equation which determines the nature of the bifurcation at the onset of instability. For the sake of clarity, most of the complicated expressions arising in this analysis are left out here and given in Appendix A.

To investigate the bifurcation at marginal instability we consider the region slightly above critical, i.e. where

$$0 < (\Lambda - \Lambda_c)/\Lambda_c \ll 1, \tag{4.22}$$

and the growth rate, p, of the perturbations is small

$$p \propto (\Lambda - \Lambda_c)/\Lambda_c. \tag{4.23}$$

In this region the magnitude of the perturbations, ϵ, is very small ($|\epsilon| \ll 1$) and we can expand the system of equations (4.7) as an asymptotic series in ϵ to obtain a sequence of linear equations in ascending powers of ϵ. In order to solve this sequence of equations we must eliminate secularity and in so doing we will arrive at a relationship (the amplitude equation) involving the amplitude of the perturbations and the timescale τ on which they evolve where

$$\tau \propto p^{-1}. \tag{4.24}$$

Secular terms arise first at third order in the expansion. This means that to eliminate them the slow time derivative ∂_t must be such that

$$\frac{\partial}{\partial t} = \epsilon^2 \frac{\partial}{\partial \tau}. \tag{4.25}$$

This implies the growth rate p is $O(\epsilon^2)$ and, with consideration of (4.23), we have

$$\lambda\epsilon^2 = (\Lambda - \Lambda_c)/\Lambda_c. \tag{4.26}$$

where λ is a constant of proportionality from (4.23).

The matrix L and vectors Φ and N are expanded as follows

$$L = L_0 + \epsilon L_1 + \epsilon^2 L_2 + \cdots, \tag{4.27}$$

$$\Phi = \epsilon \mathbf{b}_1 + \epsilon^2 \mathbf{b}_2 + \epsilon^3 \mathbf{b}_3 + \cdots, \tag{4.28}$$

$$\mathbf{N} = \epsilon^2 \mathbf{N}_2 + \epsilon^3 \mathbf{N}_3 + \cdots. \tag{4.29}$$

Substituting into (4.7) we obtain a series of linear equations. At $O(\epsilon)$ we retrieve the linear problem,

$$L_0 \mathbf{b}_1 = 0 \tag{4.30}$$

where L_0 is given in Appendix A and

$$\mathbf{b}_1 = \begin{bmatrix} b_{s1} \\ i b_{z1} \end{bmatrix} + c.c. \tag{4.31}$$

where $c.c.$ means complex conjugate. The equations (4.30) admit normal mode solutions of the form

$$\mathbf{b}_1 = A(\tau) \begin{bmatrix} b_{s1}(s,z) \\ i b_{z1}(s,z) \end{bmatrix} \exp(im\phi) + c.c. \tag{4.32}$$

The simplicity of the boundary conditions (4.16) and (4.17) also allows us to separate out the z-dependence as

$$\mathbf{b}_1 = A(\tau) \begin{bmatrix} b_{s1}(s) \cos n(z+d) \\ i b_{z1}(s) \sin n(z+d) \end{bmatrix} \exp(im\phi) + c.c. \tag{4.33}$$

[equations (4.3) and (4.4) then imply $b_{\phi 1}, u_{\phi 1}, u_{s1} \sim \cos n(z+d)$ and $u_{z1} \sim \sin n(z+d)$] where

$$n = \frac{k\pi}{2d}, \qquad k \in \mathcal{Z} \tag{4.34}$$

(see Lan, Kuang and Roberts 1992). This is the same linear problem solved by Fearn [1983b (with perfectly conducting boundaries),1988]. Although he had no

bounding plates in his model and the z-dependence of his perturbations took the form $\exp(inz)$, writing ib_{z1} in (4.32) means that our equations are identical to Eqns(2.5) of Fearn (1983b) (after elimination of u_s, u_z) and $b_{z1}(s)$ is the same as $b_z(s)$ which appears there and in Chapters 2 and 3.

At next order, $O(\epsilon^2)$, we have

$$L_0\mathbf{b}_2 + L_1\mathbf{b}_1 = \mathbf{N}_2. \tag{4.35}$$

Although the numerical solution to the system of equations permits any value of n, from (4.34), for fixed d, n is discrete so that

$$L_1 = 0. \tag{4.36}$$

The nonlinear vector $\mathbf{N}_2$ takes the form

$$\begin{aligned}\mathbf{N}_2 &= A^2\mathbf{N}_{20} + |A|^2\mathbf{N}_{11} + \overline{A}^2\mathbf{N}_{02} \\ &= A^2\begin{bmatrix} N_{201} \\ N_{202}\end{bmatrix} e^{2im\phi} + |A|^2\begin{bmatrix} N_{111} \\ N_{112}\end{bmatrix} + \overline{A}^2\begin{bmatrix} N_{021} \\ N_{022}\end{bmatrix} e^{-2im\phi},\end{aligned} \tag{4.37}$$

where $N_{201}, N_{202}, N_{111}$ and N_{112} are given in Appendix A and $N_{201} = \overline{N}_{021}$, $N_{202} = \overline{N}_{022}$ where the bar denotes complex conjugate. In the subscripts here the first two digits refer to the powers of A and $\overline{A}$ respectively. Substitution of (4.37) into (4.35) then implies $\mathbf{b}_2$ must take the form

$$\begin{aligned}\mathbf{b}_2 &= A^2\mathbf{b}_{20} + |A|^2\mathbf{b}_{11} + \overline{A}^2\mathbf{b}_{02} \\ &= A^2\begin{bmatrix} b_{s20} \\ b_{z20}\end{bmatrix} e^{2im\phi} + |A|^2\begin{bmatrix} b_{s11} \\ b_{z11}\end{bmatrix} + \overline{A}^2\begin{bmatrix} b_{s02} \\ b_{z02}\end{bmatrix} e^{-2im\phi}.\end{aligned} \tag{4.38}$$

At $O(|A|^2)$ here terms $b^{(1)}_{\phi 11}$, $u^{(1)}_{\phi 11}$ and $u^{(1)}_{s11}$ (the superscript (1) denotes terms independent of z - see Appendix A) arise which are functions only of s. In the case of $u_{\phi 11}$ this term cannot be found from the momentum equation but must be determined by considering the importance of viscosity in the boundary layers. This problem was discussed in §4.2.3 and further detail can be found in Appendix A.

Equations (4.35), with (4.37) and (4.38), can be solved in a straightforward manner with the appropriate boundary conditions given in Appendix C. The complementary function which arises in this solution is proportional to $\mathbf{b}_1$ and can therefore simply be absorbed into it. It is at the next order, $O(\epsilon^3)$, that secular terms arise. From (4.7) and (4.27)–(4.29) with (4.36) the $O(\epsilon^3)$ equation is

$$L_0\mathbf{b}_3 = \mathbf{N}_3 - L_2\mathbf{b}_1, \tag{4.39}$$

where

$$\begin{aligned}\mathbf{N}_3 &= A^3\mathbf{N}_{30} + A|A|^2\mathbf{N}_{21} + c.c.,\\ &= A^3\begin{bmatrix}N_{301}\\ N_{302}\end{bmatrix}e^{3im\phi} + A|A|^2\begin{bmatrix}N_{211}\\ N_{212}\end{bmatrix}e^{im\phi} + c.c.,\end{aligned} \tag{4.40}$$

Secularity arises because of the second term on the right hand side of (4.40). In order to remove it we define an adjoint as follows. Let $\langle\ ,\ \rangle$ denote the inner product

$$\langle f, g\rangle \ = \ \frac{1}{2\pi}\int_0^{2\pi}\int_{-d}^{d}\int_{s_{ib}}^{1} f\bar{g}\ dsdzd\phi \tag{4.41}$$

where f, g are arbitrary functions of s, z and ϕ. Then, if $L_0^\dagger$ denotes the adjoint operator of L_0 with the property

$$\langle f, L_0 g\rangle \ = \ \langle L_0^\dagger f, g\rangle \tag{4.42}$$

the adjoint problem is

$$L_0^\dagger\mathbf{b}_1^\dagger = 0 \tag{4.43}$$

where

$$\mathbf{b}_1^\dagger = \begin{bmatrix}\zeta\sin n(z+d)\\ i\xi\cos n(z+d)\end{bmatrix}e^{im\phi} + c.c. \tag{4.44}$$

(see Appendix B). The adjoint operator $L_0^\dagger$ and the appropriate boundary conditions for $\mathbf{b}_1^\dagger$ are given in Appendix B. If we pre-multiply (4.39) by $\mathbf{b}_1^\dagger$, take the inner product and utilise the property (4.42) the solvability condition for (4.39) is then

$$\langle\mathbf{b}_1^\dagger, \mathbf{N}_{21}\rangle \ - \langle\mathbf{b}_1^\dagger, L_2\mathbf{b}_1\rangle \ = 0 \tag{4.45}$$

(only $\mathbf{N}_{21}$ appears here since the other components of $\mathbf{N}_3$ vanish after integration with respect to ϕ). When secularity has been removed, $\mathbf{b}_3$ in (4.36) takes the form

$$\begin{aligned}\mathbf{b}_3 &= A^3\mathbf{b}_{30} + A|A|^2\mathbf{b}_{21} + c.c.,\\ &= A^3\begin{bmatrix} b_{s30} \\ b_{z30}\end{bmatrix} e^{3im\phi} + A|A|^2\begin{bmatrix} b_{s21} \\ b_{z21}\end{bmatrix} e^{im\phi} + c.c.\end{aligned} \tag{4.46}$$

Finally, after substitution from (4.31), the appropriate term from (4.40) and L_2 (given in Appendix A) (4.45) gives us the amplitude equation

$$a_1\frac{dA}{d\tau} = a_2\lambda A + a_3 A|A|^2 \tag{4.47}$$

where a_1, a_2 and a_3 are given in Appendix A. Now, multiplying by ϵ^3 and defining

$$\epsilon A(\tau) \rightarrow A(t) \tag{4.48}$$

we have

$$\frac{dA}{dt} = c\Delta\Lambda A + hA|A|^2 \tag{4.49}$$

where

$$c = \frac{a_2}{a_1}, \qquad h = \frac{a_3}{a_1}, \qquad \Delta\Lambda = \frac{\Lambda - \Lambda_c}{\Lambda_c}, \tag{4.50}$$

Here $c\Delta\Lambda$ represents the growth rate from the linear problem. This is our amplitude equation. There are two possible cases to consider. The analysis here is made simpler and more elegant by writing

$$A = Re^{i\theta}, \qquad h = h_r + ih_i \tag{4.51}$$

and considering the real part of (4.49) which gives

$$\frac{dR}{dt} = c\Delta\Lambda R + h_r R^3 \tag{4.52}$$

i) $c\Delta\Lambda > 0 \qquad h_r < 0$

The bifurcation is said to be supercritical. Stable, finite amplitude solutions to the nonlinear problem exist with

$$R = (c\Delta\Lambda/|h_r|)^{1/2}. \tag{4.53}$$

The stability of these solutions can be seen from solving (4.49) to get

$$R(t)^2 = R_e^2[(1 - \exp(-2c\Delta\Lambda t)) + \frac{R_e^2}{R_0^2}\exp(-2c\Delta\Lambda t)]^{-1} \tag{4.54}$$

so that

$$R \to R_e \quad \text{as} \quad t \to \infty \tag{4.55}$$

where $R_0 = R(0)$ [see, for example, Drazin and Reid (1981)].

ii) $c\Delta\Lambda > 0 \qquad h_r > 0$

The bifurcation is said to be subcritical. A stable finite amplitude equilibrium does not exist in the approximation $\epsilon \ll 1$. In this case (4.46) fails to determine the nonlinear equilibrium state.

4.3 RESULTS

4.3.1. A check on the results

To serve as a test on parts of the code we make a comparison between the eigenvalues of the linear problem (4.30) and the adjoint problem (4.43). From the definition of the adjoint problem the eigenvalues of (4.30) and (4.43) should be complex conjugates and can therefore serve as an indicator of the reliability of our solution to first order. In Figure 4.1 the modulus of the critical frequency is plotted against the number of grid points N for both the linear stability problem (4.30) and the adjoint problem (4.43). They can be seen to be near identical at fairly modest values of N indicating the solutions to (4.30) and (4.43) are correct (note that the determination of h depends on solutions to the linear stability problem, $\mathbf{b}_1$, the adjoint problem, $\mathbf{b}_1^\dagger$ and the solution of differential equations for $\mathbf{b}_2$, the solution for the latter depending also on $\mathbf{b}_1$).

4.3.2 Sub- or supercritical instability?

As in previous chapters we consider instabilities of two basic states which are

$$F = s^\alpha, \tag{4.56}$$

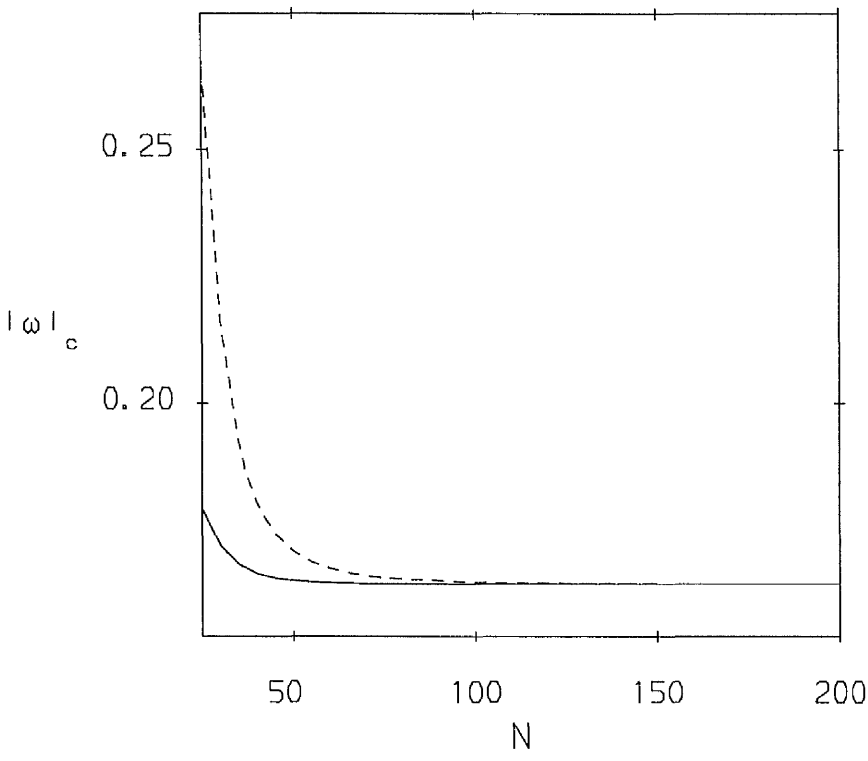

Figure 4.1 Modulus of the critical frequency ω_c of a resistive instability of field (4.56) versus number of grid points N for the linear stability problem (full line) and adjoint problem (dashed line). The parameters are $\alpha = 1$, $\Lambda_c = 28.9$, $\omega_c = 0.16$, $m = 1$, and $n = 3$.

unstable only to field gradient instability, and

$$F = \frac{4(1 - s^\beta)(s^\beta - s^\beta_{ib})}{(1 - s^\beta_{ib})^2}, \tag{4.57}$$

which admits both field gradient and resistive instability. In this section we consider only the case $\Re_m = 0$. Figures 4.2–4.4 illustrate solutions up to second order of an ideal instability of the field (4.56), including the geostrophic flow $u^{(1)}_{\phi 11}$ and $b^{(1)}_{\phi 11}$ both of which are concentrated, as would be expected, in the outer part of

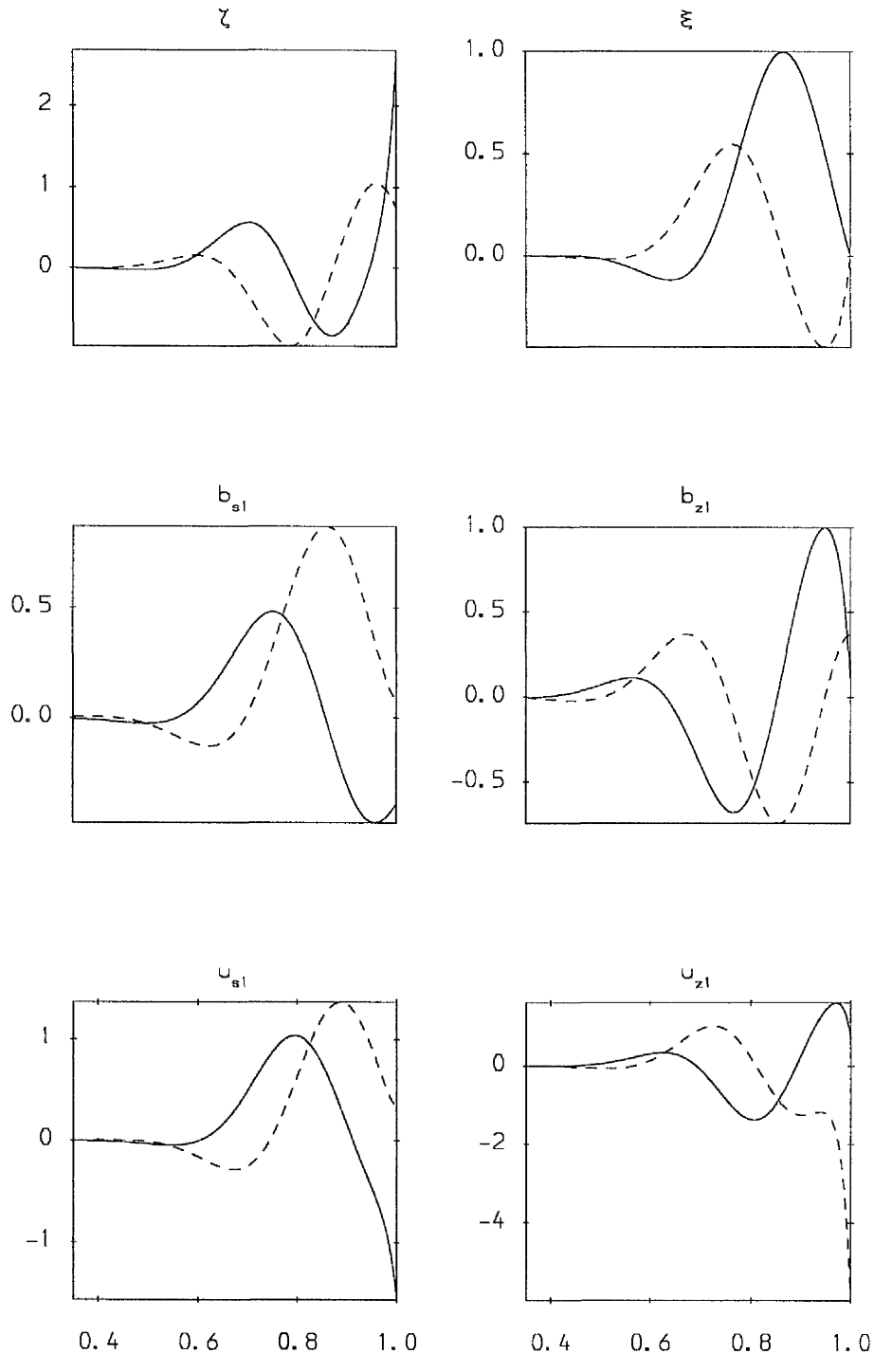

Figure 4.2 Adjoint and linear eigenfunctions of an ideal mode of the basic state (4.56) with $\alpha = 2$, $m = 1$, $\Lambda_c = 387$, $n_c = 8.64$ and $\omega_c = -1.11$.

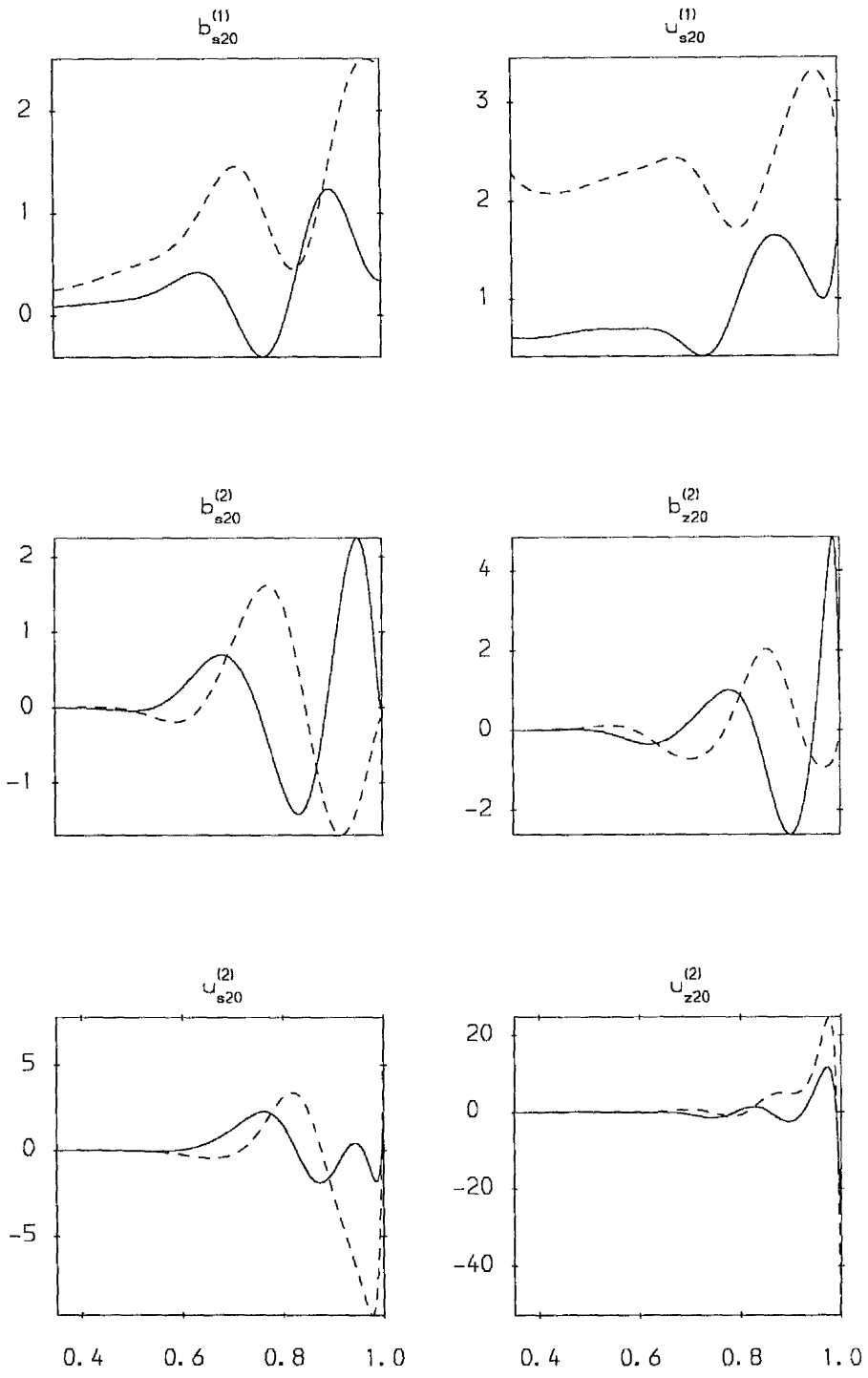

Figure 4.3 Order A^2 solutions for the mode of Figure (4.2) (note $b^{(1)}_{z20} \equiv u^{(1)}_{z20} \equiv 0$).

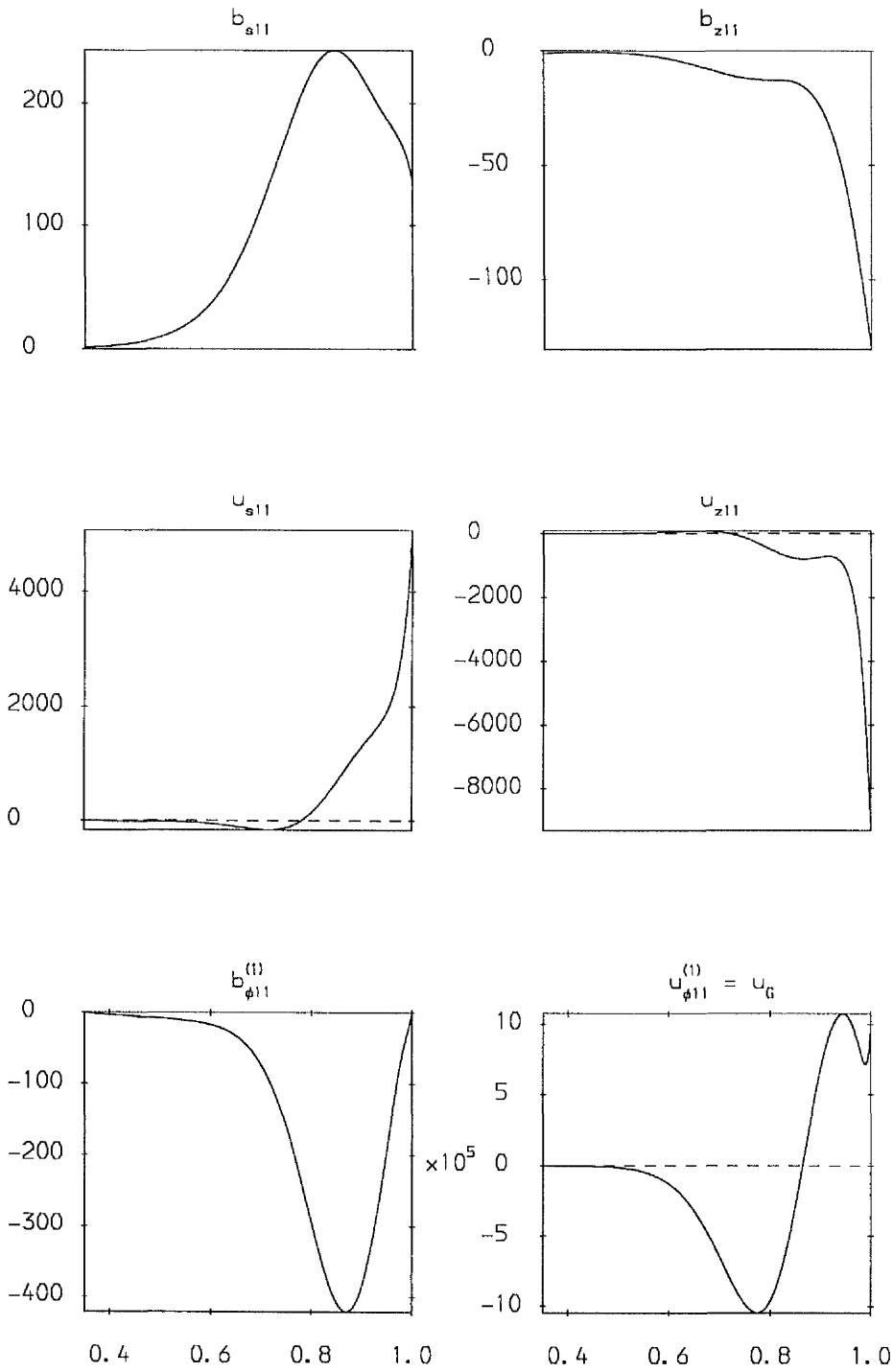

Figure 4.4 Order $|A|^2$ solutions, including the geostrophic flow (with $E = 10^{-10}$), for the mode of Figure (4.2) (note $b^{(1)}_{s11} \equiv b^{(1)}_{z11} \equiv u^{(1)}_{z11} \equiv 0$).

the annulus where the field gradient is largest and therefore most unstable. This instability was found to be subcritical, as was each case of the basic state (4.56).

For the field (4.57) the picture is less straightforward. When $m = 1$ modes were investigated [these modes are not easily classified as ideal or resistive - see Fearn (1988)] the criticality depended on the field geometry, the cases $\beta = 1$, 2 and 3 were found to be subcritical but $\beta = 4$ was supercritical. For $m = 2$, all cases considered were subcritical. Samples of the linear and nonlinear states of an $m = 1$ and $m = 2$ mode of field (4.57) are illustrated in Figures 4.5–4.6 and 4.7–4.8 respectively.

4.3.3 The effect of the geostrophic flow on Λ_c

In this section we consider how the geostrophic flow generated by the nonlinear interactions of the perturbations will influence the stability of the basic state. To do this we consider the flow $u^{(1)}_{\phi 11}$ calculated for the case $\Re_m = 0$. Using this flow (normalised so that $\max|u^{(1)}_{\phi 11}| = 1$) as input into the linear code [i.e., we let Ω take the form of $u^{(1)}_{\phi 11}$ in (4.6)] we increase $\Re_m$ slightly from $\Re_m = 0$ and calculate Λ_c. This is illustrated in Figure 4.9.

As expected, for the case of subcritical instability the differential rotation plays a destabilising role and instability is found at lower Λ_c. For supercritical instability the differential rotation is a stabilising effect and Λ_c is increased.

4.4 CONCLUSION

In this chapter we have investigated the weakly nonlinear stability of a toroidal magnetic field in an electrically conducting fluid bounded by cylindrical insulating walls and perfectly conducting horizontal plates. The simplicity of the boundary conditions on the perfectly conducting plates allowed us to separate out the z-dependence of the perturbations in a simple way permitting consideration of discrete modes of instability in the absence of the sideband effect (the $O(\epsilon)$ correction to n that would occur as Λ is increased above Λ_c if n were continuous - this would result in a 'band' of modes for a given value of Λ rather than a discrete mode).

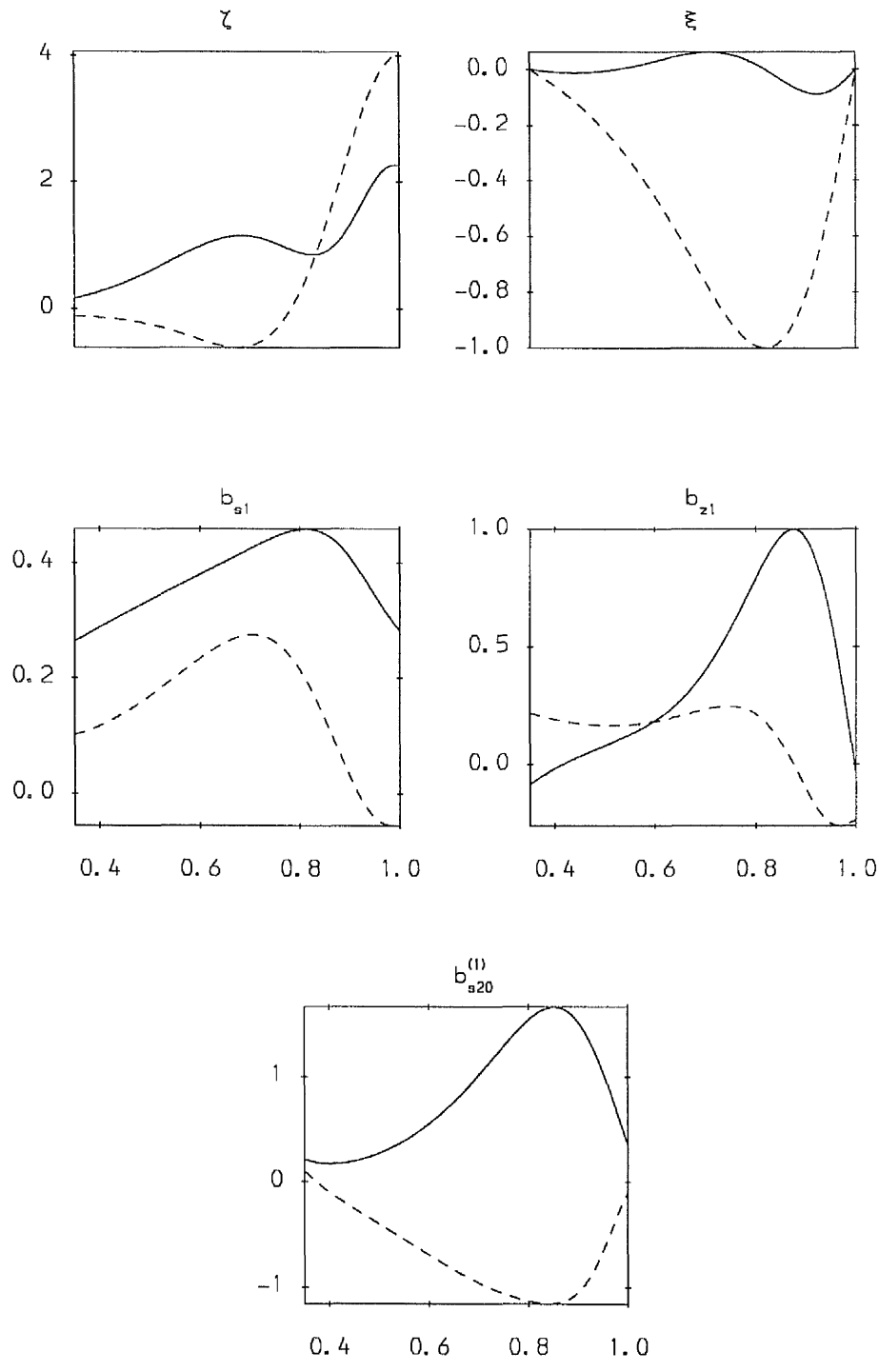

Figure 4.5 The adjoint state, linear eigenfunctions and $O(A^2)$ solution of the most unstable $m = 1$ mode of the basic state (4.57) for the case $\beta = 4$ with $\Lambda_c = 16.3$, $n = 3$ and $\omega_c = -1.04$. The mode is supercritical.

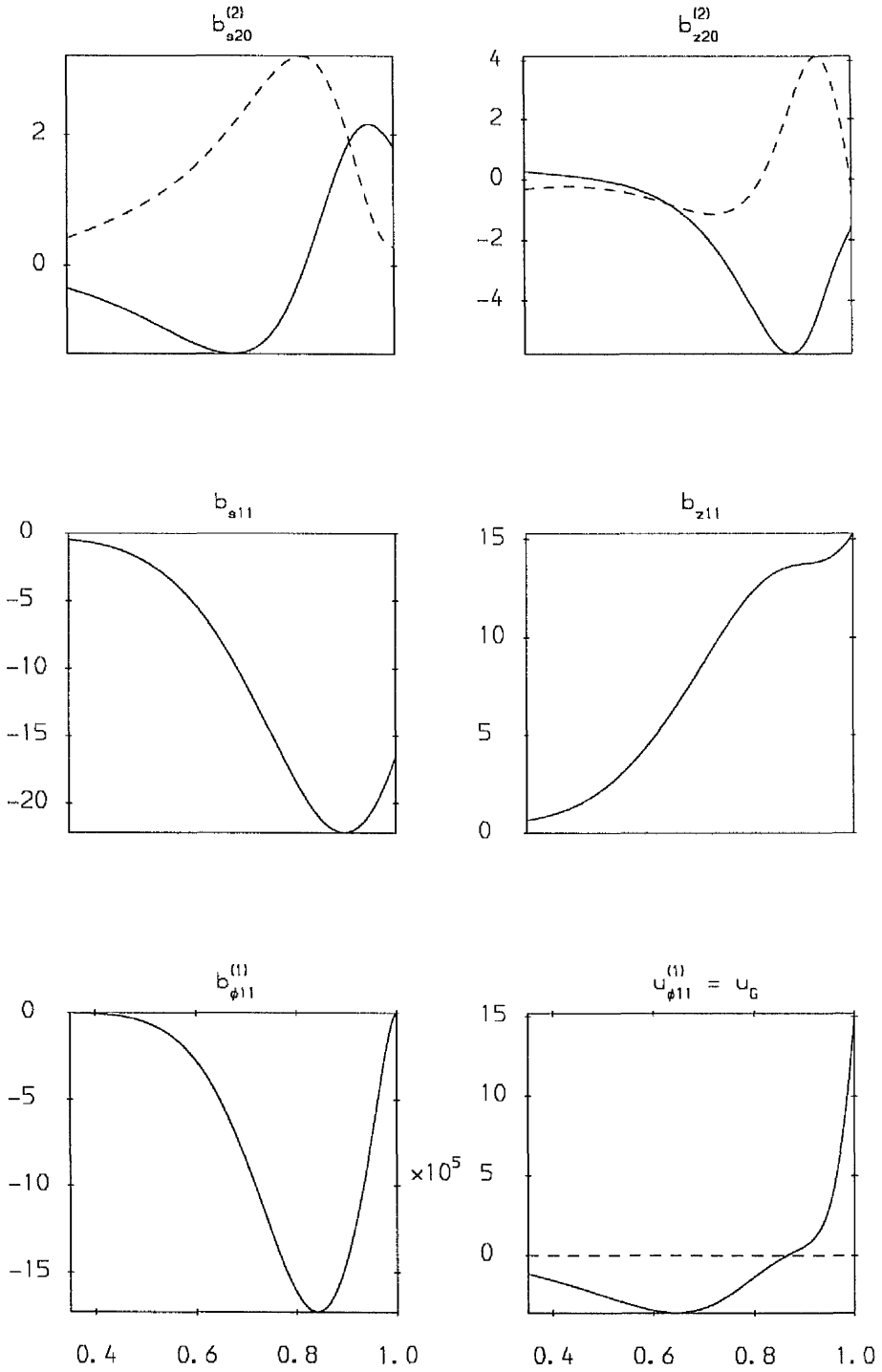

Figure 4.6 $O(A^2)$ and $O(|A|^2)$ solutions, including the geostrophic flow (with $E = 10^{-10}$), for the mode of Figure (4.5).

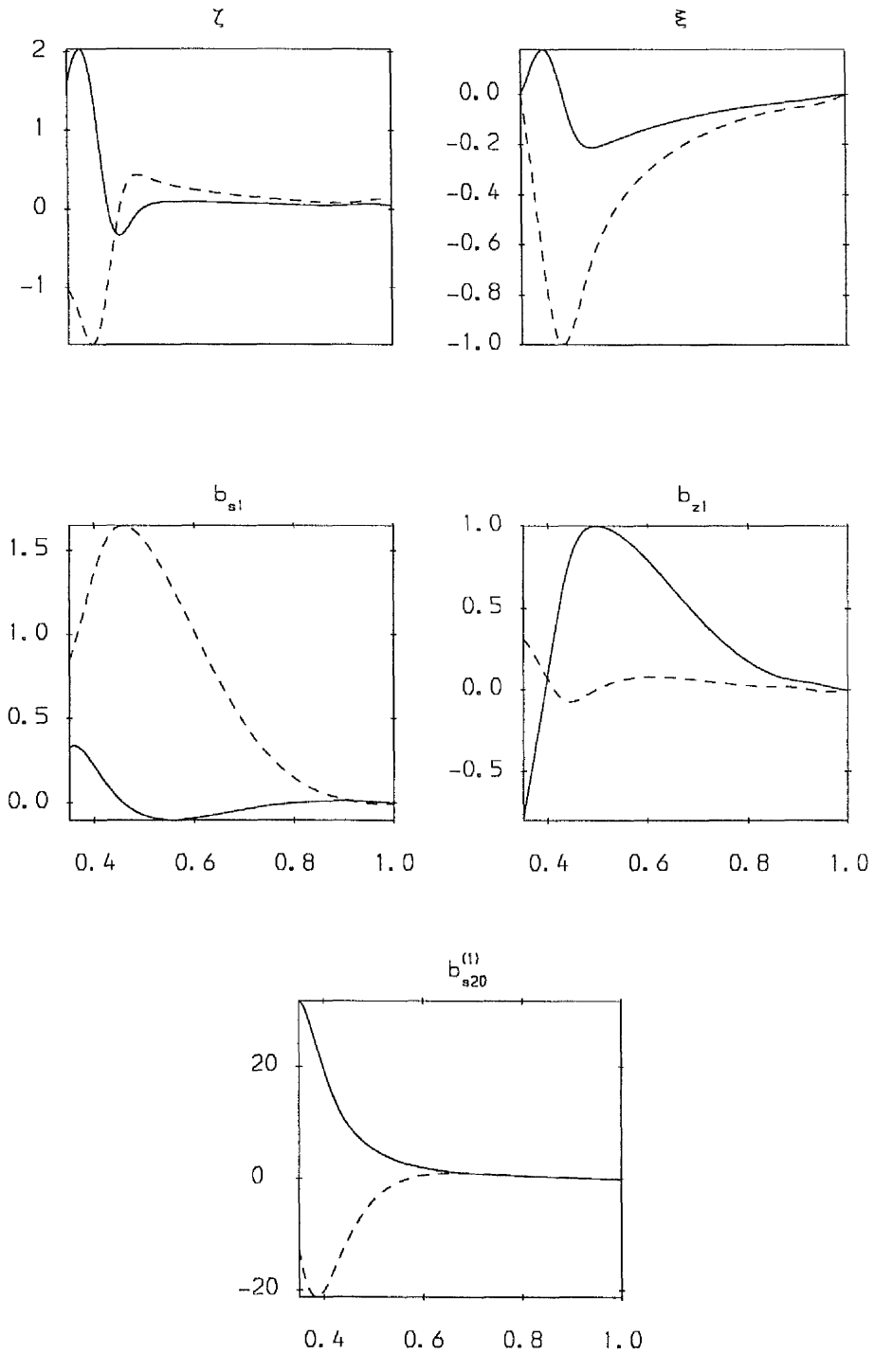

Figure 4.7 The adjoint state, linear eigenfunctions and $O(A^2)$ solution of an ideal mode of the basic state (4.57) with $\beta = 1$, $m = 2$, $\Lambda_c = 501$, $n = 9.4$ and $\omega_c = -0.928$. The mode is subcritical.

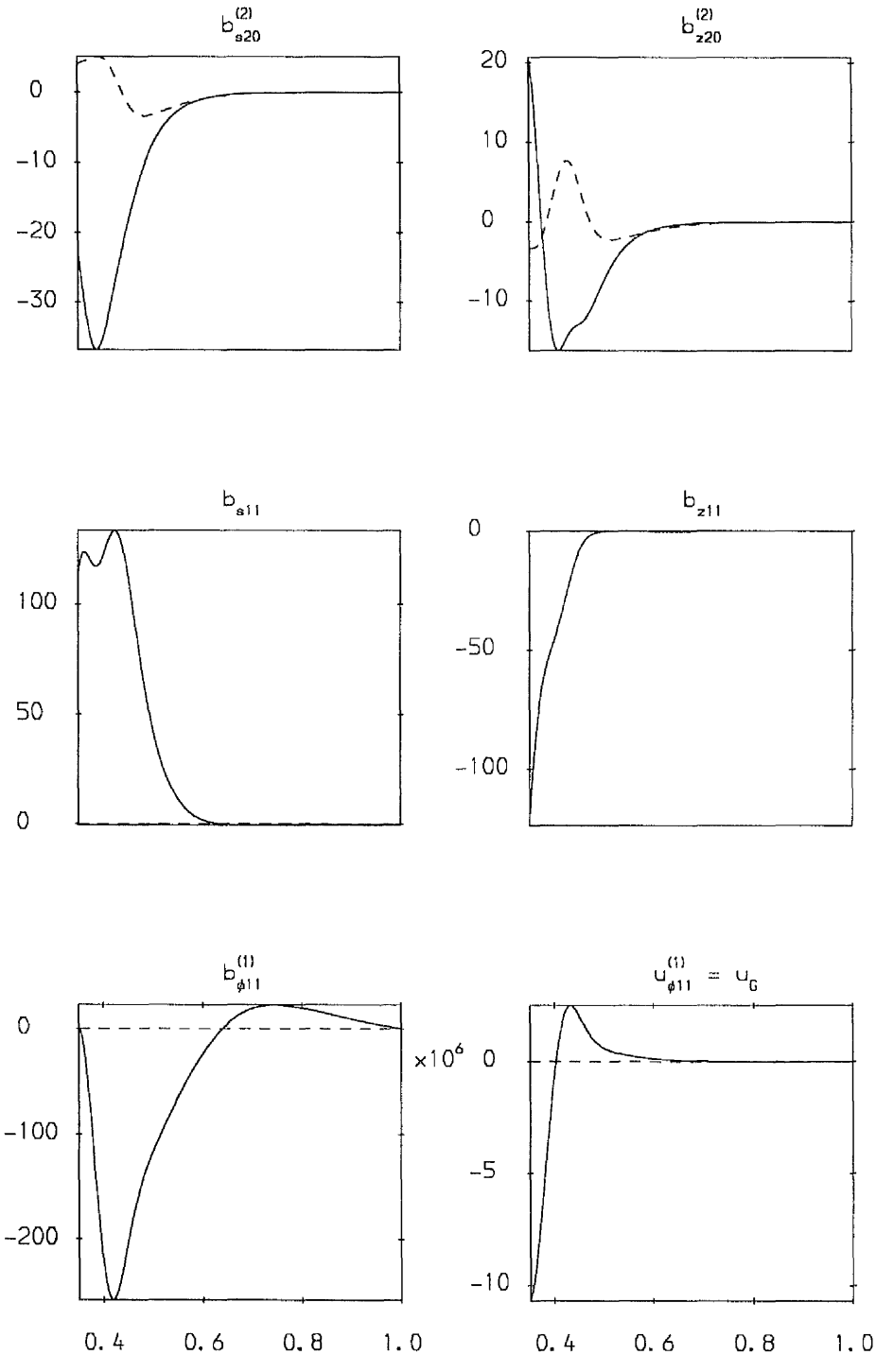

Figure 4.8 $O(A^2)$ and $O(|A|^2)$ solutions, including the geostrophic flow (with $E = 10^{-10}$), for the mode of Figure (4.7).

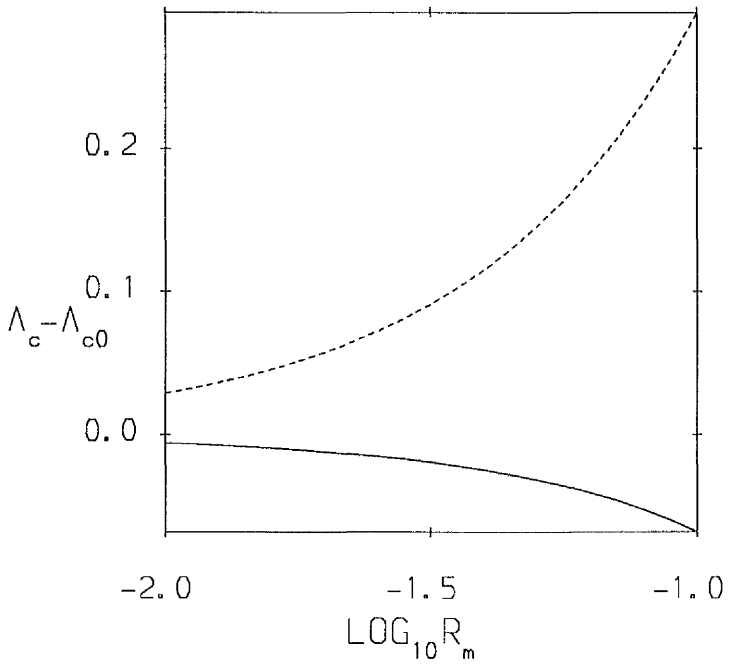

Figure 4.9 The effect of the geostrophic flow $u_{\phi 11}$ on the critical field strength Λ_c. Each curve is an instability of field (4.57); the full line is a subcritical resistive instability with $\beta = 1$, $m = 2$, $n = 3$, $\Lambda_c = 28.9$, $\omega_c = 0.160$ (at $\Re_m = 0$), the dashed line a supercritical 'mixed' mode with $\beta = 4$, $m = 1$, $n = 3$, $\Lambda_c = 16.4$, $\omega_c = -1.04$ (at $\Re_m = 0$). Λ_{c0} refers to Λ_c at $\Re_m = 0$.

The interactions of the perturbations were found to give rise to terms independent of z and ϕ which were modifications to the basic state. Of these the geostrophic velocity was determined by considering the importance of viscosity in the boundary layers (eg. Fearn, Roberts and Soward, 1988). The magnitude of this velocity is proportional to $E^{-1/2}$. For sufficiently small values of E therefore this term dominates the nonlinear terms in the expression determining h. By including all of these nonlinear terms we were able to estimate its relative importance and found that very small values of E were required before the integrand of (A63) was dominated by the geostrophic flow (typically, at $E = 10^{-8}$, the geostrophic flow accounted for $\sim$ 50–80% of the integral (A63).

Of primary interest of course is the most unstable mode of a given basic state. For the case of a monotonic field, unstable only to the field gradient instability, we found that the most unstable mode, and indeed every mode, was a subcritical instability. The more interesting case of a field vanishing at the boundaries was less straightforward. With $m = 1$ the modes were sub- or supercritical depending on the geometry of the field. For $\beta = 1$ (when the maximum of the field (4.57) is in in the centre of the annulus) and $\beta = 2$ the modes were found to be subcritical but for $\beta = 4$ with the field maximum near the outer boundary supercritical instability was found. Of these cases, the latter also corresponds to the lowest Λ_c i.e., the most unstable mode considered. With $m = 2$ or $m = 3$ only subcritical instability was found although again only $\beta \leq 4$ was considered.

The method we have used here does not allow us to determine the nonlinear equilibrium state of subcritical instability since an assumption that the perturbations are small is made. To do this an alternative approach will be required. However, the general predominance of subcritical instability in the cases we have considered here of both ideal and resistive instability enhances the possibility that instability of this type may be responsible for some of the rapid phenomenon observed in the Earth's magnetic field, in particular the very short timescales on which polarity reversals occur.

CHAPTER 5

Conclusion

The work discussed in this thesis represents a further step towards understanding the importance of magnetic instability in the dynamics of the Earth's core. We have focused here on two aspects of magnetic instability. The first was to investigate the role of the boundary conditions in the linear stability analysis; the second was to make some progress beyond the linear regime into the nonlinear regime.

Previous studies of magnetic instability have assumed the boundaries to be either perfectly insulating or perfectly conducting. This simplifies the problem since the need to solve equations in the inner core or mantle is avoided. The aim of Chapters 2 and 3 was to explore more realistic boundary conditions. In Chapter 2 we incorporated a finitely conducting inner core into the problem and found that instability was most readily excited when the conductivity of the inner core was comparable with that of the outer core. This is significant since it represents the situation in the Earth and suggests that the inclusion of a finitely conducting core in future studies of magnetic instability would be worthwhile. When the conductivity of the D'' layer (the conducting layer at the base of the largely insulating mantle) was considered in Chapter 3, its influence on the field strengths required for the onset of instability was found to be small. This is unsurprising since the layer is relatively very thin. However, it was found that the direction of propagation of resistive instabilities was dependent on the conductivity of the D'' layer which may be of interest in view of the observed westward drift of some features of the Earth's field.

The second general aspect we considered was the question of whether the instabilities thought most likely to be important within the Earth, the field gradient

and resistive instabilities, are sub- or supercritical. We found them to be predominantly subcritical, although for the more interesting case of a field vanishing at the boundaries this was dependent on the azimuthal wave number, m, and the exact field geometry. Subcritical instability is of particular interest since it provides for the rapid evolution of the field into a stable finite amplitude equilibrium at field strengths lower than that required for marginal stability. This could be of relevance to the polarity reversals observed in the Earth since there is evidence these are triggered by fluid instability in the outer core (McFadden and Merrill, 1993).

Although many authors have carried out stability analyses of both magnetically and thermally driven instability in the Earth there is much that remains to be done. In particular, the finite amplitude analysis mentioned above was able to tell us whether the instabilities were sub- or supercritical but in the case of subcritical instability it was unable to describe the stable finite amplitude states. To do this some alternative approach is required. It is, of course, also highly desirable to carry out these studies in the more realistic spherical geometry. This is of added importance in the light of ongoing attempts to solve the full nonlinear dynamo problem numerically.

REFERENCES

Abramowitz, M. and Stegun, I.A., 1965. *Handbook of Mathematical Functions,* Dover, New York

Acheson, D.J., 1972. On the hydromagnetic stability of a rotating fluid annulus, *J. Fluid Mech.* **52**, 529–541

Acheson, D.J., 1973. Hydromagnetic wavelike instabilities in a rapidly rotating stratified fluid, *J. Fluid Mech.* **61**, 609–624

Acheson, D.J., 1980. 'Stable' density stratification as a catalyst for instability, *J. Fluid Mech.* **96**, 723–733

Acheson, D.J., 1983. Local analysis of thermal and magnetic instabilities in a rapidly rotating fluid, *Geophys. Astrophys. Fluid Dynam.* **27**, 123–136

Backus, G.E., 1957. The axisymmetric self-excited fluid dynamo, *Astrophys. J.* **125** 500–524

Backus, G.E. and Chandresekhar, S., 1956. On Cowling's theorem on the impossibility of self-maintained axisymmetric homogeneous dynamos, *Proc. Natl. Acad. Sci. USA,* **42** 105–109

Bataille, K. and Flatté, S.M., 1988. Inhomogeneities near the core-mantle boundary inferred from short-period scattering PKP waves recorded at the global digital seismograph network, *J. Geophys. Res.* **93**, 15,057–15,064

Benton, E. R. and Whaler, K.A., 1983. Rapid diffusion of the poloidal geomagnetic field through the weakly conducting mantle: a perturbation solution, *Geophys. J. R. Astr. Soc.* **75**, 77–100

Bloxham, J., Gubbins, D. and Jackson A., 1989. Geomagnetic secular variation, *Phil. Trans. R. Soc. Lond.* A**329**, 415–502

Bloxham, J. and Jackson A., 1991. Fluid flow near the surface of the Earth's outer core, (Abstract), *Geophys. Astrophys. Fluid Dynam.* **60**, 366–368

Condi, F.J., 1978. Sidewall boundary layers in rapidly rotating convection, Woods Hole Oceanographic Institution Technical Report WHOI-78-67 Vol. II, 18–24

Cowling, T.G., 1957. The dynamo maintenance of steady magnetic fields, *Q.J. Mech. Appl. Math.* **10** 129–136

Drazin, P.G. and Reid, W.H., 1981. *Hydrodynamic Stability* , Cambridge

University Press

Drew, S.J., 1991. Thermal convection in a spherical shell with a variable radius ratio, *Geophys. Astrophys. Fluid Dynam.* **59**, 165–183

Drew, S.J., 1993. Magnetic field expulsion into a conducting mantle, *Geophys. J. Int.* **115**, 303–312

DuCruix, J., Courtillot, V. and le Mouël, J.-L., 1980. The late 1960's secular variation impulse, the eleven year magnetic variation and the electrical conductivity of the deep mantle, *Geophys. J. R. Astr. Soc.* **61**, 73–94

Eltayeb, I.A. and Kumar S., 1977. Hydromagnetic convective instability of a rotating self-gravitating fluid sphere containing a uniform distribution of heat sources, *Proc R. Soc. Lond.* A**353**, 145–162

Fearn, D.R., 1979. Thermally driven hydromagnetic instabilities in a rapidly rotating fluid sphere, *Proc R. Soc. Lond.* A**369**, 227–242

Fearn, D.R., 1983a. Boundary conditions for a rapidly rotating hydromagnetic system in a cylindrical container, *Geophys. Astrophys. Fluid Dynam.* **25**, 65–75

Fearn, D.R., 1983b. Hydromagnetic waves in a differentially rotating annulus I. A test of local stability analysis, *Geophys. Astrophys. Fluid Dynam.* **27**, 137–162

Fearn, D.R., 1984. Hydromagnetic waves in a differentially rotating annulus II. Resistive instabilities, *Geophys. Astrophys. Fluid Dynam.* **30**, 227–239

Fearn, D.R., 1985. Hydromagnetic waves in a differentially rotating annulus III. The effect of an axial field, *Geophys. Astrophys. Fluid Dynam.* **33**, 185–197

Fearn, D.R., 1988. Hydromagnetic waves in a differentially rotating annulus IV. Insulating boundaries, *Geophys. Astrophys. Fluid Dynam.* **44**, 55–75

Fearn, D.R., 1989. Compositional convection and the Earth's core, in *Geomagnetism and Paleomagnetism* pp. 335–346 (ed. F. J. Lowes *et al*) , Kluwer Academic Publishers, Dordrecht

Fearn, D.R., 1991. Eigensolution of boundary value problems using inverse iteration, *J. Comp. Appl. Math.* **34**, 201–209

Fearn, D.R., 1993. Magnetic instabilities in rapidly rotating systems, in *Theory of Solar and Planetary Dynamos* (ed. M.R.E. Proctor, P.C. Matthews & A.M. Rucklidge), Cambridge University Press, in press

Fearn, D.R., 1994. Nonlinear planetary dynamos, in *Stellar and Planetary Dynamos* (ed. M.R.E. Proctor & A.D. Gilbert), Cambridge University Press, in press

Fearn, D.R. and Kuang, W., 1993. Resistive instability in the absence of critical levels, *Geophys. Astrophys. Fluid Dynam.* , in press

Fearn, D.R. and Proctor M.R.E., 1983a. Hydromagnetic waves in a differentially rotating sphere, *J. Fluid Mech.* **128**, 1–20

Fearn, D.R. and Proctor M.R.E., 1983b. The stabilising role of differential rotation on hydromagnetic waves, *J. Fluid Mech.* **128**, 21–36

Fearn, D.R. and Proctor M.R.E., 1987. Dynamically consistent magnetic fields produced by differential rotation, *J. Fluid Mech.* **178**, 521–534

Fearn, D.R. and Proctor M.R.E., 1992. Magnetostrophic balance in non-axisymmetric non standard dynamo models, *Geophys. Astrophys. Fluid Dynam.* **67**, 117–128

Fearn, D.R. and Weiglhofer, W.S., 1991a. Magnetic instabilities in rapidly rotating spherical geometries I. from cylinders to spheres, *Geophys. Astrophys. Fluid Dynam.* **56**, 159–181

Fearn, D.R. and Weiglhofer, W.S., 1991b. Magnetic instabilities in rapidly rotating spherical geometries II. more realistic fields and resistive instabilities, *Geophys. Astrophys. Fluid Dynam.* **60**, 275–294

Fearn, D.R. and Weiglhofer, W.S., 1992. Resistive instabilities and the magnetostrophic approximation, *Geophys. Astrophys. Fluid Dynam.* **63**, 111–158

Furth, H.P., Killeen, J., and Rosenbluth, M.N., 1963. Finite-resistivity instabilities of a sheet pinch, *Phys. Fluids* **6** 459–484

Gilbert, W., 1600. *De Magnete*, Dover Publications Inc., New York, 1958 (English translation P. Fleury Mottelay 1893)

Gubbins, D., 1973. Numerical solutions of the kinematic dynamo problem, *Phil. Trans. R. Soc. Lond.* A**274**, 493–521

Gubbins, D., 1977. Energetics of the Earth's core, *J. Geophys.* 43 453–464

Gubbins, D., 1982. Finding core motions from magnetic observations, *Phil. Trans. R. Soc. Lond.* A**306**, 247–254

Gubbins, D., 1991. On unique determination of toroidal or geostrophic flow

in the Earth's core, *Geophys. Astrophys. Fluid Dynam.* **60**, 165–176

Gubbins, D. and Roberts, P.H., 1987. Magnetohydrodynamics of the Earth's core, in *Geomagnetism* Vol. 2, pp 1–177, ed. Jacobs. J., Academic Press, London.

Hide, R., 1966. Free hydromagnetic oscillations of the Earth's core and the theory of the geomagnetic secular variation, *Phil. Trans. R. Soc. Lond.* A**259**, 615–647

Jeanloz, R., 1990. The nature of the Earth's core, *Ann. Rev. Earth Planet. Sci.* **18**, 357–386

Jeanloz, R. and Lay, T., 1993. The core-mantle boundary, *Scientific American* **268** May, 48–55

Kuang, W., 1992. Thesis, University of California, Los Angeles,

Kuang, W. and Roberts, P.H., 1990. Resistive instabilities in rapidly rotating fluids: Linear theory of the tearing mode, *Geophys. Astrophys. Fluid Dynam.* **55**, 199–239

Kuang, W. and Roberts, P.H., 1991. Resistive instabilities in rapidly rotating fluids: Linear theory of the g-mode, *Geophys. Astrophys. Fluid Dynam.* **60**, 295–332

Kuang, W. and Roberts, P.H., 1992. Resistive instabilities in rapidly rotating fluids: Linear theory of the convective modes, *Geophys. Astrophys. Fluid Dynam.* **67**, 129–162

Kumar, S. and Roberts, P.H., 1975. A three-dimensional kinematic dynamo, *Proc R. Soc. Lond.* A**344**, 235–258

Lamb, C.J., 1994a. Magnetic instability in a rapidly rotating cylindrical annulus with a finitely conducting inner core, *Geophys. Astrophys. Fluid Dynam.* , in press

Lamb, C.J., 1994b. The effect of a finitely conducting layer in the mantle on magnetic instability in the core, *Geophys. J. Int.* , submitted

Lan, S., Kuang, W. and Roberts, P.H., 1993. Ideal instabilities in rapidly rotating MHD systems that have critical layers, *Geophys. Astrophys. Fluid Dynam.* **69**, 133–160

Li, X. and Jeanloz, R., 1987. Electrical conductivity of (Mg,Fe)SiO_3 perovskite and a perovskite-dominated assemblage at lower mantle conditions, *Geophys.*

Res. Lett. **14**, 1075–1078

Loper, D.E., 1989. Dynamo energetics and the structure of the outer core, *Geophys. Astrophys. Fluid Dynam.* **49**, 213–217

Malkus, W.V.R., 1967. Hydromagnetic planetary waves, *J. Fluid Mech.* **28**, 793–802

McFadden, P.L. and Merrill, R.T., 1993. Inhibition and geomagnetic field reversals, *J. Geophys. Res.* **98**, 6189–6199

Peters, G. and Wilkinson, J.H., 1971a. Eigenvectors of real and complex matrices by LR and QR triangularisations, in *Handbook for Automatic computation* Vol. 2: Linear Algebra, eds. Wilkinson, J.H. and Reinsch, C. pp. 370–395, Springer.

Peters, G. and Wilkinson, J.H., 1971b. The calculation of specified eigenvectors by inverse iteration, in *Handbook for Automatic computation* Vol. 2: Linear Algebra, eds. Wilkinson, J.H. and Reinsch, C. pp. 418–439, Springer.

Peyronneau, J. and Poirier, J.P., 1989. Electrical conductivity of the Earth's lower mantle, *Nature* **342**, 537–539

Roberts, P.H., 1968. On the thermal instability of a rotating fluid sphere containing heat sources, *Phil. Trans. R. Soc. Lond.* **A263**, 93–117

Roberts, P.H. and Loper, D.E., 1979. On the diffusive instability of some simple steady magnetohydrodynamic flows, *J. Fluid Mech.* **90**, 641–668

Roberts, P.H. and Stewartson, K., 1974. On finite amplitude convection in a rotating magnetic system, *Proc R. Soc. Lond.* **A277**, 93–117

Roberts, P.H. and Stewartson, K., 1975. Double roll convection in a rotating magnetic system, *J. Fluid Mech.* **68**, 447–466

Skinner, P.H. and Soward, A.M., 1988. Convection in a rotating magnetic system and Taylor's constraint, *Geophys. Astrophys. Fluid Dynam.* **44**, 91–116

Soward, A.M., 1979. Thermal and magnetically driven convection in a rapidly rotating fluid layer, *J. Fluid Mech.* **90**, 669–684

Soward, A.M., 1980. Finite amplitude thermal convection and geostrophic flow in a rotating magnetic system, *J. Fluid Mech.* **98**, 449–471

Soward, A.M., 1986. Non-linear marginal convection in a rotating magnetic

system, *Geophys. Astrophys. Fluid Dynam.* **35**, 329–371

Soward, A.M., 1989. Geodynamo Theory, in *Geomagnetism and Paleomagnetism* pp. 297–317 (ed. F. J. Lowes *et al*) , Kluwer Academic Publishers, Dordrecht

Soward, A.M. and Jones, C.A., 1983. α^2-dynamos and Taylor's constraint, *Geophys. Astrophys. Fluid Dynam.* **27**, 87–122

Sparrow, E.M., Goldstein, R.J. and Jonsson, V.K., 1963. Thermal instability in a horizontal fluid layer: effect of boundary conditions and non-linear temperature profile, *J. Fluid Mech.* **18**, 513–528

Taylor, J.B., 1963. The magneto-hydrodynamics of a rotating fluid and the earth's dynamo problem, *Proc R. Soc. Lond.* A**274**, 274–283

Young, C.J. and Lay, T., 1987. The core-mantle boundary, *Ann. Rev. Earth Planet. Sci.* **15**, 25–46

Zhang, K. and Fearn, D.R., 1993. How strong is the invisible component of the magnetic field in the Earth's core?, *Geophys. Res. Lett.* , submitted

Zhang, K. and Fearn, D.R., 1994. Hydromagnetic waaves in rapidly rotating spherical shells generated by magnetic toroidal decay modes, *Geophys. Astrophys. Fluid Dynam.* , submitted

Appendix A: Matrix and nonlinear vector expressions

We give here the expressions omitted from the main text of §4.2.3 for clarity. Removal of secular terms from the asymptotic expansion requires that

$$p = O(\epsilon^2), \tag{A1}$$

and from (4.20) this leads to

$$\lambda\epsilon^2 = (\Lambda - \Lambda_c)/\Lambda_c, \tag{A2}$$

or

$$\Lambda^{-1} = \Lambda_c^{-1}(1 - \lambda\epsilon^2 + O(\epsilon^4)). \tag{A3}$$

While the growth rate is $O(\epsilon^2)$ the frequency, ω_i, is $O(1)$ so that we write

$$\omega_i = \omega_c(1 + \delta\epsilon^2), \tag{A4}$$

where $\lambda, \delta = O(1)$. Then, taking (A3)-(A4) together with (4.24) we have

$$L_0 = \begin{bmatrix} L_{01} & L_{02} \\ L_{03} & L_{04} \end{bmatrix} \tag{A5}$$

where

$$\begin{aligned} L_{01} = [&(F^2 + sFF' - sF^2D - \Re_m\Omega)\partial_\phi - \partial\tau_c \\ &+ \Lambda_c^{-1}(3s^{-1}D + D^2 + s^{-2}(1 + \partial_\phi^2) + \partial_z^2)]\partial_z \end{aligned} \tag{A6}$$

$$L_{02} = -F^2s^{-1}(\partial_\phi^2 + s^2\partial_z^2)\partial_\phi + 2s^{-1}\Lambda_c^{-1}\partial_z^2 \tag{A7}$$

$$L_{03} = [Fs^{-1}(1 + \partial_\phi^2) + F^2sD^2 + 3F^2D - 3FF' - sFF'']\partial_\phi \tag{A8}$$

$$\begin{aligned} L_{04} = [&(F(sFD + 4F + sF') - \Re_m\Omega)\partial_\phi - \partial\tau_c \\ &+ \Lambda_c^{-1}(s^{-1}D + D^2 + s^{-2}\partial_\phi^2 + \partial_z^2)]\partial_z \end{aligned} \tag{A9}$$

$$L_2 = \begin{bmatrix} [-\partial_\tau - \lambda\Lambda_c^{-1}(3s^{-1}D + D^2 \\ +s^{-2}(1+\partial_\phi^2) + \partial_z^2)]\partial_z & -2s^{-1}\lambda\Lambda_c^{-1}\partial_z^2 \\ 0 & [-\partial_\tau - \lambda\Lambda_c^{-1}(s^{-1}D + \\ & D^2 + s^{-2}\partial_\phi^2 + \partial_z^2)]\partial_z \end{bmatrix} \tag{A10}$$

where $\partial_z \equiv \frac{\partial}{\partial z}$ and $D \equiv d/ds$. In L_0 above $\partial\tau_c$ means the derivative evaluated at marginal stability (giving the O(1) terms, i.e., the frequency) and in L_2 $\partial\tau$ applies only to the O(ϵ^2 + h.o.t) terms in the time dependence. For example, in (4.32) [with (4.35)] $-\partial\tau_c \mathbf{b}_{20} = 2i\omega_c \mathbf{b}_{20}$ and $\partial\tau$ applies only to the remaining parts of the time dependence.

The nonlinear term in the order ϵ^2 problem is

$$\mathbf{N}_2 = A^2 \begin{bmatrix} N_{201} \\ N_{202} \end{bmatrix} e^{2im\phi} + |A|^2 \begin{bmatrix} N_{111} \\ N_{112} \end{bmatrix} + \overline{A}^2 \begin{bmatrix} N_{021} \\ N_{022} \end{bmatrix} e^{-2im\phi}, \tag{A11}$$

where $N_{201} = \overline{N}_{021}$, $N_{202} = \overline{N}_{022}$. Each of the components in (A11) is determined in terms of the first order solutions from (4.9) giving

$$\begin{aligned} N_{201} = \{ & \frac{2n}{s}[im(u_{s1}b_{\phi 1} - u_{\phi 1}b_{s1}) - in(u_{s1}b_{z1} - u_{z1}b_{s1})] \\ & - \frac{2m^2F}{s}[\frac{b_{\phi 1}}{s}(-mb_{z1} + nsb_{\phi 1}) + b_{s1}(iDb_{z1} + nb_{s1})] \\ & + \frac{2imnF}{s^2}[ib_{z1}(-mb_{z1} + nsb_{\phi 1}) + b_{s1}(D(sb\phi 1) - imb_{s1})]\} \sin 2n(z+d) \end{aligned} \tag{A12}$$

and

$$N_{202} = N_{202}^{(1)} + N_{202}^{(2)} \cos 2n(z+d), \tag{A13}$$

where

$$\begin{aligned} N_{202}^{(1)} = \{ & \frac{im^2FD}{s}[mb_{z1}(ib_{z1} + nsb_{\phi 1}) + b_{s1}(D(sb_{\phi 1}) - imb_{s1})] \\ & + \frac{2m^2F}{s}[-ib_{z1}(iDb_{z1} + nb_{s1}) - \frac{1}{s}b_{\phi 1}(D(sb_{\phi 1}) - imb_{s1})]\}, \end{aligned} \tag{A14}$$

$$N_{202}^{(2)} = \{\frac{n}{s}[iD(u_{s1}b_{z1} - u_{z1}b_{s1}) - 2m(u_{\phi 1}b_{z1} - u_{z1}b_{\phi 1})]$$
$$+ \frac{im^2FD}{s}[-ib_{z1}(mb_{z1} - nsb_{\phi 1}) + b_{s1}(D(sb_{\phi 1}) - imb_{s1})]$$
$$+ \frac{2m^2F}{s}[ib_{z1}(iDb_{z1} + nb_{s1}) - \frac{1}{s}b_{\phi 1}(D(sb_{\phi 1}) - imb_{s1})]\}, \qquad (A15)$$

and

$$N_{111} = \frac{2n^2}{s}[-iu_{s1}\overline{b}_{z1} - i\overline{u}_{s1}b_{z1} - iu_{z1}\overline{b}_{s1} + i\overline{u}_{z1}b_{s1}]\sin 2n(z+d), \qquad (A16)$$

$$N_{112} = \frac{n}{s}D[-iu_{s1}\overline{b}_{z1} - i\overline{u}_{s1}b_{z1} - iu_{z1}\overline{b}_{s1} + i\overline{u}_{z1}b_{s1}]\cos 2n(z+d). \qquad (A17)$$

In (4.35) we therefore have

$$\mathbf{b}_{20} = \begin{bmatrix} b_{s20}^{(1)} + b_{s20}^{(2)}\cos 2n(z+d) \\ b_{z20}^{(1)} + b_{z20}^{(2)}\sin 2n(z+d) \end{bmatrix} e^{2im\phi}, \qquad (A18)$$

and

$$\mathbf{b}_{11} = \begin{bmatrix} b_{s11}^{(1)} + b_{s11}^{(2)}\cos 2n(z+d) \\ b_{z11}^{(1)} + b_{z11}^{(2)}\sin 2n(z+d) \end{bmatrix}. \qquad (A19)$$

Taking the A^2 part of (4.32) and substituting in for L_0, $\mathbf{b}_{20}$ and $\mathbf{N}_{20}$ we find

$$b_{z20}^{(1)} \equiv 0, \qquad (A20)$$

which implies, from (4.4).$\hat{\mathbf{z}}$,

$$u_{z20}^{(1)} \equiv 0, \qquad (A21)$$

Consideration of the appropriate equations shows

$$b_{s11}^{(1)} \equiv b_{z11}^{(1)} \equiv u_{z11}^{(1)} \equiv 0. \qquad (A22)$$

so we write

$$\mathbf{b}_{11} = \begin{bmatrix} b_{s11}\cos 2n(z+d) \\ b_{z11}\sin 2n(z+d) \end{bmatrix}. \qquad (A23)$$

At $O(|A|^2)$ in the momentum equation the perturbations take the form

$$u_{s11} = u_{s11}^{(1)} + u_{s11}^{(2)}\cos 2n(z+d), \qquad (A24)$$

$$u_{\phi 11} = u^{(1)}_{\phi 11} + u^{(2)}_{\phi 11} \sin 2n(z+d), \tag{A25}$$

and, from the induction equation,

$$b_{\phi 11} = b^{(1)}_{\phi 11} + b^{(2)}_{\phi 11} \sin 2n(z+d). \tag{A26}$$

The terms in (A24)–(A26) with superscript (1) are functions only of s and represent modifications to the basic state. The terms $b^{(1)}_{\phi 11}$ and $u^{(1)}_{s11}$ can be found directly from (4.3).$\hat{\phi}$ and (4.4).$\hat{\phi}$ respectively. However, $u^{(1)}_{\phi 11}$ cannot be determined from the momentum equation because (4.3).$\hat{\mathbf{s}}$ determines only the z-derivative of u_ϕ. This is the problem discussed in §4.2.4 - $u^{(1)}_{\phi 11}$ is the geostrophic flow and is determined by reinstating viscous effects important only in the Ekman boundary layers. It can be shown (see §4.2.4 and references therein) that

$$u^{(1)}_{\phi 11} \equiv u_G = \frac{1}{2\pi}(2E)^{-1/2} \int\int_{C(s)} [(\nabla \times \mathbf{B}) \times \mathbf{B}]_\phi d\phi dz. \tag{A27}$$

(note that $u^{(1)}_{s11} = (2d)^{-1}(2E)^{1/2} u^{(1)}_{\phi 11}$).

At the next order the nonlinear terms are

$$\mathbf{N}_3 = A^3 \begin{bmatrix} N_{301} \\ N_{302} \end{bmatrix} e^{3im\phi} + A|A|^2 \begin{bmatrix} N_{211} \\ N_{212} \end{bmatrix} e^{im\phi} + c.c. \tag{A28}$$

We need only consider N_{21} here since it is this term that appears in our solvability condition (4.42). From (4.10) we obtain

$$N_{211} = N^{(1)}_{211} \sin n(z+d) + N^{(2)}_{211} \sin 3n(z+d), \tag{A29}$$

and

$$N_{212} = N^{(1)}_{212} \cos n(z+d) + N^{(2)}_{212} \cos 3n(z+d), \tag{A30}$$

where

$$\begin{aligned} N^{(1)}_{211} = \frac{1}{2s}[&inm(w_1+w_2) + n^2(w_3+w_4+w_5) \\ &- m^2 F(\frac{1}{s}(k_1-k_2) + k_3 - k_4 + k_5) + \frac{inmF}{s}(q_1+q_2+q_3)], \end{aligned} \tag{A31}$$

$$N_{211}^{(2)} = -\frac{1}{2s}[inmw_1 + 9n^2(w_3 - w_4) - m^2F(\frac{1}{s}(k_1 + k_2) + k_3 + k_4) + \frac{3inmF}{s}(-q_1 + q_2)], \quad (A32)$$

$$N_{212}^{(1)} = \frac{1}{2s}[nD(t_1 - t_2 + t_3) + inm(t_4 + t_5 + t_6) - \frac{imF}{s}(1 - D)(q_1 + q_2 + q_3) + m^2F(r_1 - \frac{1}{s}(r_2 + r_3)], \quad (A33)$$

$$N_{212}^{(2)} = \frac{1}{2s}[3nD(t_1 + t_2) + 3imn(t_4 + t_5) + \frac{imF}{s}(1 - D)(q_1 - q_2) - m^2F(r_1 - \frac{1}{s}r_2], \quad (A34)$$

with

$$k_1 = 2[ns(b_{\phi 1}b_{\phi 11}^{(2)} + \bar{b}_{\phi 1}b_{z20}^{(2)}) + im\bar{b}_{\phi 1}b_{\phi 20}^{(2)}], \quad (A35)$$

$$k_2 = -b_{\phi 20}^{(2)}(m\bar{b}_{z1} - ns\bar{b}_{\phi 1}) - b_{\phi 11}^{(2)}(mb_{z1} - nsb_{\phi 1}), \quad (A36)$$

$$k_3 = b_{s1}(Db_{z11} + 2nb_{s11}) + \bar{b}_{s1}(Db_{z20}^{(2)} + 2nb_{s20}^{(2)}), \quad (A37)$$

$$k_4 = b_{s20}^{(2)}(-iD\bar{b}_{z1} + n\bar{b}_{s1}) + b_{s11}(iDb_{z1} + nb_{s1}), \quad (A38)$$

$$k_5 = 2b_{s20}^{(1)}(n\bar{b}_{s1} - iD\bar{b}_{z1}) + 2s^{-1}[b_{\phi 20}^{(1)}(ns\bar{b}_{\phi 1} - m\bar{b}_{z1}) + b_{\phi 11}^{(1)}(nsb_{\phi 1} - mb_{z1})], \quad (A39)$$

$$q_1 = -ib_{z1}(2nsb_{\phi 11}^{(2)} + imb_{z11}) - i\bar{b}_{z1}(imb_{z20}^{(2)} + 2nsb_{\phi 20}^{(2)}), - ns\bar{b}_{\phi 1}b_{z20}^{(2)} - nsb_{\phi 1}b_{z11}, \quad (A40)$$

$$q_2 = b_{s1}(D(sb_{\phi 11}^{(2)}) - imb_{s11}) + \bar{b}_{s1}(D(sb_{\phi 20}^{(2)}) - imb_{s20}^{(2)}) + b_{s20}^{(2)}D(s\bar{b}_{\phi 1}) + b_{s11}D(sb_{\phi 1}), \quad (A41)$$

$$q_3 = 2[b_{s1}D(sb_{\phi 11}^{(1)}) + \bar{b}_{s1}D(sb_{\phi 20}^{(1)}) + b_{s20}^{(1)}D(s\bar{b}_{\phi 1}) - im\bar{b}_{s1}b_{s20}^{(1)})], \quad (A42)$$

$$r_1 = -[ib_{z1}(Db_{z11} + 2nb_{s11}) - i\bar{b}_{z1}(Db_{z20}^{(2)} - 2nb_{s20}) - b_{z20}^{(2)}(iD\bar{b}_{z1} - \bar{b}_{s1}) + b_{z11}(iDb_{z1} + nb_{s1})], \quad (A43)$$

$$r_2 = b_{\phi 1}(D(sb^{(2)}_{\phi 11}) + b_{\phi 11}) + b^{(2)}_{\phi 20}D(s\overline{b}_{\phi 1}) + \overline{b}_{\phi 1}D(sb^{(2)}_{\phi 20}) - 2im\overline{b}_{\phi 1}b^{(2)}_{s20} + b_{\phi 11}(sDb_{\phi 1} + imb_{s1}) + im\overline{b}_{s1}b^{(2)}_{\phi 20}, \quad (A44)$$

$$r_3 = 2[b_{\phi 1}(D(sb^{(1)}_{\phi 11}) + b^{(1)}_{\phi 11}) + \overline{b}_{\phi 1}(D(sb^{(1)}_{\phi 20}) + b^{(1)}_{\phi 20}) - 2imb^{(1)}_{s20}\overline{b}_{\phi 1} + b^{(1)}_{\phi 20}(sD\overline{b}_{\phi 1} + im\overline{b}_{s1} + b^{(1)}_{\phi 11}(sDb_{\phi 1} - imb_{s1})], \quad (A45)$$

$$t_1 = u_{s1}b_{z11} + \overline{u}_{s1}b^{(2)}_{z20} - u^{(2)}_{z20}\overline{b}_{s1} - u_{z11}b_{s1}, \quad (A46)$$

$$t_2 = -iu^{(2)}_{s20}\overline{b}_{z1} + iu^{(2)}_{s11}b_{z1} - iu_{z1}b_{s11} + i\overline{u}_{z1}b^{(2)}_{s20}, \quad (A47)$$

$$t_3 = 2i(\overline{u}_{z1}b^{(1)}_{s20} - u^{(1)}_{s20}\overline{b}_{z1} + u^{(1)}_{s11}b_{z1}), \quad (A48)$$

$$t_4 = u_{\phi 1}b_{z11} + \overline{u}_{\phi 1}b^{(2)}_{z20} + u^{(2)}_{z20}\overline{b}_{\phi 1} - u_{z11}b_{\phi 1}, \quad (A49)$$

$$t_5 = iu^{(2)}_{\phi 20}\overline{b}_{z1} - iu^{(2)}_{\phi 11}b_{z1} + iu_{z1}b^{(2)}_{\phi 11} - i\overline{u}_{z1}b^{(2)}_{\phi 20}, \quad (A50)$$

$$t_6 = -2i(u^{(1)}_{\phi 20}\overline{b}_{z1} - \overline{u}_{z1}b^{(1)}_{\phi 20} - u^{(1)}_{\phi 11}b_{z1} + u_{z1}b^{(1)}_{\phi 11}), \quad (A51)$$

and

$$w_1 = u_{s1}b^{(2)}_{\phi 11} + \overline{u}_{s1}b^{(2)}_{\phi 20} + u^{(2)}_{s20}\overline{b}_{\phi 1} + u^{(2)}_{s11}b_{\phi 1} - u_{\phi 1}b_{s11} - \overline{u}_{\phi 1}b^{(2)}_{s20} - u^{(2)}_{\phi 20}\overline{b}_{s1} - u^{(2)}_{\phi 11}b_{s1}, \quad (A52)$$

$$w_2 = 2(u_{s1}b^{(1)}_{\phi 11} + \overline{u}_{s1}b^{(1)}_{\phi 20} + u^{(1)}_{s20}\overline{b}_{\phi 1} + u^{(1)}_{s11}b_{\phi 1} - \overline{u}_{\phi 1}b^{(1)}_{s20} - u^{(1)}_{\phi 20}\overline{b}_{s1}) - u^{(1)}_{\phi 11}b_{s1}, \quad (A53)$$

$$w_3 = u_{s1}b_{z11} + \overline{u}_{s1}b^{(2)}_{z20} - u^{(2)}_{z20}\overline{b}_{s1} - u_{z11}b_{s1}, \quad (A54)$$

$$w_4 = -iu^{(2)}_{s20}\overline{b}_{z1} - iu^{(2)}_{s11}b_{z1} + iu_{z1}b_{s11} - i\overline{u}_{z1}b^{(2)}_{s20}, \quad (A55)$$

$$w_5 = -2i(u^{(1)}_{s20}\overline{b}_{z1} - u^{(1)}_{s11}b_{z1} - \overline{u}_{z1}b^{(1)}_{s20}). \quad (A56)$$

The solvability condition is

$$a_1\frac{dA}{d\tau} = a_2\lambda A + a_3 A|A|^2. \quad (A57)$$

where

$$a_1 = \int_{-d}^{d}\int_{s_{ib}}^{1} [n\overline{\zeta}\sin n(z+d)b_{s1}\sin n(z+d) - n\overline{\xi}\cos n(z+d)b_{z1}\cos n(z+d)]\, dsdz, \qquad (A58)$$

$$a_2 = -\Lambda_c^{-1}\int_{-d}^{d}\int_{s_{ib}}^{1} \overline{\zeta}\sin n(z+d)[(3s^{-1}D + D^2 + s^{-2}(1-m^2) - n^2)nb_{s1} - 2is^{-1}n^2 b_{z1}]\sin n(z+d) + \overline{\xi}\cos n(z+d)[(s^{-1}D + D^2 - s^{-2}m^2 - n^2)nb_{z1}\cos n(z+d)]\, dsdz, \qquad (A59)$$

$$a_3 = \int_{-d}^{d}\int_{s_{ib}}^{1} \overline{\zeta}\sin n(z+d)[N_{211}^{(1)}\sin n(z+d) + N_{211}^{(2)} sin3n(z+d)] - i\overline{\xi}\cos n(z+d)[N_{212}^{(1)}\cos n(z+d) + N_{212}^{(2)}\cos 3n(z+d)]\, dsdz. \qquad (A60)$$

After integration with respect to z these become

$$a_1 = nd\int_{s_{ib}}^{1} [\overline{\zeta}b_{s1} - \overline{\xi}b_{z1}]\, ds, \qquad (A61)$$

$$a_2 = -nd\Lambda_c^{-1}\int_{s_{ib}}^{1} \overline{\zeta}[(3s^{-1}D + D^2 + s^{-2}(1-m^2) - n^2)b_{s1} + 2ins^{-1}b_{z1}] - \overline{\xi}[(s^{-1}D + D^2 - s^{-2}m^2 - n^2)b_{z1}]\, ds, \qquad (A62)$$

$$a_3 = d\int_{s_{ib}}^{1} [\overline{\zeta}N_{211}^{(1)} - i\overline{\xi}N_{212}^{(1)}]\, ds. \qquad (A63)$$

The amplitude equation (A57) then becomes, after multiplying by ϵ^3 and redefining $A(\tau) \to \epsilon A(t)$,

$$\frac{dA}{dt} = c\Delta\Lambda A + hA|A|^2, \qquad (A64)$$

where

$$c = \frac{a_2}{a_1}, \qquad h = \frac{a_3}{a_1}, \qquad \Delta\Lambda = \frac{\Lambda - \Lambda_c}{\Lambda_c}, \qquad (A65)$$

For realistic values of the Ekman number E in (A25) the integrand in (A61) is dominated by the geostrophic flow and it follows that h, the parameter that determines if an instability is sub- or supercritical, is in turn dominated by $u_{\phi 11}^{(1)}$.

Appendix B: The adjoint problem

In the adjoint problem we are seeking to determine $\mathbf{b}_1^\dagger$ satisfying

$$L_0^\dagger \mathbf{b}_1^\dagger = \mathbf{0}, \tag{B1}$$

where the adjoint operator $L_0^\dagger$ is determined using the property

$$\langle \mathbf{b}_1^\dagger, L_0 \mathbf{b}_1 \rangle \;=\; \langle L_0^\dagger \mathbf{b}_1^\dagger, \mathbf{b}_1 \rangle. \tag{B2}$$

Starting with the left hand side of (B2) and integrating by parts with respect to z we obtain

$$\langle \mathbf{b}_1^\dagger, L_0 \mathbf{b}_1 \rangle \;= A + C + \int_{-d}^{d} \int_{s_{ib}}^{1} \mathbf{b}_1 \overline{L}_0^\dagger \mathbf{b}_1^\dagger \, ds dz, \tag{B3}$$

where, after taking onto account (4.12) and (4.13),

$$\begin{aligned} A = \int_{s_{ib}}^{1} [& \Lambda_c^{-1} \partial_z^2 \zeta - im\zeta(F^2 + sFF' - sF^2 D - \Re_m \Omega) \\ & + \Lambda_c^{-1}(3s^{-1} D + D^2 + s^{-2}(1 - m^2)) - i\omega_c) \overline{b}_{s1} \\ & + \Lambda_c^{-1} \zeta \partial_z^2 \overline{b}_{s1} + (\zeta(msF^2 + 2s^{-1}\Lambda_c^{-1}) + i\Lambda_c^{-1} \partial_z \xi) \partial_z \overline{b}_{z1}]_{-d}^{d} ds, \end{aligned} \tag{B4}$$

$$\begin{aligned} C = \int_{-d}^{d} [& \overline{b}_{s1}(imsF^2 + 3s^{-1}\Lambda_c^{-1} - \Lambda_c^{-1} D) \partial_z \zeta + \Lambda_c^{-1} D \overline{b}_{s1} \partial_z \zeta \\ & - im\overline{b}_{s1}(3F^2 - (F^2 + 2sFF' + sF^2 D)) \xi - imsF^2 D \overline{b}_{s1} \zeta \\ & + \overline{b}_{z1}(msF^2 + is^{-1}\Lambda_c^{-1} + i\Lambda_c^{-1} D) \partial_z \xi - i\Lambda_c^{-1} D \overline{b}_{z1} \partial_z \xi]_{s_{ib}}^{1} dz, \end{aligned} \tag{B5}$$

and

$$L_0^\dagger = \begin{bmatrix} L_{01}^\dagger & L_{02}^\dagger \\ L_{03}^\dagger & L_{04}^\dagger \end{bmatrix} \tag{B6}$$

where

$$\begin{aligned} L_{01}^\dagger = [& -im(2F^2 + 3sFF' + sF^2 D - \Re_m \Omega) - i\omega_c \\ & + \Lambda_c^{-1}(D^2 + 3s^{-1} D + s^{-2}(4 - m^2) + \partial_z^2)] \partial_z \end{aligned} \tag{B7}$$

$$L_{02}^{\dagger} = -im[Fs^{-1}(1-m^2) - 5FF' + 2sF'^2 - sFF'' + (F^2D + 4sFF')D + sF^2D^2] \quad (B8)$$

$$L_{03}^{\dagger} = -mF^2s^{-1}(-m^2 + s^2\partial_z^2) + 2is^{-1}\Lambda_c^{-1}\partial_z^2 \quad (B9)$$

$$L_{04}^{\dagger} = [im(sF^2D - 3F^2 + sFF') + \Re_m\Omega) - i\omega_c + \Lambda_c^{-1}(D^2 - s^{-1}D + s^{-2}(1-m^2) + \partial_z^2)]\partial_z \quad (B10)$$

The appropriate z-dependence for ζ and ξ is determined from the requirement that, to satisfy (B2), $A = 0$ for all values of s. Since $\partial_z\bar{b}_{z1}$, $\bar{b}_{s1}$ and $\partial_z^2\bar{b}_{s1}$ are non-zero on $z = \pm d$ we require their coefficients in (B4) to be zero. The latter of these gives

$$\zeta = 0, \qquad z = \pm d, \quad (B11)$$

The requirement

$$[\partial_z^2\zeta - im\zeta((F^2 + sFF' - sF^2D - \Re_m\Omega) + \Lambda^{-1}(3s^{-1}D + D^2 + s^{-2}(1-m^2)) - i\omega_c)\partial_z\bar{b}_{s1}]_{-d}^{d} = 0, \quad (B12)$$

then reduces to

$$\partial_z^2\zeta = 0, \qquad z = \pm d \quad (B13)$$

and setting the coefficient of $\partial_z\bar{b}_{z1}$ to zero gives

$$\partial_z\xi = 0, \qquad z = \pm d, \quad (B14)$$

To satisfy (B11),(B13)–(B14) we take

$$\zeta \sim \sin n(z+d), \qquad \xi \sim \cos n(z+d). \quad (B15)$$

The boundary conditions for ζ, ξ at $s = s_{ib}, 1$ are found in a similar manner to above from the requirement $C = 0$. This leads to

$$\zeta = 0, \qquad s = s_{ib}, 1, \quad (B16)$$

$$\Lambda^{-1}D\zeta + (\Lambda^{-1}\gamma^{-1} + msF^2/n)iD\xi = 0, \qquad s = s_{ib}, 1, \tag{B17}$$

where γ is given in (4.18).

Appendix C: Boundary conditions for higher order terms

The boundary conditions as they apply to the linear problem are given in §4.2.2. Here we give them as they apply to higher order terms. The boundary conditions on the perfectly conducting plates at $z = \pm d$ are simple and satisfied by the z-dependence of the variables at each order. The conditions that must be satisfied at $s = s_{ib}, 1$ are less straightforward and detailed further below.

For the terms $b_{20}^{(2)}$ and b_{11} the boundary conditions are essentially as before with only minor differences. For the terms $\mathbf{b}_{20}^{(2)}$ the condition that the current normal to the boundary vanishes becomes

$$sD(sb_{s20}^{(2)}) + 2(m^2 + n^2)b_{z20}^{(2)}/n = 0 \tag{C1}$$

and matching to an external potential field gives

$$b_{s20}^{(2)} = \gamma_1 b_{z20}^{(2)} \tag{C2}$$

where

$$\gamma_1 = \begin{cases} -[I_{2m+1}(2ns_{ib})/I_2m(2ns_{ib}) + m/ns_{ib}]/2 & s = s_{ib} \\ [K_{2m+1}(2n)/K_2m(2n) - m/n]/2 & s = 1 \end{cases} \tag{C3}$$

Similarly, for b_{11} terms we obtain

$$D(sb_{s11}) - 2nsb_{z11} = 0 \tag{C4}$$

and

$$b_{s20}^{(2)} = \gamma_2 b_z \tag{C5}$$

where

$$\gamma_2 = \begin{cases} -[I_1(2ns_{ib})/I_0(2ns_{ib})]/2 & s = s_{ib} \\ [K_1(2n)/K_0(2n)]/2 & s = 1 \end{cases} \tag{C6}$$

For the terms $\mathbf{b}_{20}^{(1)}$ there is no z-dependence and $b_{z20}^{(1)} \equiv 0$ so that the condition that the current normal to the boundary is zero is satisfied identically. To obtain a condition for $b_{s20}^{(1)}$ we again match the field to a potential field in the insulating regions.

$$\mathbf{b}_{20}^{(1)} = \mathbf{b}^{(e)} \qquad s = s_{ib}, 1 \tag{C7}$$

where

$$\mathbf{b}^{(e)} = -\nabla V, \tag{C8}$$

and $V = V(s)\exp(2im\phi)$ satisfies

$$\frac{1}{s}D(sDV) - \frac{4m^2}{s^2}V = 0. \tag{C9}$$

Solving (C9) we obtain

$$V(s) = As^{2m} + Cs^{-2m}, \tag{C10}$$

where $A = 0$ in $s \geq 1$ and $C = 0$ in $s \leq s_{ib}$. The s and ϕ components of (C8) are

$$b_s^{(e)} = -DV, \tag{C11}$$

and

$$b_\phi^{(e)} = -s^{-1}\partial_\phi V. \tag{C12}$$

which can be solved, with (C10), to give

$$\begin{aligned} b_s^{(e)} &= -2mAs^{2m-1}, \qquad s \leq s_{ib}, \\ &= 2mCs^{-2m-1}, \qquad s \geq 1, \end{aligned} \tag{C13}$$

$$\begin{aligned} b_\phi^{(e)} &= -2imAs^{2m-1}, \qquad s \leq s_{ib}, \\ &= -2imCs^{-2m-1}, \qquad s \geq 1. \end{aligned} \tag{C14}$$

Eliminating the constant between (C13) and (C14) gives

$$\begin{aligned} b_\phi^{(e)} &= ib_s^{(e)}, \qquad s \leq s_{ib}, \\ &= -ib_s^{(e)}, \qquad s \geq 1. \end{aligned} \tag{C15}$$

From $\nabla \cdot \mathbf{b} = 0$, which must be satisfied everywhere, we have

$$D(sb_{s20}^{(1)}) + \partial_\phi b_{\phi 20}^{(1)} = 0, \tag{C16}$$

which with (C15) and the continuity of b_s, b_ϕ at the boundaries becomes

$$\begin{aligned} sDb_{s20}^{(1)} &= -(1-2m)b_{s20}^{(1)} \qquad s = s_{ib}, \\ &= -(1+2m)b_{s20}^{(1)} \qquad s = 1. \end{aligned} \tag{C17}$$